

# AN ABSTRACT OF THE THESIS OF

Christoph Pluess for the degree of Master of Science in Industrial Engineering presented on September 10, 2004.

Title: Application of Controlled Thermal Expansion in Diffusion Bonding for the High-Volume Microlamination of MECS Devices

Abstract approved:

Redacted for privacy

---

Brian K. Paul

Diffusion bonding has been widely used within microlamination architectures for the fabrication of Micro Energy and Chemical Systems (MECS). MECS are microsystems with the ability to process bulk amounts of fluid within highly-parallel microchannel arrays capable of accelerated heat and mass transfer. Thus far, diffusion bonding of the microchannel arrays is commonly done in a vacuum hot press system. The use of the hot press greatly restricts the production rate due to vacuum pump-down time and heating-up and cool-down periods. Furthermore, larger substrates are gaining interest in the system design of MECS devices and it is not apparent that uniaxial pressing within a hydraulic vacuum hot press will provide the bonding pressure uniformity necessary for large substrate bonding.

This thesis presents a novel fabrication approach for the high-volume thermal bonding of MECS devices with the use of controlled thermal expansion. A thermal bonding fixture based on the principle of differential thermal expansion was developed with focus on controlling the bonding pressure magnitude, the pressure timing and its sensitivity. The application of such a fixture within a conveyORIZED furnace system could be the key to a continuous thermal bonding approach for the mass production of MECS devices. The conceptual design and the feasibility of such a device was validated and explored by building a finite element model. Subsequently, a fixture prototype was fabricated. Functionality of the prototype  $\Delta$ CTE-fixture was confirmed at low temperatures (180°C) with the use of pressure sensitive film. An experimental comparison of at the diffusion bonding quality of the fixture versus the hot press was conducted under various bonding conditions. A  $2^4$  full factorial experimental design with

one replicate was conducted with mode (fixture/hot press), bonding pressure (3MPa/6MPa), bonding temperature (500°C/800°C) and bonding time (30min/60min) as experimental factors. The metallurgical examination of void fraction at the bond line (pressure magnitude) and the amount of measured fin warpage (pressure timing) were used to compare the bonding quality of the two approaches. An analysis of variance (ANOVA) revealed that there is no statistically significant difference in the levels of warpage found within samples prepared in the  $\Delta$ CTE-fixture compared to samples processed in the hot press indicating no major issues in pressure timing. The comparison of void fractions has shown that there was a difference in the level of pressure reached within the  $\Delta$ CTE-fixture although the bonding quality of the  $\Delta$ CTE-fixture was found to be satisfactory, especially at higher temperatures. Recommendations for design improvements were made to eliminate current issues with the level of pressure reached.

This study has shown that diffusion bonding conditions can be controlled using a static  $\Delta$ CTE bonding fixture. Results obtained conclude that the investigated concept is a plausible approach towards the high-volume microlamination of diffusion-bonded MECS devices.

© Copyright by Christoph Pluess

September 10, 2004

All Rights Reserved

Application of Controlled Thermal Expansion in Diffusion Bonding  
for the High-Volume Microlamination of MECS Devices

by  
Christoph Pluess

A THESIS

submitted to

Oregon State University

in partial fulfillment of  
the requirements for the  
degree of

Master of Science

Presented September 10, 2004

Commencement June 2005

Master of Science thesis of Christoph Pluess presented on September 10, 2004.

APPROVED:

Redacted for privacy

---

Major Professor representing Industrial Engineering

Redacted for privacy

---

Head of the Department of Industrial & Manufacturing Engineering

Redacted for privacy

---

Dean of the Graduate School

I understand that my thesis will become part of the permanent collection of Oregon State University libraries. My signature below authorizes release of my thesis to any reader upon request.

Redacted for privacy

---

Christoph Pluess, Author

## ACKNOWLEDGEMENTS

First of all, I would like to deeply express my sincere gratitude to my professor Dr. Brian K. Paul, for his valuable guidance in every aspect during my graduate studies at Oregon State University. My appreciation is extended to my graduate committee members Dr. Sundar V. Atre, Dr. Kevin M. Drost, Dr. Timothy C. Kennedy and Dr. Zhaohui Wu for their recommendations, advice and support throughout my thesis project. Specially, I would like to thank Dr. Timothy C. Kennedy for serving as my minor professor in Mechanical Engineering. My appreciation is extended to Mr. Steven Etringer, for his valuable machining work and assistance in every aspect of my research activities at Oregon State University.

I would like to thank in addition Dr. Chris A. Bell, Associate Dean of the College of Engineering, for his assistance and his continuous support and interest in sustaining the relationship with the School of Engineering in Burgdorf, Switzerland. In addition, I am very grateful for the noble efforts of Adele and Hans Neukomm in supporting and promoting students from Switzerland to undertake such a valuable experience. I am also especially thankful for the companionship, encouragement and assistance of my friend Stefan Meier and his decision and willingness to be part of this unique experience of studying abroad. Moreover, I would like to express my truthful appreciation and thankfulness to my parents, Esther and Thomas Plüss, for their endless support in all aspects of my personal education, mentally as well as financially.

Finally, I am truly and endless grateful for my partner Caroline, for her constantly mental support during my graduate studies at Oregon State University and her selfless sacrifice to join me on this endeavor far away from her family and friends.

# TABLE OF CONTENTS

	<u>Page</u>
1 Introduction.....	1
2 Literature Review .....	5
2.1 Microfluidic Devices.....	5
2.2 Research and Development of Bulk Microfluidic Devices .....	6
2.3 Fabrication of Bulk Microfluidic Devices .....	6
2.3.1 Microlamination .....	7
2.3.2 Materials.....	8
2.3.3 Solid-State Diffusion Bonding .....	8
2.4 Applications Using Differential Thermal Expansion.....	10
3 Theoretical Analysis and Device Design .....	12
3.1 Definition of Differential Thermal Expansion Bonding .....	12
3.1.1 Simplified Theoretical Model .....	12
3.1.2 Sensitivity Analysis of the Theoretical Model .....	15
3.2 Applicable Materials for Fixture Design .....	17
3.3 Process Considerations for Diffusion Bonding.....	18
3.4 Design Concepts.....	20
3.4.1 Concept 1: Basic Fixture Model .....	20
3.4.2 Concept 2: Bonding Fixture with Force Decomposing.....	21
3.4.3 Concept 3: Bonding Fixture with a Preload Mechanism .....	21
3.4.4 Concept 4: Bonding Fixture with Expansion Tubes .....	23
3.4.5 Evaluation of Design Concepts.....	24
3.5 Experimental Fixture Design .....	25
3.5.1 Timing of Bonding Pressure.....	26

## TABLE OF CONTENTS (Continued)

	<u>Page</u>
3.5.2 Adjustment of the Bonding Pressure Magnitude .....	28
3.5.3 Controlled Pressure Sensitivity .....	29
3.6 Fin Buckling Limit Analysis for Initial Gap Setting .....	31
3.7 Conceptual Design of a Large Substrate Bonding Unit .....	34
3.8 Finite Element Model of the Bonding Unit.....	37
3.8.1 FE-Model Overview and Features .....	38
4 Experimental Approach.....	43
4.1 Overview .....	43
4.2 Prototype Bonding Unit .....	43
4.3 Test Article Design .....	45
4.4 Test Article Fabrication.....	45
4.5 Orientation Experiment of Test Article .....	47
4.6 Effect of Pressure Timing on Fin Warpage .....	48
4.7 Load Cell Validation .....	49
4.8 Calibration of the $\Delta$ CTE-Fixture .....	50
4.8.1 Pressure Uniformity .....	50
4.8.2 Timing of the Bonding Pressure.....	51
4.9 Experimental Design for $\Delta$ CTE-Fixture Validation .....	52
4.10 Thermocouple Setup and Measurements.....	53
4.11 Optimization of the Furnace Cool Down Time .....	58
5 Results and Discussion.....	61
5.1 Theoretical Results FE-Model .....	61
5.1.1 Thermal Expansion Behavior of Fixture Model.....	61

## TABLE OF CONTENTS (Continued)

	<u>Page</u>
5.1.2 Stress Distribution in the Fixture Model.....	63
5.1.3 Initial Gap and Pressure Timing Analysis.....	64
5.1.4 Sensitivity Analysis .....	67
5.1.5 Pressure Uniformity .....	69
5.2 Effect of Pressure Timing on Fin Warpage .....	70
5.2.1 Comparison of Fin Warpage with the Finite Element Model.....	74
5.3 Load Cell Design Modifications .....	76
5.4 Analysis of Pressure Uniformity with Fuji Prescale Film .....	78
5.4.1 Pressure Uniformity based on Bonding Platens Accuracy.....	78
5.5 Analysis of Pressure Timing at Low Temperatures.....	81
5.6 Fixture Validation at High Temperatures .....	84
5.6.1 Failure of Aremcolox 502-1100 Ceramic Fixture Posts .....	84
5.6.2 Method for Initial Gap Adjustment of very Small Gaps .....	85
5.6.3 High Temperature Cycle Tests with Steatite L-5 Posts .....	85
5.7 Validation of the $\Delta$ CTE-Fixture .....	87
5.7.1 Results and Analysis of Fin Warpage .....	87
5.7.2 Results and Analysis of Void Fraction.....	89
6 Conclusions .....	95
6.1 Thesis Summary .....	95
6.2 Recommendations for Future Work.....	97
7 References .....	100
8 Appendices .....	103

# LIST OF FIGURES

<u>Figure</u>	<u>Page</u>
2-1: Classification of Microfluidic Devices .....	5
2-2: Schematic of a Microlamination Approach .....	7
3-1: Schematic of a Simple CTE Bonding Unit.....	13
3-2: Thermal Expansion Behavior of the $\Delta$ CTE-Fixture .....	14
3-3: General Bonding Cycle for Microlamination .....	19
3-4: Basic $\Delta$ CTE-Fixture Concept .....	20
3-5: $\Delta$ CTE-Fixture Concept with Force Decomposing .....	21
3-6: $\Delta$ CTE-Fixture Concept with Preload Mechanism .....	22
3-7: $\Delta$ CTE-Fixture Concept with Expansion Tube .....	23
3-8: Design of the Experimental $\Delta$ CTE Bonding Unit .....	25
3-9: Pressure Application during Temperature Ramping.....	27
3-10: Sensitivity Behavior .....	30
3-11: Fin Geometry and Column Buckling Behavior.....	32
3-12: Critical Temperature Difference for Fin Buckling .....	34
3-13: Concept of a Large Substrate $\Delta$ CTE Bonding Unit.....	35
3-14: Concept of a Large Substrate Fixture with a Gas Expander.....	36
3-15: FE-Model Overview of the Fixture Design (1/4 Symmetry Expansion) .....	37
3-16: Modeled Section of the $\Delta$ CTE-Fixture .....	39
3-17: Initial Strain Situation in LINK10 Elements of Load Cell Fasteners .....	40
3-18: Load Step Definition .....	41
4-1: Differential Thermal Expansion Bonding Unit Prototype.....	43
4-2: Load Cell .....	44
4-3: Bonding Platens .....	44

## LIST OF FIGURES (Continued)

<u>Figure</u>	<u>Page</u>
4-4: Laser Cut Layers of Test Article.....	45
4-5: Deburring of Laser Machined Laminae .....	46
4-6: Mean Fin Warpage based on Test Article Orientation in Fixture .....	47
4-7: Load Cell Validation.....	49
4-8: Temperature Limit of Fuji Pressure Sensitive Film.....	51
4-9: Test Article with Bending Features for High Temperature Experiments .....	52
4-10: Experimental Design of Comparison Experiment.....	53
4-11: TC Setup on Pressmaster Vacuum Hot Press .....	54
4-12: Temperature Profile Hot Zone vs. Heating Elements .....	55
4-13: Thermocouple Setup of the $\Delta$ CTE Fixture.....	56
4-14: Thermocouple Measurements on $\Delta$ CTE Fixture (no vacuum).....	56
4-15: Improved Temperature Profile (in vacuum).....	58
4-16: Cooling Curves in Helium vs. Vacuum.....	59
5-1: Thermal Expansion of Fixture in Z-Direction at 800°C (Units shown in m) .....	61
5-2: Thermal Expansion of Frame and Inner Parts.....	62
5-3: Stress in Z-Direction (Values shown in Pa).....	64
5-4: Variation of Initial Gap and Effect on Contact Temperature .....	65
5-5: Effect of Contact Temperature on Pressure Timing .....	66
5-6: Pressure Sensitivity Depending on Temperature Fluctuations.....	68
5-7: Copper Substrate of the FE-Model (mapped mesh).....	69
5-8: Path Plots of Pressure Distribution at Substrate .....	69
5-9: Metallographic Cross-Sections of Fin Warpage .....	71
5-10: Experimental Fin Warpage Measured in the Center of the Fins .....	72

## LIST OF FIGURES (Continued)

<u>Figure</u>	<u>Page</u>
5-11: Experimental Fin Warpage Measured to the Right and Left of the Fins.....	73
5-12: FE Model of the Test Article (half cut) .....	74
5-13: Real Test Article (left) and FE-Model Half Cut (right) .....	74
5-14: Theoretical Fin Warpage of Test Article based on FE-Analysis.....	75
5-15: Load Cell with Graphite Bolts.....	77
5-16: Final Load Cell Design.....	78
5-17: Axis Definition of the Graphite Bonding Platens .....	79
5-18: Initial Surface Roughness and Waviness in X-X Direction .....	80
5-19: Non-uniform Pressure Distribution due to Expanded Frame Bolts .....	82
5-20: Fixture Frame Fastening Modification with Disc Springs.....	82
5-21: Ceramic Post Failures and Thread Wear .....	84
5-22: Gauge Ring for Small Gap Adjustments .....	85
5-23: Temperature Profile of 800°C Bonding Cycle .....	86
5-24: Plot of Mean Fin Warpage based on the Experimental Mode .....	87
5-25: Interaction of Temperature and Pressure on Fin Warpage.....	88
5-26: Interaction of Mode and Pressure on Fin Warpage.....	89
5-27: Mean Void Fraction for Experimental Factor Mode .....	90
5-28: Interaction of Experimental Mode and Pressure on Void Fraction.....	92
5-29: Interaction of Mode and Temperature on Void Fraction .....	92
6-1: Design Recommendation for Future Fixture Post Design .....	98

## LIST OF TABLES

<u>Table</u>	<u>Page</u>
3-1: Low CTE-Materials for High Temperature Frame Applications .....	17
3-2: High CTE-Materials for High Temperature Inner Part Applications .....	18
3-3: Design Concept Evaluation.....	24
4-1: Physical Properties of Molybdenum and SS 321 .....	57
4-2: Physical Properties of Typical Furnace Quenching Gases.....	58
5-1: Experimental Results of Fin Warpage.....	72
5-2: FE-Simulation Results of Fin Warpage .....	75
5-3: Initial Pressure Film Readings of Bonding Platens.....	79
5-4: Initial Bonding Platens Waviness and Roughness in X and Y-Direction .....	80
5-5: Corrected Bonding Platens Waviness and Roughness in X and Y-Direction.....	81
5-6: Final Film Readings of Bonding Platens .....	81
5-7: Low Temperature Pressure Film Readings for Fixture Validation.....	82
5-8: Mean Void Fractions observed at Bonding Conditions.....	90
5-9: Void Fraction Comparison Hot Press vs. $\Delta$ CTE-Fixture .....	93

## LIST OF APPENDICES

<u>Appendix</u>	<u>Page</u>
A: Fixture Drawings .....	104
B: APDL-Macro FE-Model .....	112
C: FE-Model Simulation Settings .....	115
D: Experimental Data.....	119
E: Fixture Timing with Fuji Film.....	131
F: Data Comparison Experiment.....	135

# DEDICATION

Dedicated to my beloved grandfather

Erwin Andres-Künzli,  
17.7.1925 – 1.3.2004

## PREFACE

The strategy of “smaller is better” has begun to transform the world of fluidics as it has transformed the world of electronics. As microchannels become smaller, their surface area to volume ratio increases dramatically making microfluidic devices highly sensitive to surface effects. Hence, heat and mass transfer are greater at the microscale and energy transfer and chemical processes can be performed in smaller volumes of space. Moreover, reactions, separations, phase changes and mixing of fluids can be realized in an accelerated manner leading to more precise process control.

So far, the research on microfluidic systems has focused on the development of individual functions, units and devices and no standards exist, even for the simplest components. The field remains open for exploration and most major research institutions have groups working on R&D of microfluidic systems. MIT Technology Review named microfluidics one of ten technologies that will change the world. Microfluidic technology is on its way to commercialization but it is still a long way to go and many problems remain to be solved.

## 1 INTRODUCTION

In recent years, there has been a growing emphasis in manufacturing research on the fabrication of Micro Energy and Chemical Systems (MECS). MECS are microsystems with the ability to process bulk amounts of fluid within highly-parallel microchannel arrays capable of accelerated heat and mass transfer. Small characteristic sizes provide the benefits of large surface-to-volume ratios, laminar flow conditions and the opportunity of operating at elevated pressures. Examples of devices which would result from the application of MECS technology include miniature heat pumps, chemical synthesis systems, waste clean-up devices, miniature power sources and biological reactors. Important application areas for MECS devices are portable systems and devices for on-site and on-demand synthesis. Applying MECS technology to energy systems has the potential of reducing the size, weight, and cost of miniature power generating equipment. Combustion driven electrical generators could be packaged to the size of conventional batteries with lifetimes exceeding those of batteries by many times. This could have a huge impact on the whole portable communications and computing industry. On-site and on-demand fuel reforming to drive fuel cells in cars would make the storage of hydrogen in tanks unnecessary and reduce the risks of fuel cell technology for the automotive industry.

The vast majority of ongoing research and development in the field of microfluidic devices is based on silicon microfabrication techniques [36][38]. However, the functionality of MECS require that the devices have thermal, chemical and physical properties of more traditional engineering materials such as polymers, metals or ceramics some of which, for instance, are capable of working at high temperatures. Further, MECS system sizes dictate the use of more economical materials than single crystal silicon.

One approach to building microfluidic systems with embedded microfeatures in engineering materials is an architecture known as microlamination [13][37] shown in Figure 2-2. Microlamination involves the patterning, registration and bonding of thin layers of material referred to as laminae and is commonly used to fabricate monolithic, multi-layered fluidic devices with complex shapes, internal cavities, flow chambers and

interconnects suitable for microfluidic applications. Diffusion bonding is commonly used to join metal laminae. During diffusion bonding laminae are heated up to the appropriate bonding temperature under an applied bonding pressure and held at these conditions for a period of time necessary to join the individual laminae into a monolithic device due to solid state diffusion across the faying surfaces of the materials. The bonding pressure has to be distributed uniformly throughout the microchannel device to prevent poor bonding conditions which would lead to fluid leakage.

Common diffusion bonding processes use a hydraulic vacuum hot press which in most cases is not the appropriate machine tool for the mass production of diffusion bonded devices. Vacuum hot presses require batch operation which restricts throughput. Furthermore, it has been observed that 50 to 80% of the total diffusion bonding cycle time within a vacuum hot press is due to vacuum pump-down time, heat-up and cool-down time of the vacuum hot press. Another deficiency of hot press systems is the cost of the system as the size of the work envelope increases. Large substrates are gaining interest in the system design of microlaminated MECS devices. For MECS devices having large volumes, it is expected to be cheaper to produce microsystems with larger substrate sizes thereby reducing the number of laminae needed [23]. For MECS devices having small volumes, large substrates permit batch production with the ability to distribute the patterning and bonding costs over a greater number of devices. Further larger substrates permit the integration of multiple unit operations onto the same substrate layer. This integral design concept provides an optimal solution to achieve a compact system design with minimal dead volumes among the unit operations compared to small, stand alone unit operations connected by tubing. Large hot press systems which would be capable of bonding substrates up to sizes of 10 x 10 inches can be found on the market, but require large capital expenditures and pump-down, heat-up and cool-down phases of such huge systems are even worse than observed on small systems. Moreover, the costs associated with the operating and maintaining hydraulic vacuum hot press systems to meet capacity needs are high. Also, it is not apparent that uniaxial pressing with a hydraulic ram will provide a certain uniformity of bonding pressure, especially for joining large substrates. Hence, a new approach to diffusion bonding (and thermal bonding in general) has to be investigated

towards a more economical production of large-substrate microlaminated MECS devices.

Paul and Thomas [20] have shown a technique that uses the difference in the coefficients of thermal expansion (CTE's) between the bonding fixture material and the laminae material to precisely align prismatic laminae for diffusion bonding. Through this work and the work of Wattanutchariya and Paul [20][21][22], it has been observed that very high pressures can be generated based on differential thermal expansion. In this thesis, a fixture design is pursued that would use differential thermal expansion between a static fixture and the laminae to produce a bonding pressure. This would permit diffusion bonding to be accomplished within a conveyORIZED furnace or oven with much shorter cycle times. The frame construction of the thermal expansion fixture should be fabricated out of a high temperature material with a lower thermal expansion coefficient compared to the expansion parts inside the clamp which will apply the pressure onto the laminae. The difference in thermal expansion will transmit bonding pressure to the laminae at a particular temperature once an interference is produced between the inside dimension of the fixture and the outside dimension of the laminae stack. The size of the substrate would not be constrained by the pressure distribution and cavity size of a uniaxial vacuum hot press. An appropriately designed bonding fixture would allow the diffusion bonding of large substrates for integrated systems in a batch inert gas or vacuum furnace. Moreover, by replacing the batch furnace with a conveyORIZED inert gas furnace, as used in the material processing and electronics industry, a continuous diffusion bonding approach for high-volume production of microlaminated devices would be feasible. The use of such a bonding approach would substantially reduce the operating and fabrication costs of a microlaminated device. It is unknown if a static clamping system as described could provide a controlled bonding pressure over a certain temperature range while maintaining a uniform pressure distribution over the substrate. Such an approach could be the key to the high-volume production and commercialization of large-scale microlaminated MECS devices and might be of potential interest for industrial applications.

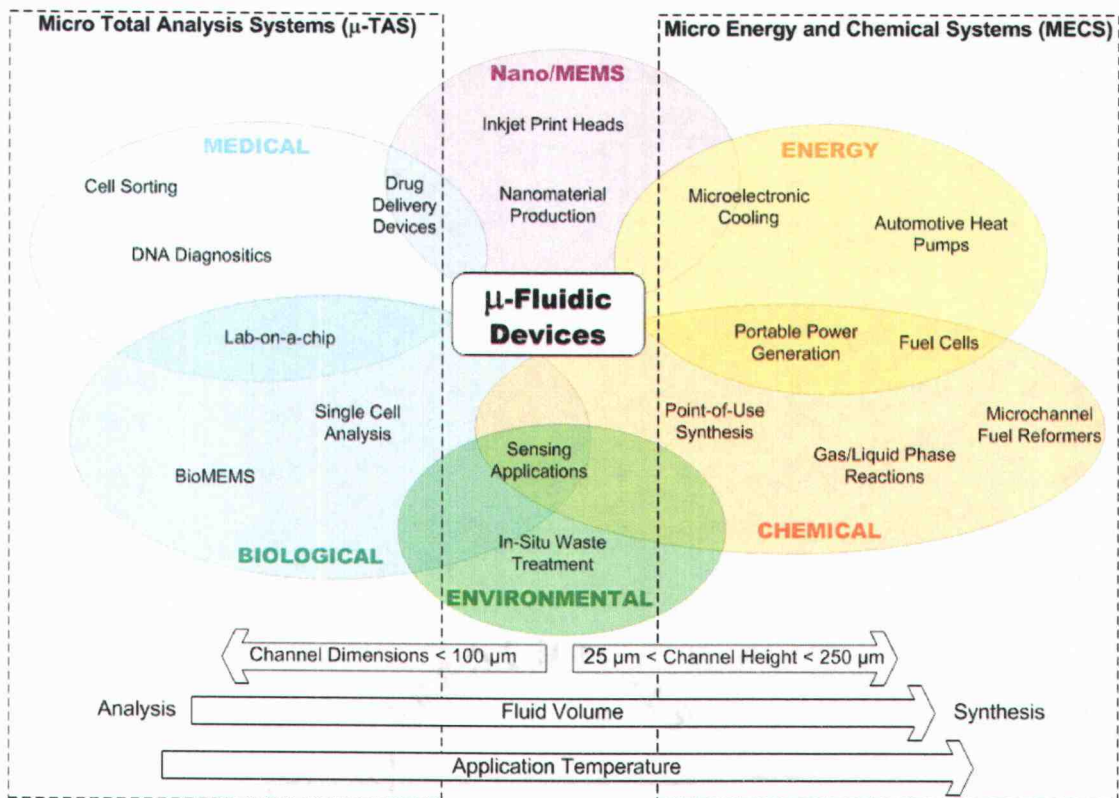
This thesis investigates a new approach for consistently diffusion bonding microlaminated devices with a bonding fixture based on the principle of differential thermal expansion. It is unknown if the necessary bonding pressure can be controlled

through a static fixture design which allows some modularity in the stack height for the laminae under a given set of material and processing conditions. In addition, parameters like pressure magnitude, timing, uniformity and sensitivity, and their effect on the bonding quality will be examined to conclude if the new technique might be a plausible approach towards the high-volume production of diffusion-bonded MECS devices.

## 2 LITERATURE REVIEW

### 2.1 MICROFLUIDIC DEVICES

The continuous progress in research and development of microfluidic devices can be seen in a wide range of applications (medical, biological, environmental, chemical, energy, consumer) as shown in Figure 2-1.



**Figure 2-1: Classification of Microfluidic Devices**

The potential benefits of microfluidic devices include reduced size, improved performance, disposability, integration in other microsystems and lower costs. Besides the categorization into different fields of application, microfluidic devices can mainly be classified into two groups: analytical microfluidic devices, referred to as micro total analysis systems (μ-TAS) and bulk microfluidic devices, referred to as MECS. These two major categories have significant differences in their function, in the fabrication technologies needed to produce them and in the materials used. While analytical devices are dealing with picoliters of fluids, bulk fluidic devices are designed to process

maximal amounts of fluids. This affects the architecture of the device and dictates more or less fabrication methods and materials.

## **2.2 RESEARCH AND DEVELOPMENT OF BULK MICROFLUIDIC DEVICES**

Fewer research efforts have been made in the area of MECS and only a few institutions and companies are active in this emerging research area. The function of bulk fluidic devices is to process large amounts of fluids at small scales. Bulk microfluidic devices are concerned about energy transfer or synthesis of products, not the information extracted from processing of the fluid like in  $\mu$ -TAS. MECS has emerged from the miniaturizing of macroscale fluidic devices (reactors, mixers, heat exchangers etc.), since heat and mass transfer is favorable at a smaller scale due to the higher surface-to-volume ratio. Today, a variety of microfluidic units already exists and proofed their functionality in the laboratory [29]. Future steps in the development of microfluidic devices should focus on the integration of different functions and aspects of low-cost and high-volume production to build complete, economical microfluidic systems [30]. Full commercial potential of microfluidic systems will be realized through the integration of various chemical and energy unit operations.

The innovative design of a thermal expansion bonding unit presented in this thesis could be a key technology for the mass production and commercialization of microlaminated devices and a provisional patent has been filed by Paul and Pluess. The use of thermal expansion as a driving force for the pressure application during a microlamination approach was first stated by Pacific Northwest National Laboratory (PNNL) in 1999 [18].

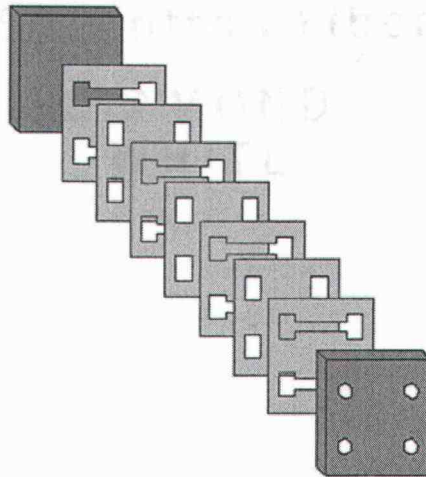
## **2.3 FABRICATION OF BULK MICROFLUIDIC DEVICES**

Bulk microfluidic devices are at least partially fabricated by using microtechnology and precision engineering methods for fabricating the microchannel geometries. Peripheral components like connectors, housing or isolation devices, are normally fabricated by conventional fabrication methods. The characteristic dimensions of internal microchannels are in the range of 10 to 500  $\mu\text{m}$  [27]. Compared to silicon-based micro total analysis systems ( $\mu$ -TAS), bulk microfluidic devices are more spatially-intensified since their function involves the processing of maximal amounts of fluids. Hence, these devices are mostly multilayered and by numbering up the microstructured channels the

performance can be multiplied. In the vast majority of applications, the fabrication of bulk microfluidic devices is based on a microlamination approach [3][4][16][17].

### 2.3.1 MICROLAMINATION

Microlamination is a process commonly used to fabricate monolithic, multi-layered bulk microfluidic devices with complex shapes, internal cavities, flow chambers and interconnects suitable for microfluidic applications [13][27]. Most conventional microfabrication techniques cannot easily form sets of internal channels and chambers. Microlamination involves the patterning and bonding of thin layers of material, called laminae, to produce monolithic devices containing embedded features. Thin layers can be “designed for function” and for example the deposition of catalytic materials on specific layers can be used in the fabrication of microreactors [26]. Hence, microlamination is a favorable fabrication technique for chemical process intensification.



**Figure 2-2: Schematic of a Microlamination Approach**

For the patterning of the fluid layers different techniques are commonly used. Good feature resolution can be achieved with photochemical etching. The laminae can be etched either single-sided or double-sided and complex cavity shapes are possible. Direct-writing methods like laser machining offer a higher flexibility in the production of substrates compared to photochemical etching. Stamping of patterns could be an alternative to laser machining for mass production, if the channel features are not too small. This is one advantage of the microlamination approach. Precision is generally required in the z-axis which for metals is controlled by cold rolling processes

traditionally known as a precise, high-volume process (e.g. process is used to make shim stock). In a typical microchannel array, the lateral patterns on laminae are much larger requiring less precision. For the patterning of very complex channel features in metallic substrates, fabrication methods like electrochemical micromachining (ECMM) or electro discharge micromachining (EDMM) could be of potential interest. Wire-EDM is capable of cutting hundreds of layers at the same time by stacking up the substrates.

After patterning of the individual fluidic layers the bonding process follows. Diffusion bonding is commonly used to join metallic and ceramic structures. A critical step during the bonding of the patterned layers is the proper alignment and registration of the layers relative to each other. Commonly, alignment of the layers is achieved with pins and precise pinholes in the layers [27]. Thomas and Paul [20] have shown an innovative alignment technique by using the difference in thermal expansion between fixture and laminae. During diffusion bonding laminae are heated up to bonding temperature under an applied bonding pressure and held at these conditions for a period of time necessary to join the layers to a monolithic device due to solid state diffusion. Insufficient bonding conditions can lead to poor bonding and leakage while too great of bonding conditions can lead to deformed or collapsed channel features.

### 2.3.2 MATERIALS

The application portfolio of bulk microfluidic devices requires that used materials have thermal, chemical and physical properties of more traditional engineering materials such as metals or ceramics with high melting temperatures and corrosion resistance. Therefore, most commonly used materials are stainless steel, copper, aluminum alloys, titanium, and many others. For high-temperature applications in microreactors, ceramics have been successfully implemented [18]. Other high temperature materials like aluminide foils have been investigated by Paul and Alman et al. for the application in microlaminated high-temperature heat exchangers [1][2][19].

### 2.3.3 SOLID-STATE DIFFUSION BONDING

Diffusion bonding is a solid state joining process, in which two cleaned and smooth surfaces are pressed together for a certain time at elevated temperatures until a bond is formed. This joining process usually happens in a protective atmosphere or in vacuum

to prevent oxidation which will act as a diffusion barrier. To form a satisfactory bond it is necessary to bring the two metal surfaces into sufficient atomic contact that the energy of interaction between their atoms will be a minimum. The interatomic forces of attraction begin to be felt at distances between  $10^{-4}$  and  $5 \cdot 10^{-4}$   $\mu\text{m}$  [39]. No matter how well machined a surface is, it presents microscopically a rough surface. Consequently the application of a certain pressure is needed to bring the surfaces close enough into contact through plastic deformation of surface asperities. The application of pressure let the contact area grow to a large fraction of the joint area. Experiments have shown that the bonding faces should have a surface finish better than  $0.4 \mu\text{m } R_a$  to achieve a bonding strength comparable to the one of the parent material [31][33]. An increased surface roughness would increase the volume fraction of voids in the bonding interface and finally decreasing the bonding strength. It is also understood that an increased temperature reduces the yield stress of the materials and activates the diffusion and mobility of atoms in the lattice. When both pressure and heat are applied together, the bonding process can be accelerated. The principal parameters activating diffusion bonding are bonding temperature, bonding pressure and processing time. Between temperature and pressure a hyperbolic relation is recommended to yield sound bonds. Bonding at higher temperatures needs less pressure than bonding at lower temperatures. The bonding process takes place at temperatures below the melting temperature  $T_m$  of the lowest melting material, typically at  $0.5\text{-}0.7 T_m$ . The pressure application is such, that macro-deformation of the joined parts is not reached, although increasing the pressure could improve the bonding strength. Typical pressure ranges are 5-10 MPa for carbon steels, 7-12 MPa for stainless steels and 3-7 MPa for aluminum alloys [31]. An optimal bonding pressure is approximately equal to the yield strength of the workpieces at the bonding temperature [39]. Where dissimilar materials are to be joined, the choice of bonding pressure is decided by the weaker of the two materials. The bonding time can vary depending on the applied temperature and pressure from several minutes to several hours. An indirect indication that a diffusion process is complete is the ultimate strength of the bond which should be ideally about the same as the parent material. The strength of the bond increases proportional to the square root of the bonding time, which is characteristic for a diffusion-controlled process.

The quality of diffusion bonded joints can be evaluated by using a range of techniques. These include metallography, ultrasonic inspection and the use of mechanical testing procedures such as tensile, impact and lap shear tests [32]. Mechanical test procedures like tensile testing have been reported as reliable methods for the assessment of bonding quality. However, these methods are not readily applicable to sheet material structures and metallographic techniques can be used by analyzing the fraction of interfacial voids.

## **2.4 APPLICATIONS USING DIFFERENTIAL THERMAL EXPANSION**

Thermal expansion is always an issue where dissimilar parts/materials have to be assembled, joined or interacted in any way in an environment that experiences changes in temperature. This can be the case in almost any engineering discipline, starting at the microscale in the microelectronics industry up to large structures in civil engineering. However, in general it is desired either to compensate or minimize the influence of thermal expansion in engineered structures. Thermal stress is one of the most serious reliability problems in engineering. The combination of different materials, each with its own set of elastic coefficients, expansion coefficients and stress limitations can lead to high stress levels at elevated temperatures.

Few applications can be found where thermal expansion is desired and actively used to fulfill a function. An early invention from 1987 shows a concept of an implantable biomedical pump for drug dispensing driven by a thermal-responsive pumping movement of a diaphragm due to differential thermal expansion [5]. A thermal expansion driven indentation system was presented by Lesko et al. in 1992 where a specimen was placed on a thermally expandable member to determine the hardness and other material properties by measuring the applied force and displacement [6]. Other applications of thermal expansion can be found in the field of compensating tolerances during thermal cycling to hold parts and tools in exact position. Alignment of layers by thermal expansion gained interest in the lamination of multilayer integrated circuits (IC) in the electronics industry [11]. Thomas and Paul [20] presented earlier an approach to precisely aligning multiple layers by differential thermal expansion for the use in a microlamination approach.

It has been recognized, that thermal expansion can favorably be applied in processes where clamping of a part is needed during a thermal cycling process. Nulman et al. have shown an improved clamping ring based on a low thermal expansion clamping mechanism for securing semiconductor wafers during physical vapor deposition (PVD) [9]. A belt press has been proposed which uses differential thermal expansion between parts of a platen assembly to generate bonding pressure for the joining of conveyor belts was patented by Willis et al. [10]. An interesting patent application was filed by McHerron et al. of the IBM Corporation (NY) which claims the method for application of pressure to a workpiece by thermal expansion [12]. The presented method and apparatus of McHerron et al. relates to the high-volume fabrication of multilayer thin film (MLTF) structures in the semiconductor industry and is considered for low temperature applications used for the lamination of polymer circuit boards.

Although the basic idea of the IBM patent application is similar to the investigation presented in this thesis, the author's fixture design shows capabilities and improvements well beyond the capabilities of the IBM patent application, especially for the use as a production unit for high-volume production at higher temperatures. Following analysis will show that a differential thermal expansion fixture based on a simple expansion block interposed between laminae and fixture frame never can produce a controllable bonding pressure and hence, bonding results can have significant variance between cycles, in particular at high temperatures. Control of bonding parameters is the key to high-volume production and the control of pressure magnitude, sensitivity and timing are essential design aspects of a differential thermal expansion bonding unit. These aspects have been addressed in this thesis.

### 3 THEORETICAL ANALYSIS AND DEVICE DESIGN

#### 3.1 DEFINITION OF DIFFERENTIAL THERMAL EXPANSION BONDING

The general design of a bonding fixture based on the principle of thermal expansion for the application of bonding pressure is rather simple as shown in Figure 3-1. The bonding unit consists of a bottom plate, a top plate and in the simplest case of an expansion block interposed between them. The bottom and top plates are structurally connected representing a rigid frame construction built of a low thermal expansion material. The expansion block has a significantly higher coefficient of thermal expansion than the frame of the fixture. All things being equal, the height of the expansion block is directly proportional to the amount of clamping pressure to be delivered. Between the expansion block and the bottom plate the laminae are placed and aligned. Typically, it is preferred to place the laminae between bonding platens as illustrated in Figure 3-1. It is believed that the coefficients of thermal expansion (CTE) should preferably differ at least by a factor of two to guarantee functionality [10]. When the bonding unit is heated up to the bonding temperature ( $T_B$ ), the expansion block and the platens inside the frame expand relatively to the frame by the difference in the sum of their coefficients of thermal expansion scaled by the product of the height of the expansion block/laminae and the change in temperature. An initial gap can be designed into the fixture assembly to scale and time the application of the bonding pressure. As soon as the initial gap ( $g_0$ ) is consumed due to the differential expansion behavior (i.e. inside of frame and inner parts come into contact), compression is applied to the laminae and increases with increasing temperature.

##### 3.1.1 SIMPLIFIED THEORETICAL MODEL

The thermal expansion of a part is determined by multiplying its length ( $L$ ) times its coefficient of thermal expansion ( $\alpha$ ) times the change in temperature ( $\Delta T$ ) according to Equation 1.

$$\Delta L_{thermal} = L \cdot \alpha \cdot (T_2 - T_1) = L \cdot \alpha \cdot \Delta T \quad (1)$$

If it is assumed that the frame construction of the proposed static fixture, consisting of a top plate, bottom plate and plate connections, is rigid and does not deflect due to

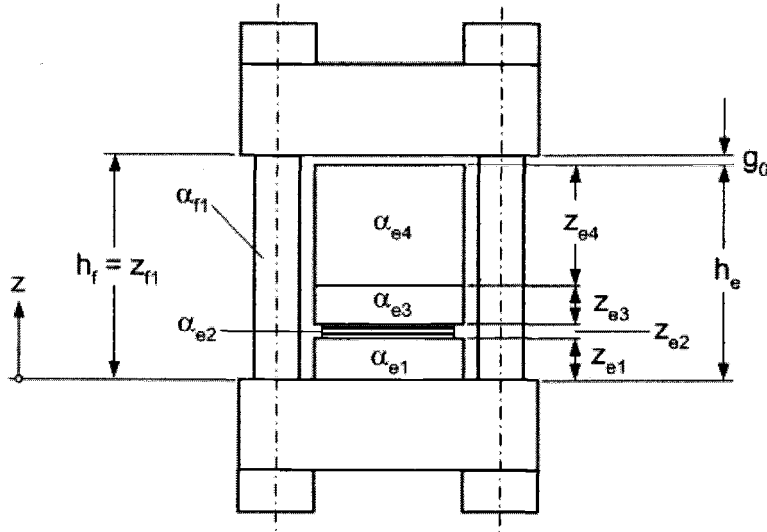
resultant forces, the following analysis applies. To determine how the frame and inner parts of the fixture expand upon a raise in temperature from room temperature ( $T_R$ ) to bonding temperature ( $T_B$ ), the sum of the coefficient of thermal expansion scaled by the individual part height times the change in temperature has to be considered. Equation 2 and 3 express the thermal expansion function of the fixture frame (subscript f) and the inner parts (subscript e).

$$\Delta z_f(T) = \sum \alpha_{f,i} \cdot z_{f,i} \cdot (T - T_R) \quad (2)$$

$$\Delta z_e(T) = \sum \alpha_{e,i} \cdot z_{e,i} \cdot (T - T_R) \quad (3)$$

Since the inner parts are designed to have a higher expansion rate, the initial gap will close as a function of temperature by the difference of Equations 2 and 3 and can be expressed according to Equation 4.

$$g(T) = g_0 - \Delta z(T) = g_0 - (\sum \alpha_{e,i} \cdot z_{e,i} - \sum \alpha_{f,i} \cdot z_{f,i}) \cdot (T - T_R) \quad (4)$$



**Figure 3-1: Schematic of a Simple CTE Bonding Unit**

It is of particular interest to set the initial gap ( $g_0$ ) such that contact between the inner platens and the frame is reached at a certain temperature. The contact temperature ( $T_C$ ) is defined as the temperature at which the initial gap has been reduced to zero.

$$g(T_C) = g_0 - (\sum \alpha_{e,i} \cdot z_{e,i} - \sum \alpha_{f,i} \cdot z_{f,i}) \cdot (T_C - T_R) = 0 \quad (5)$$

Since the contact temperature ( $T_C$ ) is unknown, it is useful to express it as a function of the known bonding temperature ( $T_B$ ). The specification of the temperature difference ( $\Delta T_{CB}$ ) between contact and bonding temperature is actually responsible for the transfer of thermal expansion to structural strain and can be used for the scaling of the bonding pressure.

$$T_C = T_B - \Delta T_{CB} \quad (6)$$

Finally, by introducing Equation 6 into Equation 5 the initial gap can be calculated according to Equation 7.

$$g_0 = (\sum \alpha_{e,i} \cdot z_{e,i} - \sum \alpha_{f,i} \cdot z_{f,i}) \cdot (T_B - \Delta T_{CB} - T_R) \quad (7)$$

After defining the initial gap ( $g_0$ ), the final amount of thermal expansion at bonding temperature  $g(T_B)$  can be calculated by using Equation 4. Since the higher expanding inner parts of the fixture will follow the expansion behavior of the more rigid frame after the contact temperature ( $T_C$ ), the value of  $g(T_B)$  will be negative, which is indicative of the amount of compression within the fixture frame above  $T_C$  (see Figure 3-2). This behavior is true for a stiff and rigid fixture frame construction.

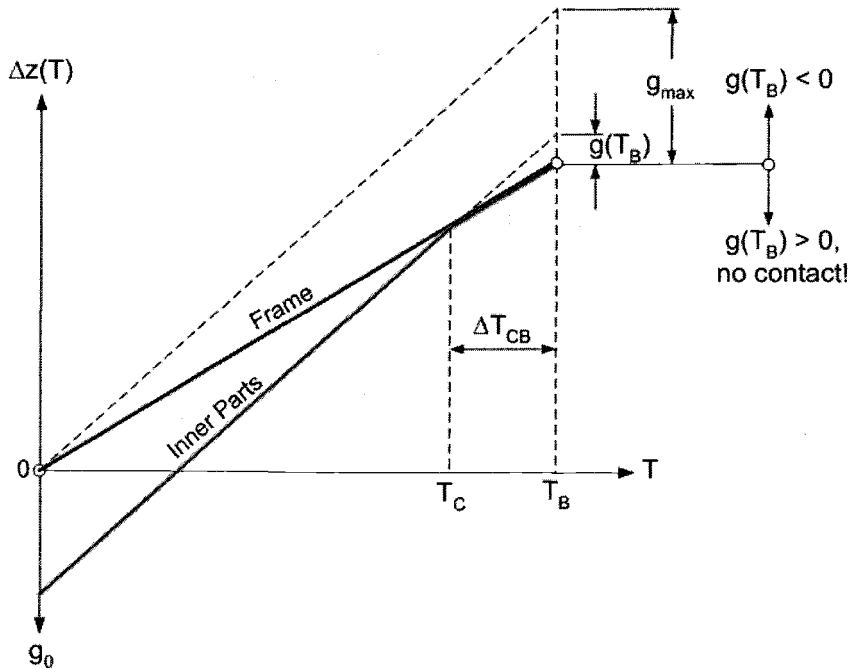


Figure 3-2: Thermal Expansion Behavior of the  $\Delta$ CTE-Fixture

The amount of compression in the laminae at the final bonding temperature finally can be expressed as the total compressive strain ( $\epsilon_{total}$ ) on the laminae with respect to the expanded frame height,  $h_f + \Delta z_f(T_B)$  as shown in Equation 8.

$$\epsilon_{total} = \frac{g(T_B)}{h_f + \Delta z_f(T_B)} \quad (8)$$

To calculate the final bonding pressure, stress-strain relations have to be applied. In this simplified theoretical model the assumption was made that the modulus of elasticity of the individual parts are similar. From Equation 8 the resulting bonding pressure can be extracted by multiplying the amount of strain by the specific modulus of elasticity of the lamina material.

$$\sigma_{lam} = \epsilon_{total} \cdot E_{lam} \quad (9)$$

### 3.1.2 SENSITIVITY ANALYSIS OF THE THEORETICAL MODEL

Applying the equations above to the fixture design shown in Figure 3-1, a sensitivity analysis of the bonding pressure can be made. Geometrical dimensions and applied materials are selected comparable to the fixture design developed in this thesis. The bonding platens were made out of graphite ( $\alpha_{e1}=\alpha_{e3}=4.6\mu\text{m}/\text{m}^\circ\text{C}$ ) and have thicknesses of  $z_{e1}=z_{e3}=15\text{mm}$ . A copper laminae stack ( $\alpha_{e2}=24.8\mu\text{m}/\text{m}^\circ\text{C}$ ) was chosen as a substrate material with a stack height of  $z_{e2}=1\text{mm}$ . The expansion block made of stainless steel 321 ( $\alpha_{e4}=20.5\mu\text{m}/\text{m}^\circ\text{C}$ ) has an initial height of  $z_{e4}=40\text{mm}$ . The summation of all inner platens gives a total height of the inner parts of  $h_e=71\text{mm}$ . A diffusion bonding cycle with a bonding temperature of  $800^\circ\text{C}$  was assumed with a realistic defined temperature difference ( $\Delta T_{CB}$ ) of  $25^\circ\text{C}$  between the contact and bonding temperature. The frame is made of a ceramic material with thermal expansion coefficient of  $5.2\mu\text{m}/\text{m}^\circ\text{C}$  and the frame height is given by  $h_f=h_e+g_0$ . Introducing this relationship into Equation 7, the initial gap size can be calculated to be  $462\mu\text{m}$ . These settings would lead to an interference of  $15\mu\text{m}$  between frame and inner parts and a resultant pressure on the laminae of  $23.4\text{MPa}$  can be calculated. This amount of pressure would be well beyond a desired pressure of about  $5\text{MPa}$  and has to be reduced. This can be achieved by either increase the initial gap size or by changing geometry and material properties of the fixture design. By increasing the gap size to

474  $\mu\text{m}$ , contact between frame and inner parts will be established  $5^\circ\text{C}$  before reaching the bonding temperature. The temperature difference ( $\Delta T_{\text{CB}}$ ) of  $5^\circ\text{C}$  reduces the interference to 3  $\mu\text{m}$  and a resultant pressure of 4.7 MPa can be produced. This concludes that an increase of 12  $\mu\text{m}$  in initial gap size ( $g_0$ ) reduced the pressure from 23.4 MPa to 4.7 MPa or changing the gap size  $\pm 1 \mu\text{m}$  would vary the resulting bonding pressure by  $\pm 1.6$  MPa. Since the initial gap has to be adjusted manually with a feeler gauge, a gap adjustment accuracy of  $\pm 5 \mu\text{m}$  has to be considered as very good. In other words, the pressure of the discussed fixture design according to Figure 3-1 has a sensitivity of  $\pm 8.0$  MPa based on the initial gap adjustment, assumed all other possible sources of error are zero. The sensitivity depending on temperature fluctuations of  $\pm 5^\circ\text{C}$  can be expressed as  $\pm 4.7$  MPa with the current fixture settings. Neither temperature nor initial gap adjustments can be adjusted that accurate in order to achieve a tolerable pressure variation of  $\pm 0.5$  MPa.

A possible approach to reduce the pressure sensitivity of the fixture is by reducing the product of the CTE and the height of the expansion block. Reducing either the height, CTE or both would decrease the potential of pressure generation. Hence, the previous height of 40 mm for the expansion block is reduced to 20 mm for further analysis. Applying same calculation as done previously, a bonding pressure of 6.6 MPa is achieved with an initial gap adjustment of 236  $\mu\text{m}$  which relates to temperature difference  $\Delta T_{\text{CB}}$  of  $10^\circ\text{C}$ . By decreasing the gap to 231  $\mu\text{m}$ , contact will be established  $25^\circ\text{C}$  before reaching the bonding temperature with a resulting pressure of 16.4 MPa (23.4 MPa for same  $\Delta T_{\text{CB}}$  with  $z_{e4}=40\text{mm}$ ). The actual change in gap size by  $\pm 1 \mu\text{m}$  relates to a pressure change of  $\pm 2.0$  MPa, which is even more sensitive than before. The pressure sensitivity depending on temperature fluctuations decreased with the shorter expansion block to  $\pm 0.65$  MPa/ $^\circ\text{C}$ . Although the expansion rate of the inner parts has decreased the pressure sensitivity depending on temperature fluctuations, the geometrical sensitivity (initial gap adjustment) increased.

The conclusion can be made, that the application of pressure due to thermal expansion of solid materials is highly sensitive and is dependent on exact process conditions and geometrical adjustments in order to achieve the desired level of pressure. Errors in the final level of pressure can be due to temperature fluctuations or geometrical settings.

The Initial gap adjustment seems to be the larger source of error and is more difficult to control than temperature. Hence, the differential expansion rate of the fixture should be large, in order to allow a better gap adjustment. Conversely, a large expansion rate increases the pressure sensitivity due to temperature fluctuations. Both requirements are difficult to balance with the proposed fixture design of McHerron et al. [12] and the application of the bonding pressure due to thermal expansion has to be provided in a different manner.

### 3.2 APPLICABLE MATERIALS FOR FIXTURE DESIGN

Similar bonding fixtures and approaches have been designed for low and moderate temperature levels to join mainly polymers [10][12]. The selection of structural materials for the above stated fixtures is not as problematic as it is for the design of a bonding unit which should be capable of providing functionality up to temperatures below 1000°C for solid state diffusion bonding of metallic substrates. The selection of applicable materials is based on the maximal service temperature of the material, the strength at service temperature, the coefficient of thermal expansion, and the manufacturability and cost of the material. Subsequently, the materials can be classified according to their CTE either for use as a material for the fixture frame (see Table 3-1) or as a material for parts where higher thermal expansion is desired (see Table 3-2).

**Table 3-1: Low CTE-Materials for High Temperature Frame Applications**

Material	FEM ID#	Max. Service Temperature [°C]	Tensile Elastic Modulus [GPa]	Poisson's Ratio	CTE linear 1000°C [μm/m°C]
Graphite ISO-63	4	3650 <sup>(1)</sup>	12.0 <sup>(1)</sup>	-	5.6 <sup>(2)</sup>
Molybdenum	1	2617 (T <sub>m</sub> ) <sup>(1)</sup>	330 <sup>(1)</sup>	0.29 <sup>(2)</sup>	6.5 <sup>(1)</sup>
Tungsten	-	3370 (T <sub>m</sub> ) <sup>(1)</sup>	400 <sup>(1)</sup>	0.28 <sup>(1)</sup>	4.4 <sup>(1)</sup>
Alumina A998	7	1750 <sup>(1)</sup>	370 <sup>(1)</sup>	0.22 <sup>(1)</sup>	8.2 <sup>(1)</sup>
Steatite L-5	-	930 <sup>(2)</sup>	100 <sup>(1)</sup>	0.24 <sup>(1)</sup>	9.5 <sup>(2)</sup>
Aremcolox™ 502-1100 full-fired	2	1150 <sup>(2)</sup>	(100)	(0.24)	5.2 <sup>(2)</sup>

(1) Material Property Source: [www.MatWeb.com](http://www.MatWeb.com)

(2) Material Property Source: Material Supplier

**Table 3-2: High CTE-Materials for High Temperature Inner Part Applications**

Material	FEM ID#	Max. Service Temperature [°C]	Tensile Elastic Modulus [GPa]	Poisson's Ratio	CTE linear 1000°C [μm/m·°C]
AISI Stainless Steel Type 309	-	980 <sup>(1)</sup>	200 <sup>(1)</sup>	0.3 <sup>(1)</sup>	17.3 <sup>(1)</sup> linear 500°C
AISI Stainless Steel Type 310	-	1035 <sup>(1)</sup>	200 <sup>(1)</sup>	0.3	19.1 <sup>(1)</sup>
AISI Stainless Steel Type 321	3	925 <sup>(1)</sup>	195 <sup>(1)</sup>	0.3	20.5 <sup>(1)</sup>
AISI Stainless Steel Type 330	-	1035 <sup>(1)</sup>	197 <sup>(1)</sup>	0.3	16.7 <sup>(1)</sup> linear 500°C
INCONEL™ 625	-	650 <sup>(1)</sup>	208 <sup>(1)</sup>	0.28 <sup>(1)</sup>	14.9 <sup>(1)</sup>

(1) Material Property Source: [www.MatWeb.com](http://www.MatWeb.com)

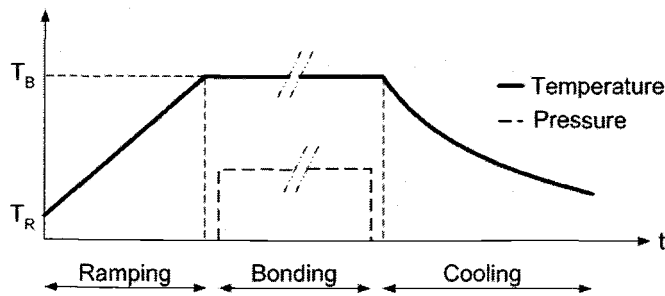
(2) Material Property Source: Material Supplier

The combination of materials contacting each other during the bonding cycle has to be considered. Especially the substrate layers should be sandwiched between materials where no bond occurs to prevent joining the fixture together. Graphite platens have been successfully used in the past to prevent bonding to the fixture. Other contacting fixture parts can be coated with a magnesia slurry to prevent solid state diffusion.

### 3.3 PROCESS CONSIDERATIONS FOR DIFFUSION BONDING

The previous theoretical study of a simple fixture design has shown that a desired bonding pressure due to differential thermal expansion is rather difficult to be controlled and a small change either in temperature or initial gap size can result in an enormous variation of bonding pressure. To yield a certain bonding quality it is absolutely necessary to control the amount of pressure caused by thermal expansion and to minimize pressure variations due to thermal fluctuations or gap adjustments. The initial gap adjustment is necessary to offset the point of contact close to the final bonding temperature and can be understood as a timing of bonding pressure. This timing of pressure during a bonding cycle as shown in Figure 3-3 is of great importance for the prevention of fin warpage inside the microlaminated device. The prevention of warpage in the microchannel structure is a major goal during the production of microlaminated devices and effects of pressure timing will be analyzed in greater detail later in the text. Kanlayasiri [25] found that in the reactive diffusion bonding of NiAl microchannel arrays, the average warpage as a percentage deviation in channel height varied from 21.4% to

36.8% (channel height 142  $\mu\text{m}$ ), depending on the bonding parameters used (bonding time, pressure and temperature). In diffusion bonding stainless steel microchannel arrays without self-registration, Wattanutchariya [24] found the average warpage as a percentage deviation in channel height to be from 31.7% to 7.7% for channel heights from 50.8  $\mu\text{m}$  to 101.6  $\mu\text{m}$  respectively. It was also found that a 20% channel height deviation could result in greater than 50% increase in the heat transfer surface area needed to compensate for this variation [24]. Essentially, this translates into roughly a 50% increase in the number of channels and consequently a 50% increase in the device size needed.



**Figure 3-3: General Bonding Cycle for Microlamination**

In general, the bonding cycle can mainly be divided into ramping, bonding and cooling. During the temperature ramp-up from room temperature ( $T_R$ ) to bonding temperature ( $T_B$ ), it is important that the patterned layers inside the clamp have the freedom to expand without restraint and that no pressure is applied to the stack. Any pressure during ramp-up would constrain the expansion of the layers due to friction and any subsequent temperature rise will cause the internal microchannel structure to warp (first elastically then plastically) since the material is still expanding. This effect will be discussed in further detail later in the text.

After the temperature has reached the bonding temperature, it is desirable to apply the bonding pressure. This initiates the bonding phase. Normally, a certain amount of lag guarantees temperature uniformity before applying the bonding pressure. The bonding phase ends with the removal of bonding pressure and the start of the cooling phase. Before the temperature starts to drop, the bonding pressure has to be removed from the bonded device to, again, prevent thermal stresses during the cooling.

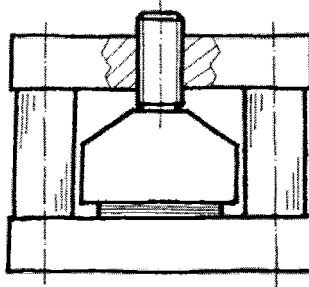
Within a vacuum hot press the timing, the magnitude and the leveling of the pressure can be achieved by controlling the hydraulic ram of the press. Developing a fixture to control these key parameters within a static fixture actuated by differential thermal expansion represents the major challenge of this investigation.

### 3.4 DESIGN CONCEPTS

The design of a thermal expansion fixture can mainly be divided into the frame construction with a lower thermal expansion behavior, and the pressure platens inside the frame with a higher thermal expansion behavior. Their difference in thermal expansion is the principal driving force of the bonding fixture. Both, frame and platens have to be designed in a rigid manner to prevent deformations and deflections since the useable stroke of thermal expansion will be in the range of  $500 \pm 200 \mu\text{m}$ . All design concepts shown below, can either be used in a vertical or horizontal arrangement depending on the cavity design of the furnace or the opening of a conveyor furnace.

#### 3.4.1 CONCEPT 1: BASIC FIXTURE MODEL

The simplest design of a bonding unit driven by thermal expansion can be seen in Figure 3-4 and represents mainly the previously discussed design of the IBM patent application by McHerron et al. [12]. The integrated set screw in the frame allows the modification of the fixture for different stack heights to guarantee certain modularity and the timing of bonding pressure by allowing an initial gap. Timing and magnitude of the resulting pressure are controlled by the gap adjustment.



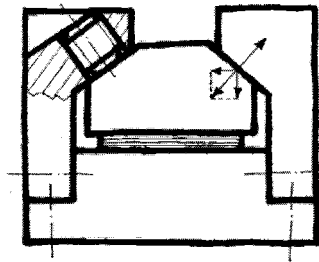
**Figure 3-4: Basic  $\Delta\text{CTE}$ -Fixture Concept**

Since the magnitude of the bonding pressure is based on stress-strain relations of the substrate material, the system will be highly sensitive to changes either in temperature or initial gap adjustments. A further limitation can be seen in the applicable substrate

size. The thermal expansion scales with the height of the expansion block, and for larger substrates, the expansion block would result in a heavy piece of material with a large thermal mass and would absorb most of the applied heat. One possible way to overcome this issue is to split up the large expansion block in several pieces and distribute them symmetrically over the substrate area.

### 3.4.2 CONCEPT 2: BONDING FIXTURE WITH FORCE DECOMPOSING

Building on concept 1, the frame design shown in Figure 3-5 should lessen the sensitivity issues of the static fixture. The frame is designed as an open structure with rigidity in the vertical direction. The frame arms at the sides allow certain bending and this flexibility allows a certain leveling of the overall pressure applied on the substrate surface.



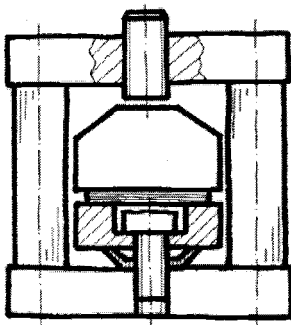
**Figure 3-5: ΔCTE-Fixture Concept with Force Decomposing**

By introducing a contact angle between frame and expansion block the contact force can be decomposed into a vertical and horizontal force component. Thus, the resulting force in vertical direction can be minimized and with that the pressure and the sensitivity of the fixture. The horizontal force components get transformed into bending of the frame arms. Moreover, the frame arms could be designed with a certain flexibility in bending that would lower the resulting pressure even more. Set screws for initial gap adjustments can be integrated on both sides of the frame arms. It would be preferable to make adjustments on the initial gap only from one side and support the other side of the expansion block with a ball point tip.

### 3.4.3 CONCEPT 3: BONDING FIXTURE WITH A PRELOAD MECHANISM

A more complex design of a thermal expansion bonding fixture is shown in Figure 3-6. Design concept 3 claims the implementation of spring elements to decrease the

pressure sensitivity of the bonding fixture. The resulting bonding pressure will be due to the amount of active spring compression related to the substrate area. By introducing spring elements into the fixture design, the amount of thermal expansion will always be consumed by the springs and the magnitude of the bonding pressure is no longer dependent on the material properties of the fixture platens. The application of disc (Belleville) springs is considered as favorable, since disc springs work with minimal compression by high load forces. Besides disc springs are available in various materials and alloys some of which, for instance, are capable of working at high temperatures.



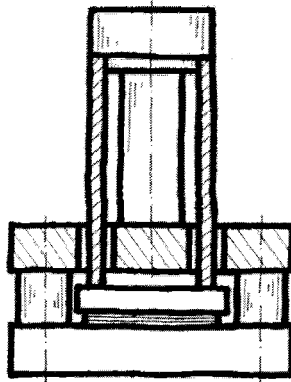
**Figure 3-6:  $\Delta$ CTE-Fixture Concept with Preload Mechanism**

Taking this concept a step further, the spring elements can even be preloaded to the desired final pressure level. The springs are held by screws in the base plate of the bonding unit in the pre-compressed state. The appropriate amount of preload force can be applied with a weight or a hydraulic press and the screws are snugged during the preload procedure to secure the amount of spring compression. During a bonding cycle, as soon as the expansion block comes in contact with the frame of the fixture, the preloaded force is transmitted into the laminae stack applying the pre-adjusted pressure. The timing of the force release can be controlled by the set screw in the fixture frame as already clarified in previous fixture concepts. The initial gap has to be compensated so that contact is made a few degrees below the final bonding temperature to guarantee release of the pre-loaded force into the laminae. Fluctuations in temperature follow differential thermal expansion behavior of the fixture modulated by the spring constant which can be modified through the design of the spring. Consequently, a thermal expansion fixture with spring elements will yield minimal bonding pressure sensitivity. However, the presented concept involves some complications in the selection of appropriate materials and components to allow the

fixture application at high temperatures without diffusion bonding structural components together or reaching limits of the maximal service temperature. Furthermore, the design of a pre-loadable bonding stage for large substrates is problematic and pressure uniformity has to be considered as an important factor.

#### 3.4.4 CONCEPT 4: BONDING FIXTURE WITH EXPANSION TUBES

The usable stroke of thermal expansion in the fixture is small as already mentioned previously and could probably be insufficient for certain high pressure applications, especially if small changes in temperature are involved. This problem is addressed in design concept 4 by introducing “expansion tubes”. As previously mentioned, the amount of thermal expansion scales with the height of the expansion driver and if higher expansion rates are desired, the application of a long, highly expanding tube could be a favorable solution as shown in Figure 3-7.



**Figure 3-7:  $\Delta$ CTE-Fixture Concept with Expansion Tube**

An expansion tube provides some significant advantages compared to a solid expansion block. Clearly, the relevant amount of thermal expansion created in the vertical direction for a tube with length  $L$  is the same as for a solid expansion block with height  $H=L$ . However, the related volume and thermal mass of the expansion block is significantly higher and would absorb much more heat than a tube. Furthermore, the free space inside the tube can be used constructive in the fixture design as shown in Figure 3-7 by extending the tubes out of the main fixture frame. This extended expansion tube design would provide a significant amount of thermal expansion along the axis of the tube. For larger substrates, multiple tubes can be distributed over the bonding area to yield a uniform pressure distribution. Unfortunately, the pressure

sensitivity of this concept would be very high and pressure timing and control are difficult to incorporate into the fixture design.

### 3.4.5 EVALUATION OF DESIGN CONCEPTS

Each of the previous design concepts illustrates some unique features and some trade-offs between fixture complexity, pressure magnification, timing and sensitivity. A reliable fixture design suited for high-volume production should have the ability to precisely control the major bonding parameters and respond insensitive to temperature changes of the furnace environment. Further, the bonding fixture has to offer certain modularity for different stack heights and substrate sizes. The overall complexity of the fixture including the number of necessary parts should be minimized since the summation of tolerances could lead to dimensional problems and incorrect pressure scaling. Table 3-3 illustrates some general trends and facts of the previously discussed design concepts. Each listed criteria is evaluated within three levels, low (L), moderate (M) and high (H). Note, that for pressure sensitivity, fixture complexity and thermal mass of the fixture the grade L (low) would be favorable.

**Table 3-3: Design Concept Evaluation**

	H/L	Concept 1			Concept 2			Concept 3			Concept 4		
		L	M	H	L	M	H	L	M	H	L	M	H
Control of Pressure Timing	H												
Control of Pressure Magnitude	H												
Pressure Sensitivity in $f(\Delta T)$	L												
Modularity in Stack Height	H												
Complexity of Fixture	L												
Thermal Mass of System	L												

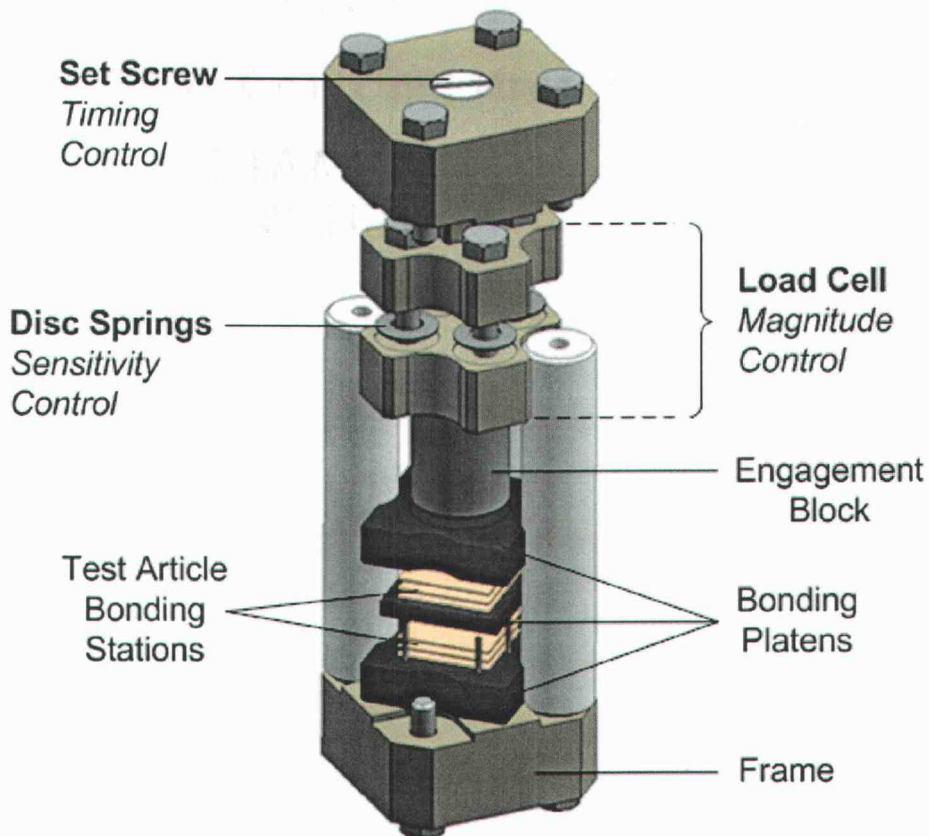
L=low / M=moderate / H=high

This simple evaluation shows that the best control of pressure timing and magnitude with least pressure sensitivity can be achieved with design concept 3. In addition, the concept with preloaded spring elements (concept 3) allows for a high level of modularity in the stack height of the substrates. It is possible, that particular concept features can be combined to yield overall improvement. As an example, the use of expansion tubes as expansion drivers to lower the overall thermal mass of the fixture.

### 3.5 EXPERIMENTAL FIXTURE DESIGN

Timing, magnitude and sensitivity of bonding pressure are the key functions which have to be addressed in the design of a differential thermal expansion bonding unit. Based on design concept 3, a final fixture design is presented in Figure 3-8 to evaluate the functionality of the fixture concept experimentally. Detailed information and fixture drawings can be found in Appendix A.

The bonding unit shown in Figure 3-8 is specially designed to fit in the three inch inside diameter of the Pressmaster vacuum hot press model HP30-4560 from Thermal Technologies Inc. to simulate the thermal cycling.



**Figure 3-8: Design of the Experimental  $\Delta$ CTE Bonding Unit**

Thus, the maximal substrate size for this particular fixture design is limited to 25x25mm. The same hot press has also been used to perform regular diffusion bonded samples which can later be used as a reference for bond quality assessment of samples bonded with the prototype fixture. The use of the same furnace system for both bonding methods assured the same environmental conditions for all samples and minimizes

experimental noise. The fixture itself is composed of multiple high temperature materials selected depending on their thermal expansion potential. The base and the top of the thermal expansion fixture are made of molybdenum connected by four ceramic standoffs to guarantee a rigid and low expanding fixture frame. Low expanding Aremcolox 502-1100 was used for the ceramic standoffs since this material is specifically designed for structural parts and can be machined in a fully fired state. The test articles are placed between isotropic graphite ISO-63 bonding platens and aligned by three tungsten alignment pins.

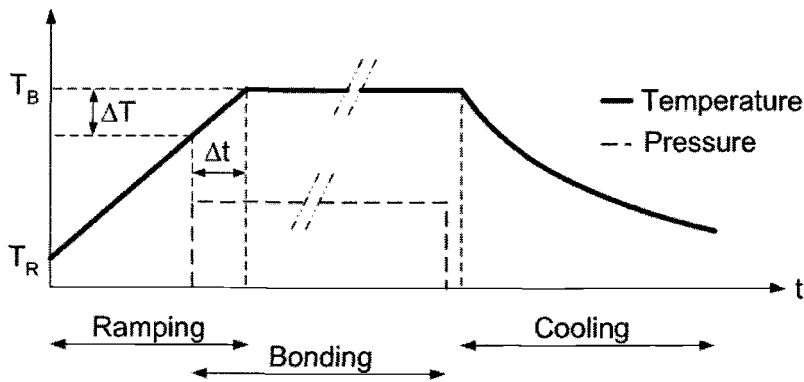
The graphite bonding platens are designed to allow the bonding of two test articles at once to reduce experimental runs. On top of the graphite bonding platen the engagement block is placed and centered. The engagement block is fabricated out of high temperature stainless steel 321 with a high coefficient of thermal expansion to drive the main displacement of the load cell sitting on top of it. The load cell consists of two molybdenum platens with four integrated Inconel™ high temperature disc springs. The device is held together by four ceramic fasteners and is mainly responsible for controlling the magnitude of the bonding pressure. The initial gap between the load cell top and the fixture frame is adjusted with a fine threaded set screw in the top plate of the fixture frame to control the timing of the bonding pressure. The set screw is made of graphite to prevent diffusion bonding to the molybdenum top plate.

### 3.5.1 TIMING OF BONDING PRESSURE

In the diffusion bonding of microlaminated devices it is of significant importance that the bonding pressure not be applied before the bonding temperature is reached to prevent warpage of the finned microchannel structures inside the laminae stack. If the bonding pressure is applied a certain time ( $\Delta t$ ) before the bonding temperature ( $T_B$ ) is reached as illustrated in Figure 3-9, the residual temperature rise ( $\Delta T$ ) will cause the fins inside the laminae stack to warp. This warpage effect can be explained by the fact that the pressurized sections of the stack will be held in position due to frictional forces between the interfaces. Since the thermal expansion of typical graphite bonding fixture platens is significantly smaller than the expansion of the lamina material (in general by a factor 4 to 5), the lateral expansion of the pressurized laminae stack is restricted by the expansion behavior of the graphite platens. The fin sections, which are not affected by

the bonding pressure expanding without restraint and the CTE difference between the layer material and the graphite will cause the fin sections to buckle (see Figure 5-9).

In an ideal bonding cycle the pressure will be applied at the end of the heating ramp and therefore no fin warpage will result since all materials are already fully expanded. However, to guarantee a certain level of pressure at the desired bonding temperature with a differential thermal expansion unit, the contact has to be made at some temperature,  $\Delta T$ , before the final bonding temperature is reached. This temperature range also allows for any tolerances of the system. Nevertheless, the point of contact should be kept as close as possible to the actual bonding temperature to minimize warpage effects.



**Figure 3-9: Pressure Application during Temperature Ramping**

In the experimental fixture design (Figure 3-8) the initial gap size between the load cell and the fixture frame can be adjusted with a fine threaded set screw. The gap size is a function of the actual bonding temperature based on the difference in thermal expansion of the frame and platen stack inside the clamp. The gap size can be adjusted by fitting a shim or assembly of shims according to the calculated gap size by making use of Equation 7. Favorably is the use of a feeler gauge with a variety of precise shims for the adjustment of the initial gap. The author believes that with some experience the tolerance for the initial gap can be kept in the range of  $\pm 10 \mu\text{m}$ . The impact of this adjustment error ( $\Delta z_{\text{err}}$ ) on the pressure sensitivity of the proposed fixture design can be seen in Equation 10, where  $k_{\text{total}}$  represents the total spring constant and  $A_B$  the actual bonding area. The total spring constant of the load cell can be obtained by multiplying the number of spring stacks (m) within the load cell times the number of springs (n) within each stack times the spring constant (k) of a single spring.

$$\Delta\sigma(\Delta z_{err}) = \frac{k_{total} \cdot \Delta z_{err}}{A_B} = \frac{m \cdot n \cdot k \cdot \Delta z_{err}}{A_B} \quad (10)$$

The current design uses four disc springs with an individual spring constant ( $k$ ) of 2740 N/mm for a load cell total of 10'960 N/mm. Considering the maximal bonding area ( $A_B$ ) of 25x25mm and the above stated adjustment error ( $\Delta z_{err}$ ) of  $\pm 10 \mu\text{m}$ , the pressure sensitivity depending on the gap adjustment relates to  $\pm 0.175 \text{ MPa}$ , which is by a factor of 50 lower than seen for the simple  $\Delta\text{CTE}$  fixture design (Figure 3-1).

### 3.5.2 ADJUSTMENT OF THE BONDING PRESSURE MAGNITUDE

Like mentioned previously, the magnitude of bonding pressure will be adjusted with the so called load cell (see Figure 3-8). As soon as the initial gap between the load cell and the fixture frame is consumed by the difference in thermal expansion, the bonding pressure is transmitted to the laminae stack. The difficulty in the design of the load cell lies in the principle of load storage. The load cell is designed to be compressed by the desired load between the hydraulic ram of the vacuum hot press. The minimal load applicable by the used hot press model is about 400 lbs (1780 N). The appropriate level of bonding pressure for a certain material is taken from the literature or is experimentally evaluated by performing some bonding experiments. With the knowledge of the desired bonding pressure, the force load ( $F$ ) can be evaluated by multiplying the bonding pressure ( $p$ ) by the actual bonding area ( $A_B$ ).

$$F = p \cdot A_B \quad (11)$$

Storage of the pre-loaded force in the load cell is accomplished by compressing the load cell, snugly tightening the load cell fasteners and retracting the hydraulic ram. Finally, the pre-loaded load cell can be placed into the static fixture. Since the springs have to deal with high loads at high temperature under minimal compression, high temperature, nickel-based disc (Bellville) springs are used.

The initial compression of the load cell ( $\Delta z_c$ ) is critical for the adjustment of the pressure magnitude. The initial compression can roughly be calculated by dividing the compression force through the total spring constant ( $k_{total}$ ) of the load cell.

$$\Delta z_c = \frac{F}{k_{total}} = \frac{F}{m \cdot n \cdot k} \quad (12)$$

If the CTE difference between load cell fasteners and load cell plates can be neglected and the bonding unit is used for low temperature bonding applications, then Equation 12 can be used. For the case, where a significant difference in thermal expansion between fasteners and load cell plates exists, the amount of differential thermal expansion has to be included in the net compression of the load cell, especially by considering high temperature bonding cycles. This behavior can either lead to a higher compression or relaxation of the load cell at contact temperature and the initial compression procedure has to compensate differences accordingly.

$$\Delta z = \Delta z_c - \Delta z_{corr} = \frac{F}{m \cdot n \cdot k} - (l_P \cdot \alpha_P - l_F \cdot \alpha_F) \cdot (T_C - T_R) \quad (13)$$

Equation 13 shows the previous Equation 12 expanded by a correction term which includes the difference in thermal expansion of the load cell fasteners and top plate. If the CTE of the fasteners ( $\alpha_F$ ) is larger than the CTE of the load cell plate ( $\alpha_P$ ) the correction term will be negative and the difference is added to the net compression since the load cell would have been relaxed due to a temperature rise to the point of contact. Hence the amount of relaxation will be additionally added to the load cell compression at room temperature. Accordingly, if the CTE of the load cell plates ( $\alpha_P$ ) is larger than the CTE of the fasteners ( $\alpha_F$ ), the load cell would have been additionally compressed during the temperature rise. Therefore, the correction term will subtract the amount of additional compression from the initial compression value at room temperature. Taking the expansion behavior of the load cell components in account should allow the exact adjustment of the bonding pressure. Based on the above developed relationships the corrected force for the appropriate load cell compression at room temperature can be expressed as shown in Equation 14.

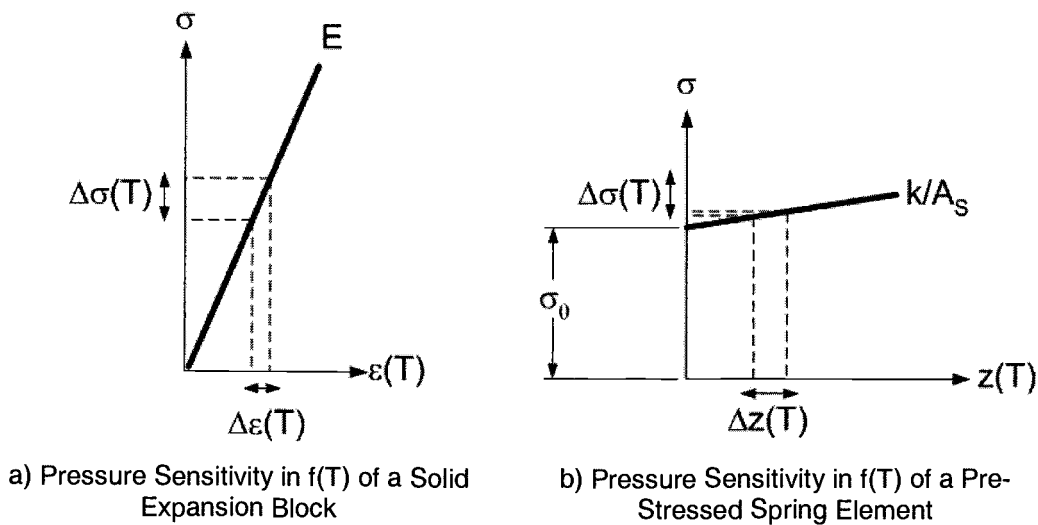
$$F = \Delta z \cdot k_{total} = p \cdot A_B - (l_P \cdot \alpha_P - l_F \cdot \alpha_F) \cdot (T_C - T_R) \cdot m \cdot n \cdot k \quad (14)$$

### 3.5.3 CONTROLLED PRESSURE SENSITIVITY

In addition to timing and magnitude of the bonding pressure, it is important to understand the sensitivity of bonding pressure as a function of temperature. Once the

fixture has applied the necessary pressure for diffusion bonding, the level of pressure should stay constant within a certain tolerance range. Typically, temperature fluctuations of  $\pm 5^\circ\text{C}$  have to be considered in a standard furnace cavity.

The simple theoretical model has shown, that the pressure sensitivity for a thermal expansion bonding unit with a solid expansion block is extremely high and slight changes in temperature effect large swings in the bonding pressure. The compressive stress between the different expanding materials is directly related over stress-strain relations and therefore scales with the slope of the tensile elastic modulus as shown in Figure 3-10a. It is obvious that a fixture having the design of a solid expansion block [12] never can provide pressure uniformity from cycle to cycle and hence, the unit is not applicable for mass production.



**Figure 3-10: Sensitivity Behavior**

In this thesis, the proposed thermal expansion bonding unit is especially designed to provide low pressure sensitivity by implementing spring elements. The previous section discussed the design of the load cell by using spring elements to provide an adjustable pressure magnitude. The same spring elements are also used to provide low pressure sensitivity as shown in Figure 3-10b. Once the spring elements are in the desired pre-stressed state, additional compression due to thermal expansion will only cause small pressure changes. The sensitivity of the load cell follows the relationship shown in Equation 15, where  $k_{\text{total}}$  is the overall spring constant of the load cell and  $\Delta z(T)$

represents the amount of thermal expansion due to thermal fluctuations. Pressure can be calculated by dividing the change in force through the bonding area  $A_B$ .

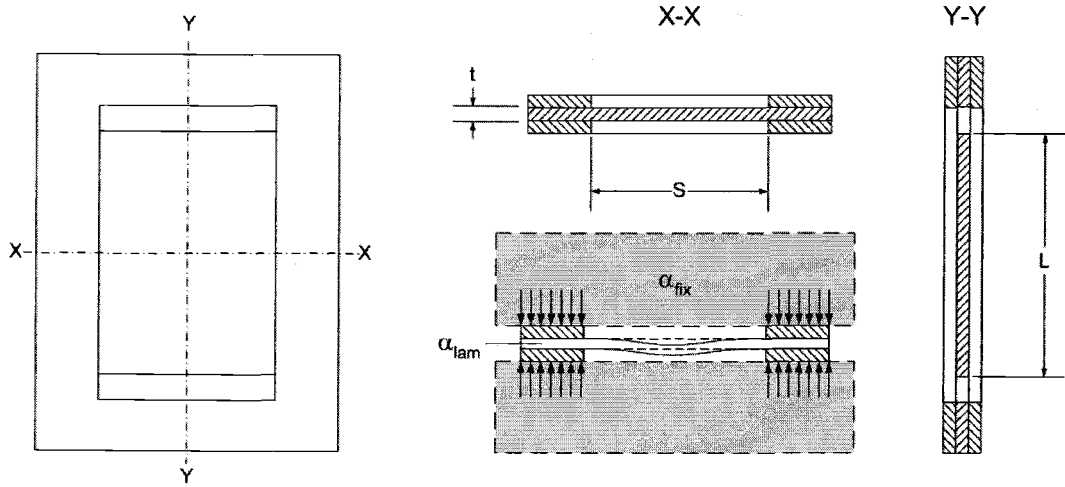
$$\Delta\sigma(T) = \frac{k_{total} \cdot \Delta z(T)}{A_B} = \frac{m \cdot n \cdot k \cdot \Delta z(T)}{A_B} \quad (15)$$

The modular design of the load cell permits the bonding pressure sensitivity to be adjusted simply by exchanging spring elements. For low pressure applications spring elements with lower spring constants can be integrated. Furthermore, it should be noted that the differential thermal expansion behavior of the fixture has a direct influence on the pressure sensitivity. A fixture with a low differential expansion behavior provides a low sensitivity but makes the exact timing of the pressure difficult (initial gap adjustment has to be more accurate). Thus, a trade-off between pressure sensitivity and timing is necessary in the fixture design.

### 3.6 FIN BUCKLING LIMIT ANALYSIS FOR INITIAL GAP SETTING

In previous sections it has been shown that application of bonding pressure within a  $\Delta$ CTE-fixture a certain temperature difference ( $\Delta T_{CB}$ ) between the contact temperature of the fixture and the bonding temperature of the microchannel device. Preferably, this temperature difference should be as small as possible to prevent any possibility of fin warpage. Thus, a fin buckling analysis [24] was applied to determine the critical temperature difference ( $\Delta T_{crit}$ ) which can be used to compute the initial gap adjustment.

To determine if a channel fin will buckle, the mode of failure needs to be confirmed by calculating the critical buckling stress ( $\sigma_c$ ). The fin buckling can be treated as column buckling since the fin cross-section ( $A$ ) and the moment of inertia ( $I$ ) are constant. As soon as the contact between the inner parts and the fixture frame is established, pressure will be transmitted to the laminae stack and the mode shape of fin buckling is derived from fixed-ended support condition as shown in Figure 3-11.



**Figure 3-11: Fin Geometry and Column Buckling Behavior**

For the fixed-ended boundary condition, the critical buckling stress can be calculated according to Equation 16, where  $P_C$  is the critical buckling load,  $A$  the area of the fin cross-section,  $L$  the length of the fin,  $S$  the fin span,  $E$  the elastic modulus of the lamina material and  $I$  the moment of inertia of the fin cross-section.

$$\sigma_C = \frac{P_C}{A} = \frac{4 \cdot \pi^2 \cdot E \cdot I}{A \cdot S^2} \quad (16)$$

As soon as pressure is applied to the laminae stack, frictional forces between the fixture platens and the laminae restrain thermal expansion of the laminae during a temperature rise. If the laminae expand faster than the fixture material, the pressurized laminae stack becomes constrained by the lower CTE of the fixture material ( $\alpha_{fix}$ ). However, the fin layers between tend to expand more freely at about the CTE of the laminae ( $\alpha_{lam}$ ). Thus, a buckling load will build-up and the force due to differential thermal expansion during a temperature rise ( $\Delta T$ ) can be expressed as shown in Equation 17.

$$P_{CTE} = A \cdot E \cdot (\alpha_{lam} - \alpha_{fix}) \cdot \Delta T \quad (17)$$

If the load due to differential thermal expansion exceeds the critical buckling load ( $P_{CTE} \geq P_C$ ), the fin will buckle. Therefore, we can solve for the critical temperature difference by setting the loads equal as shown in Equation 18.

$$\Delta T_{crit} \geq \frac{4 \cdot \pi^2 \cdot I}{A \cdot S^2 \cdot (\alpha_{lam} - \alpha_{fix})} \quad (18)$$

The cross-sectional area of the fin is given by Equation 19 and the moment of inertia for the fin can be expressed according to Equation 20.

$$A = t \cdot L \quad (19)$$

$$I = \frac{1}{12} L \cdot t^3 \quad (20)$$

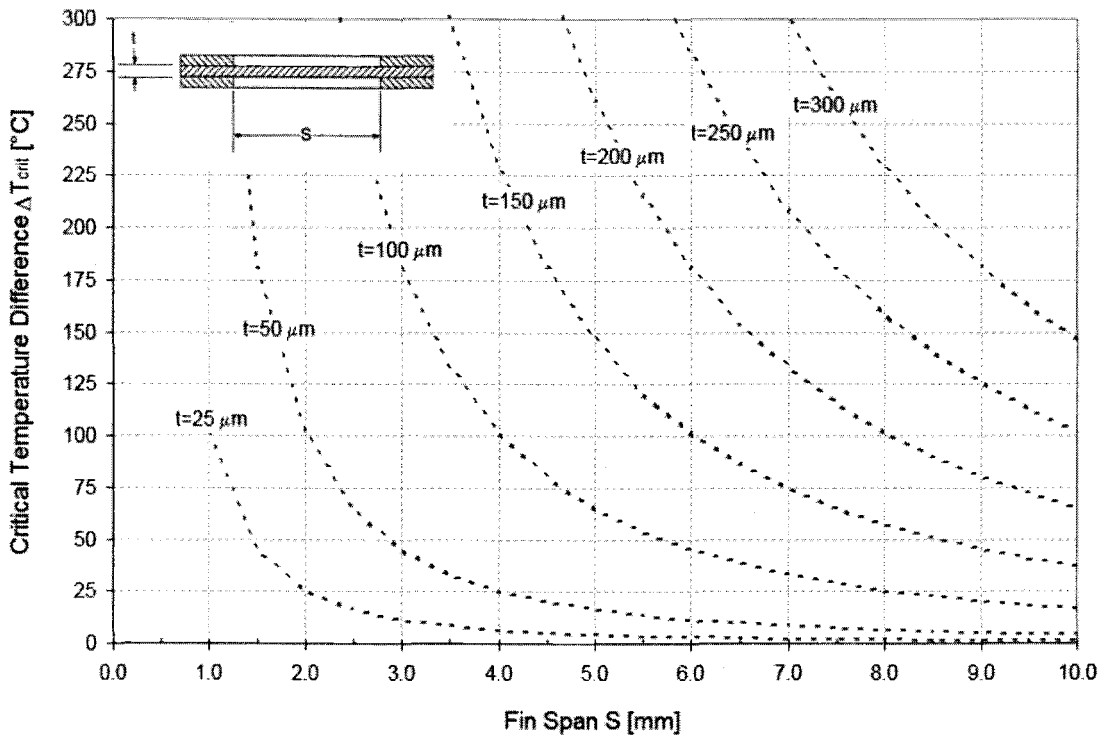
Introducing Equations 19 and 20 into Equation 18 finally simplifies the critical temperature difference to Equation 21.

$$\Delta T_{crit} \geq \frac{\pi^2 \cdot t^2}{3 \cdot S^2 \cdot (\alpha_{lam} - \alpha_{fix})} \quad (21)$$

Equation 21 shows, that only the lamina thickness ( $t$ ), the fin span ( $S$ ) and the involved CTE's have a critical influence on fin buckling. The calculation of the critical temperature can now be used to express the temperature difference between the contact and the bonding temperature of the  $\Delta$ CTE-fixture. If the temperature difference  $\Delta T_{CB}$  is smaller than the critical temperature difference  $\Delta T_{crit}$  ( $\Delta T_{CB} < \Delta T_{crit}$ ), fin warpage will be prevented. Hence, the contact temperature can be expressed as a function of the buckling limit as shown in Equation 22.

$$T_C = T_B - \Delta T_{crit} \quad (22)$$

Figure 3-12 shows the critical temperature difference plotted in function of the fin span and thickness for copper as the substrate material and graphite as the fixture material. It can be seen, that temperature differences between the bonding temperature and the contact temperature below 50°C are not critical for spans of 1.5 mm (fin aspect ratio of 60:1) or fin thicknesses greater than 200  $\mu$ m (fin aspect ratio > 50:1). However, it should be considered that the calculations above assume a perfectly flat fin lamina. Practically speaking, a perfectly flat fin is not possible and therefore any initial waviness will cause buckling right from the start as the fin expands thermally.



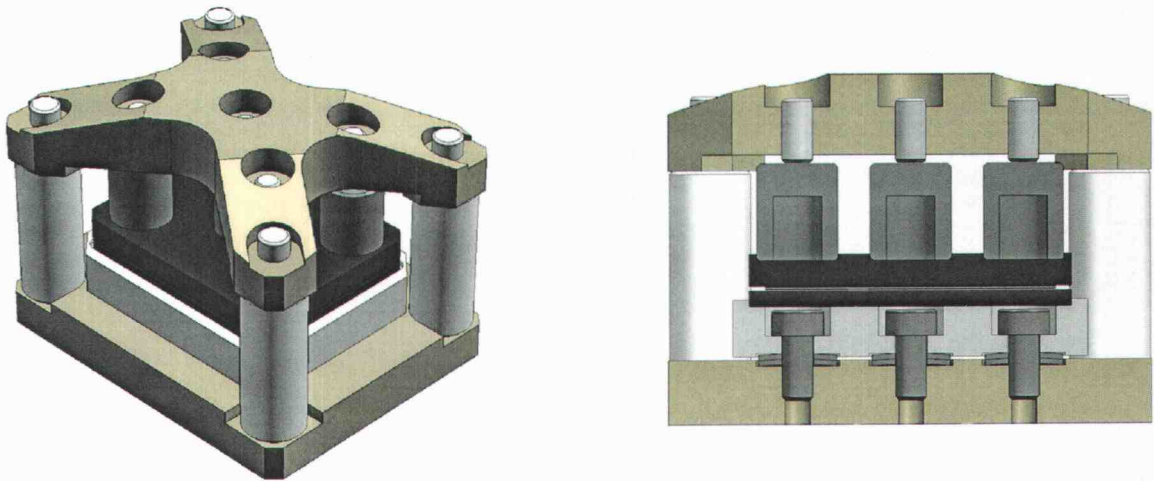
**Figure 3-12: Critical Temperature Difference for Fin Buckling**

### 3.7 CONCEPTIONAL DESIGN OF A LARGE SUBSTRATE BONDING UNIT

It would be of potential interest to apply the approach of a differential thermal expansion bonding unit in the microlamination of large substrate devices. Up to now, diffusion bonding of large substrates is only feasible with the use of large hot press systems or by hot isostatic pressing (HIP). Moreover, the uniaxial pressure application of a hot press system is problematic for the achievement of bonding pressure uniformity over a large substrate. Both methods are very cost intensive and are not applicable for mass production. Thus, a differential thermal expansion bonding unit for large substrates could be a possibly more economical approach for mass producing large-substrate microlaminated MECS devices within a continuous furnace.

Figure 3-13 shows a conceptual design of a large substrate fixture with a bonding area of 75 mm x 100 mm. The principal features of the fixture are still the same as explained for the previous design of the experimental fixture for small substrates. However, a design for large substrates needs some special attention and further design

considerations for establishing a certain pressure uniformity, which will be a major concern of the design. The frame construction for the small substrate fixture could be designed to be stiff and rigid to minimize the impact of frame deformation. Since distances between fixture posts and points of force introduction are increasing for a large substrate design, the frame will experience higher bending moments and as a result more deformation. In order to keep the weight and the thermal mass of the fixture small, the frame would be desirable to be lean. Consequently, the fixture frame has to be optimized using finite element software for maximal stiffness with the smallest possible weight.

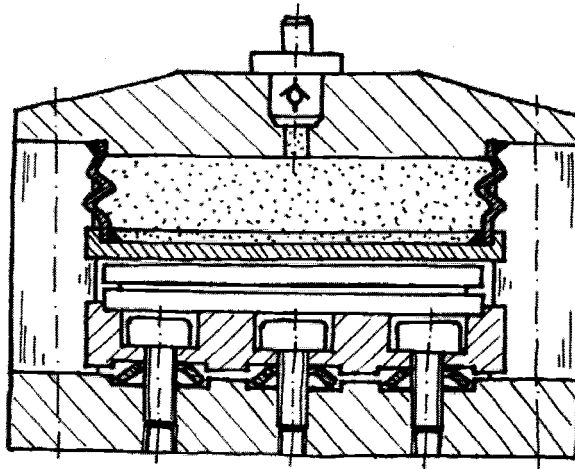


**Figure 3-13: Concept of a Large Substrate  $\Delta$ CTE Bonding Unit**

The preload storage of the fixture concept shown in Figure 3-13 is similar to the previous load cell, but for large substrates the unit is more comparable to a load stage and will not be taken out of the fixture for preloading. The spring elements are located between frame base and load stage. The graphite bonding platens are centered in the load stage and exchangeable based on substrate size and alignment features between the bonding platens. The engagement blocks on top of the bonding platens take advantage of the previous clarified expansion tube design. Multiple engagement blocks are distributed over the substrate area (4 in the corner, 1 in the center) and individual initial gap sizes can be adjusted for each engagement block. This can be favorable to compensate the deformation by adjusting a smaller initial gap in the center than in the corner sections since the deformation will be maximal in the top frame center. Hence,

the individual contact adjustments can possibly level out pressure differences across the substrate area.

The weight and size of a large substrate bonding fixture applicable for mass production will be mainly constrained by the specifications of the continuous furnace system (furnace openings and total load capacity of the conveyor belt). The large substrate concept shown in Figure 3-13 could potentially exceed these limitations of the furnace system due to the weight and structural height of the solid engagement blocks. A potential solution to overcome the issues of fixture size and weight is presented in Figure 3-14, where the solid expansion blocks are replaced with a gas/liquid expander.



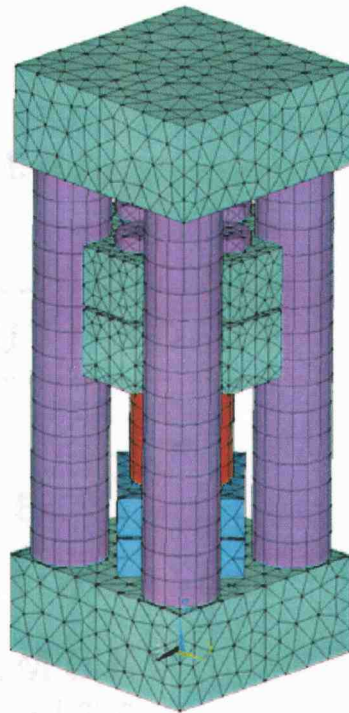
**Figure 3-14: Concept of a Large Substrate Fixture with a Gas Expander**

The pressure engagement unit in the fixture now represents a bellows filled with a fluid, which may be a liquid or a gas, with a much higher thermal expansion compared to the fixture frame. The pressure magnitude and sensitivity is still controlled by using the concept of a preloadable load stage with high temperature spring elements. Pressure engagement (pressure timing) is now controlled by the volumetric expansion of the bellows due to the temperature rise from room to bonding temperature. Initial gap settings can be controlled by setting a primary level of pressure inside the bellows with the use of an inlet valve. Additionally, a pressure relief valve may be implemented that if a preset pressure threshold is reached any excess pressure is relieved. Hence, the pressure sensitivity of the fixture can be further reduced by setting an upper pressure limit. Furthermore, it is believed that the use of a gas/liquid expander can provide a

more uniform pressure engagement over a large substrate area and the fixture design might be more durable and robust for continuous use.

### 3.8 FINITE ELEMENT MODEL OF THE BONDING UNIT

To provide a more fundamental understanding of the bonding unit, a finite element model was created in ANSYS. The ANSYS software is one of the most mature, widely distributed and popular FEM programs available. Figure 3-15 shows the meshed model of a differential thermal expansion bonding unit with the different types of material shaded in different colors.



**Figure 3-15: FE-Model Overview of the Fixture Design (1/4 Symmetry Expansion)**

The model was used to study theoretically the behavior of the differential thermal expansion unit and prove its feasibility. Moreover, the use of the model was very helpful in the material selection process to evaluate the appropriate expansion behavior. The theoretical assessment of the resulting bonding pressure, timing of the pressure and its sensitivity depending on changes in temperature was of interest in this finite element study.

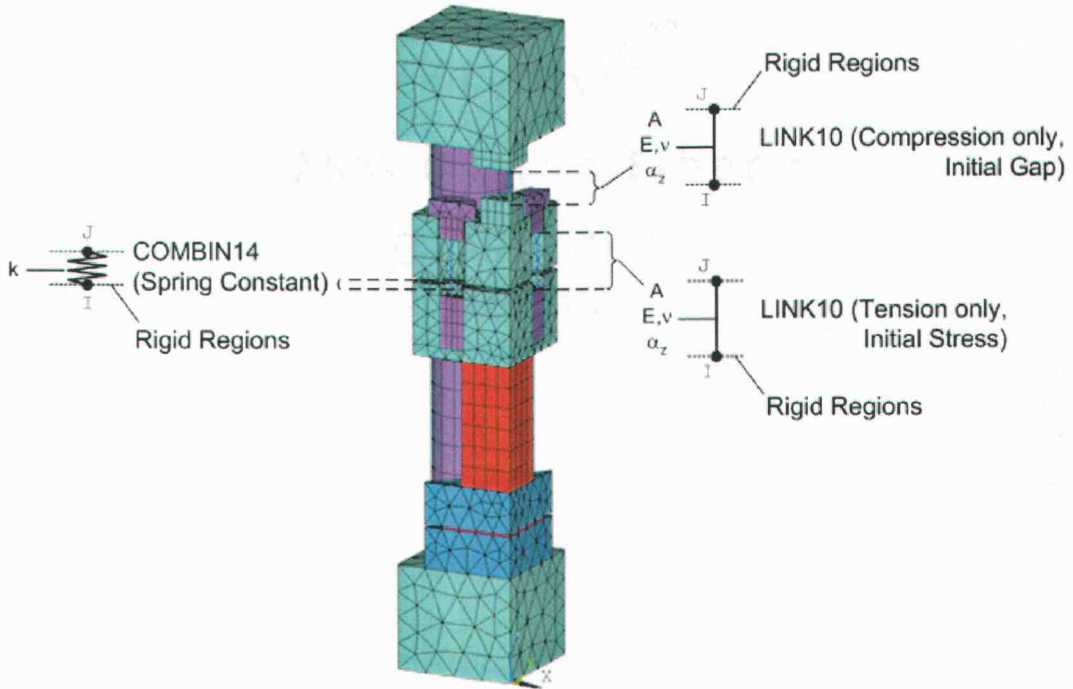
For reasons of simplification and to prevent the use of nonlinear contact elements, all volumes are connected to one solid model. SOLID95 [40] was used throughout the

model as structural element for the modeling. Critical volumes for meshing such as extruding circular shapes out of rectangular plates involved mapped meshing of the circular areas first with element PLANE42. Following extrusion processes with SOLID95 ended up in a careful meshed volume as shown in Figure 3-15. A further assumption was made in the simulation by applying the coefficients of thermal expansion for the different materials only in z-direction (orthotropic) to prevent unreal interfacial stresses in regions where two different materials are connected. This assumption can be supported by the fact, that no forces will be transmitted through the structure until the bonding unit has reached the contact temperature. Hence, all parts can freely expand in planar directions up to this point and the thermal expansion in x- and y-directions can be neglected. The model does not incorporate any thermal elements and the simulation was performed as a structural analysis by applying uniform temperature load steps on all volumes. Thus, a further assumption was made that no thermal gradients exist throughout the bonding fixture and all parts have the same uniform temperature at each point in time.

### 3.8.1 FE-MODEL OVERVIEW AND FEATURES

The finite element model required some special modeling techniques and features to allow all functions which can be found in the real bonding fixture. To enhance the simulation performance of the model, symmetry boundary conditions in the XZ- and YZ-planes were used like shown in Figure 3-16. By applying symmetry the model could be reduced to 6655 elements defined by over 17'000 nodes associated with 40'680 equations. The major challenge was to determine how to model the load cell, which should store the pre-loaded force without transmitting any stresses to the surrounding structure until the initial gap is consumed. Between the load cell platens the disc springs were modeled with the spring element COMBIN14 [40] which allows the definition of a spring constant over a real constant set. To prevent stress locations at the connection nodes of the COMBIN14 element, surrounding nodes within the diameter of the disc springs were coupled by rigid regions to distribute the force uniformly to the load cell platens. However, the implementation of rigid regions makes it necessary to provide all possible degrees of freedom (DOF) at the end nodes of the COMBIN14 element. Since the COMBIN14 element only has DOF in x-, y-, z-direction, a dummy PIPE16 element was introduced at the connection locations. PIPE16 can be easily modeled as a link and

provides all six DOF at the end nodes. The stiffness of the dummy PIPE16 element was defined small enough that the dummy elements have no significant influence in the stiffness matrix of the model. Similarly, the connection of the load cell fasteners was made to preload the spring element COMBIN14.

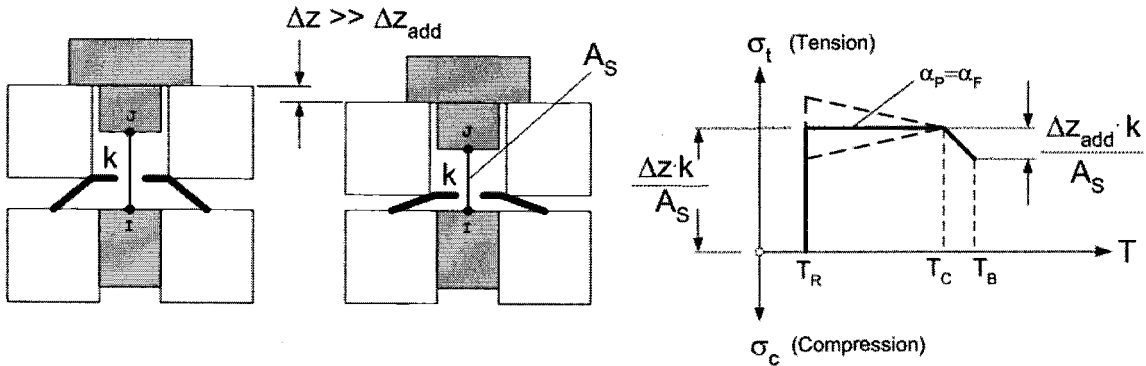


**Figure 3-16: Modeled Section of the  $\Delta$ CTE-Fixture**

Top and bottom pieces of the fasteners have been modeled as solid elements to simulate the connection as real as possible. The center section of the fasteners were cut out and replaced with the link element LINK10 [40] as shown in Figure 3-17. The end nodes of the LINK10 element were coupled with the whole cross-sections of the fasteners by rigid regions. LINK10 is a bilinear link element which can be configured by key options either as a compression-only or tension-only link element. In tension-only mode, an initial strain with respect to the initial element length defined by the end nodes I and J ( $L_{IJ}$ ) can be applied over a real constant. This allows an initial compression of the load cell by applying initial strain to the fasteners.

$$ISTRN = \frac{\Delta z}{L_{IJ}} \quad (23)$$

It should be considered, that the initial compression of the load cell due to the initial strain definition of the fasteners already supplies an initial gap in the finite element model since the initial state of the load cell is uncompressed. For the calculation of the initial gap in the LINK10 compression-only element which represents the set screw, the amount of the load cell compression ( $\Delta z$ ) has to be subtracted from the overall gap size  $g_0$ .

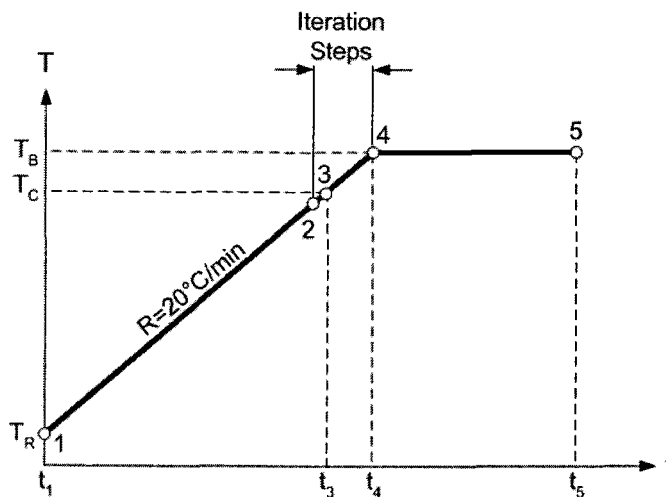


**Figure 3-17: Initial Strain Situation in LINK10 Elements of Load Cell Fasteners**

As described above, the pre-loading of the spring elements is based on the initial strain state of the LINK10 elements in the load cell which are representing the fasteners. If the LINK10 element goes to compression in the tension-only mode, it will go slack and does not transmit any displacement. Thus, the implementation of the LINK10 element avoids the use of nonlinear surface-to-surface contact between the fastener heads and the load cell top platens due to its bilinear capabilities. However, the initial strain in the LINK10 elements for the compression of the springs has to be defined high enough that the initial load cell compression  $\Delta z$  is established. Consequently, the zero strain state, when the element would actually switch-off, will never be reached since the additional load cell compression ( $\Delta z_{add}$ ) from contact to bonding temperature is minimal compared to the initial compression ( $\Delta z$ ) as visualized in Figure 3-17. Hence, the LINK10 elements are still under tension at contact temperature and forces will also be transmitted through the fasteners which would not be the case in the physical fixture.

To overcome this problem, element birth and death capabilities have been introduced to the LINK10 elements. Element birth and death involves mainly the activation and deactivation of elements based on elements results or load step definitions. The main idea is to deactivate the LINK10 elements in the load cell as soon as the load cell is

getting into contact with the frame. Unfortunately, element birth and death definition can not be saved in load step files manually and the implementation of element birth and death made it necessary to write an APDL<sup>1</sup>-macro which automatically selects the LINK10 elements at the appropriate load step and deactivates them during the bonding cycle simulation. The macro file can be found in Appendix B. Values for room temperature ( $T_R$ ), expected contact temperature ( $T_C$ ), final bonding temperature ( $T_B$ ) and temperature ramp rate ( $R$ ) can be input as scalar parameters in ANSYS and the macro file will automatically read-in the values and define the load steps as illustrated in Figure 3-18 and save them for subsequent calculations. Some degrees before reaching the contact temperature, the macro will start to do iterations every 5°C change in temperature to record results of the pressure transition section of interest. After the bonding temperature has been reached, the temperature will remain for a certain time and the simulation is finished.



**Figure 3-18: Load Step Definition**

The LINK10 element can also be used favorably to model the timing of the pressure by an initial gap between fixture frame and load cell top. By switching the key option of the LINK10 element to compression-only mode, only compressive forces can be transmitted through the linked connection which is true for the contact between frame and load cell. The force introduction at the connection nodes is also coupled with rigid

<sup>1</sup> APDL = ANSYS Parametric Design Language

regions to prevent local stresses. Recall, that the initial compression of the load cell already created an initial gap between load cell and fixture frame and therefore the LINK10 element in compression-only mode, which represents the set screw in the model, only has to consider the remaining value of the total initial gap.

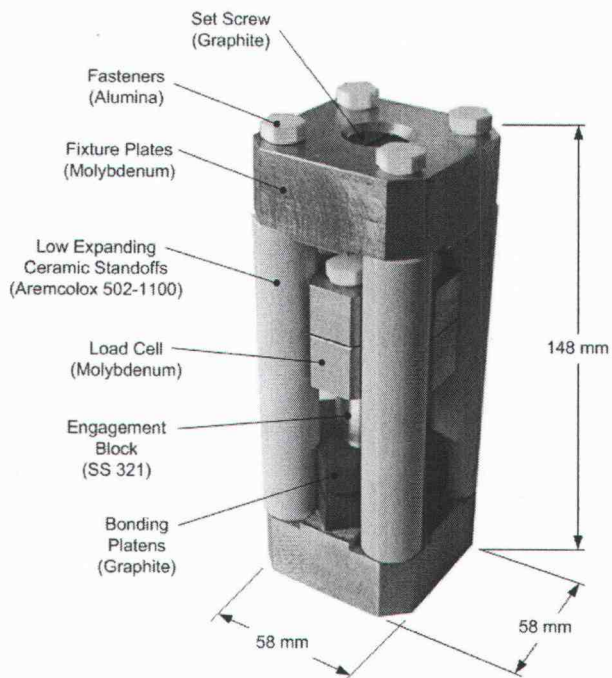
By using bilinear LINK10 and COMBIN14 elements, the main fixture parameters like spring constant, initial compression of the load cell and initial gap size can be controlled over a set of real constants and no changes in the actual model geometry are necessary. The definition of process parameters over the scalar parameter input and the automatic load step definition by the ADPL-macro makes it simple to run the model for different conditions without any model modifications. Furthermore, LINK10 elements caused a less complex model by avoiding the use of problematic nonlinear contact elements.

## 4 EXPERIMENTAL APPROACH

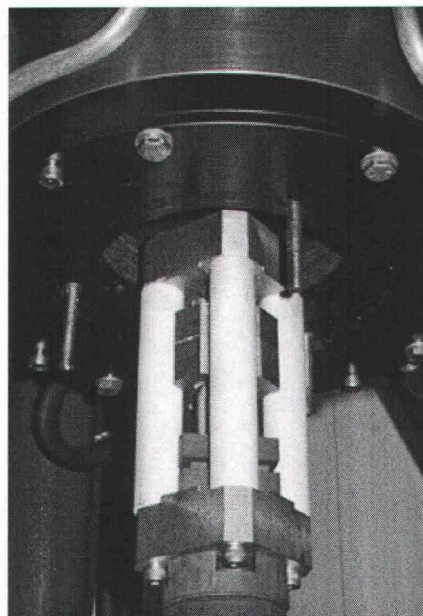
### 4.1 OVERVIEW

Different experimental designs were applied to prove the functionality of the proposed bonding method. Fuji pressure sensitive measurement film was used to evaluate pressure uniformity, magnitude and timing in the low temperature regime. Special test articles were designed to study the timing of pressure at higher temperature during microlamination. The behavior of fin warpage was used as a reference for the calibration of the bonding fixture (pressure timing). The test articles were also used for the metallurgical assessment of the bond line. The void fractions of bonded samples were compared with samples bonded within the hot press under similar conditions. Finally, an analysis of variance (ANOVA) was performed to compare samples bonded in the thermal expansion fixture and samples bonded within the hot press to determine if the differential thermal expansion fixture is capable and repeatable.

### 4.2 PROTOTYPE BONDING UNIT



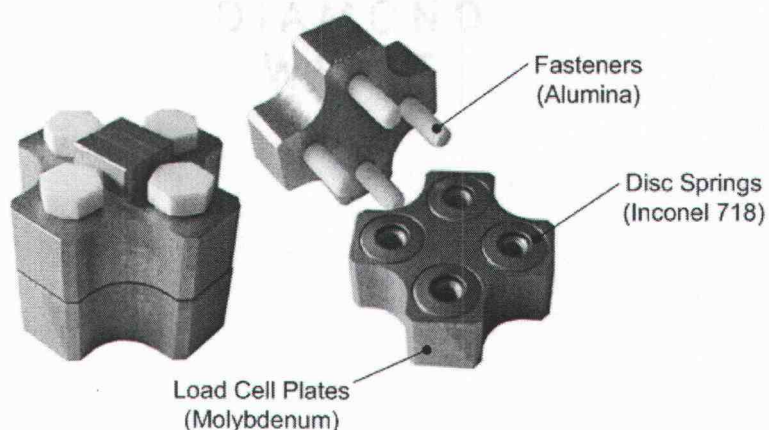
a) Fixture Overview



b) Fixture entering Hot Press

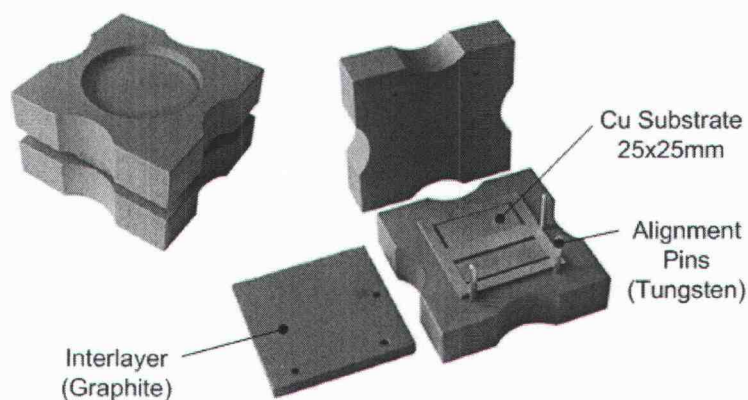
Figure 4-1: Differential Thermal Expansion Bonding Unit Prototype

Figure 4-1 shows the final assembled differential thermal expansion fixture prototype designed for the Pressmaster hot press. The load cell and bonding platens can be seen in more detail in Figure 4-2 and Figure 4-3.



**Figure 4-2: Load Cell**

The disc springs are placed between the load cell platens and are kept in position within the spring pockets. Besides positioning, the spring pockets are used to prevent the disc springs from flat loading.

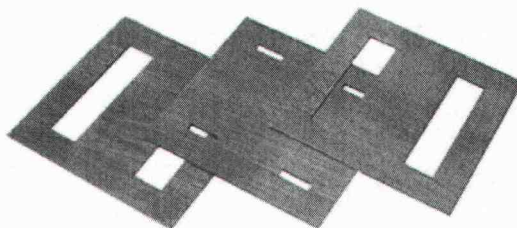


**Figure 4-3: Bonding Platens**

Similarly, the top plate of the bonding platens has a centering pocket to secure the exact position of the engagement block relative to the laminae stack. Detailed information and drawings of the fixture can be found in Appendix A.

### 4.3 TEST ARTICLE DESIGN

The test article used for fin warpage detection consisted of a fin layer sandwiched between two channel layers. The test article incorporates two fin regions to increase the number of measurements for less experimental runs. Since the fin layer is sandwiched between two open channel layers, the warpage of the fin can be measured by using the Dektak<sup>3</sup> surface profiler and scanning over the fin.



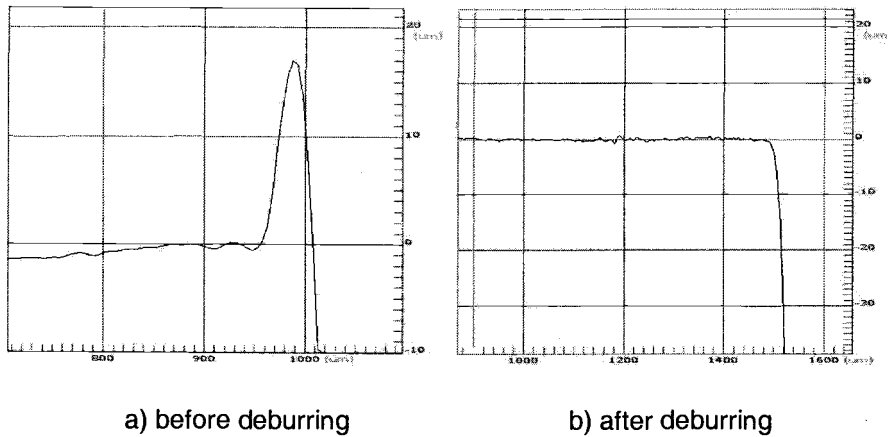
**Figure 4-4: Laser Cut Layers of Test Article**

Copper was selected as a substrate material since it is a soft material with a high coefficient of thermal expansion. That would make a finned structure highly sensitive to warpage effects and processing differences are easier detectable. In addition, copper can be diffusion bonded in a wide range of bonding parameter and effects on the resulting bonding strength can be studied. The dimensions of the test article can be found in Appendix A.

### 4.4 TEST ARTICLE FABRICATION

All layers of the test article were made from copper shim stock alloy 110 with a thickness of 8 mil (203  $\mu\text{m}$ ). An ESI 4410 Nd:YAG laser trimming system from Electro Scientific Industries (ESI) operating at the second harmonic (532 nm) was used to pattern the copper shims. The material was cut with a cutting speed of 6 mm/s and a pulse frequency of 3000 Hz (bite size 2  $\mu\text{m}$ ). 25 to 30 profile repetitions were necessary to cut through the 8 mil shim stock. The edge quality of the laser machined laminae was observed with a Dektak<sup>3</sup> Profiler (Veeco Metrology Systems) with a 12.5- $\mu\text{m}$  diamond-tipped stylus on ten randomly selected layers at different locations. The measurements showed an average laser burr of 14.2  $\mu\text{m}$  with a standard deviation of 7.3  $\mu\text{m}$ . Burrs resulting from any patterning process have to be systematically removed in order to bring the bonding surfaces into contact for solid-state diffusion bonding. All laminae were polished and deburred with ultra fine 3M Scotch-Brite<sup>TM</sup> and cleaned in an

ultrasonic cleaner afterwards. Recorded profile measurements of the lamina edge before and after deburring are shown in Figure 4-5.



**Figure 4-5: Deburring of Laser Machined Laminae**

The surface roughness of 12 randomly selected laminae was measured with a Mitutoyo Surftest 212. Two measurements perpendicular to each other were taken for each sample for a total of 24 measurements. The measurements showed an average surface roughness ( $R_a$ ) of  $0.284 \mu\text{m}$  with a standard deviation of  $0.061 \mu\text{m}$  which is below the general recommended surface roughness limit of  $0.4 \mu\text{m}$  for diffusion bonding. Since the primary function of the test article is to detect effects on fin warpage an initial flatness of the laminae has to be established. The patterned and deburred layers were stacked between graphite platens and flattened at a temperature of  $500^\circ\text{C}$  and a pressure of  $2.4 \text{ MPa}$  ( $350 \text{ psi}$ ) for 30 minutes which also served to relieve any residual stress from the cold rolling process. The flattening procedure was performed in the earlier mentioned Pressmaster hot press in vacuum ( $10^{-4} \text{ torr}$ ) to prevent oxidation of the copper laminae. The flatness was examined according to 24 samples measured with the Dektak<sup>3</sup> profiler over a scan length of 20 mm. The flattening procedure delivered an average flatness of  $4.98 \mu\text{m}$  with a standard deviation of  $1.82 \mu\text{m}$ .

Before bonding, all laminae were cleaned in the ultrasonic cleaner with acetone, methanol and de-ionized water (AMD rinse) to remove grease or any residues on the surfaces. The bonding fixture assembly was then put in the vacuum chamber and the chamber was pumped down to an approximate level of  $10^{-4} \text{ torr}$  before the bonding cycle was started. For all bonding cycles a temperature ramp of  $20^\circ\text{C}/\text{min}$  was applied.

The point of pressure application, the magnitude of bonding pressure and the bonding duration were dependent on the individual experiments.

#### 4.5 ORIENTATION EXPERIMENT OF TEST ARTICLE

The bonding fixtures used in the experiments were designed to process two test articles simultaneously in order to save experimental runs. Since the finned structure on the test article can be oriented  $0^\circ$  or  $90^\circ$  out of phase relative to the fixture a preliminary experiment was conducted to evaluate if the fin orientation has an influence on the resultant fin warpage. Four test articles according to drawing A1-013 (Appendix A) were processed in two experimental runs at a bonding temperature of  $600^\circ\text{C}$  with an applied pressure of 8 MPa (1160 psi) for 30 minutes. The fabrication of the test articles followed the steps explained in the previous section. The fin orientation of the test articles was maintained different between the two bonding stations of the bonding fixture. In the first run the fin orientation was  $0^\circ$  out of phase at the lower bonding station and  $90^\circ$  out of phase at the upper station and vice versa in the second experimental run. The fin warpage of the two fins of each test article was examined by profiling the fins at three positions (left, middle, right) with one repetition for a total of 48 measurements. The warpage profile measurements were taken with the Dektak<sup>3</sup> profiler with a scan length of five millimeter over the fin window. The collected data was analyzed by a multifactor analysis of variance to determine if the orientation of the test article has a statistical significant effect on fin warpage.

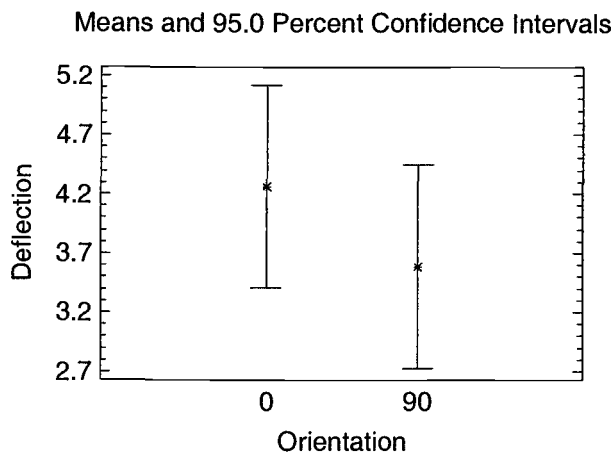


Figure 4-6: Mean Fin Warpage based on Test Article Orientation in Fixture

The F-test in the ANOVA table confirmed that the orientation of the test article has no significant influence on fin warpage with a p-value of 0.2692. Figure 4-6 shows the mean fin warpage in  $\mu\text{m}$  with a 95% confidence interval based on the test article orientation in the fixture. Additional information to the orientation experiment can be found in Appendix D.

#### **4.6 EFFECT OF PRESSURE TIMING ON FIN WARPAGE**

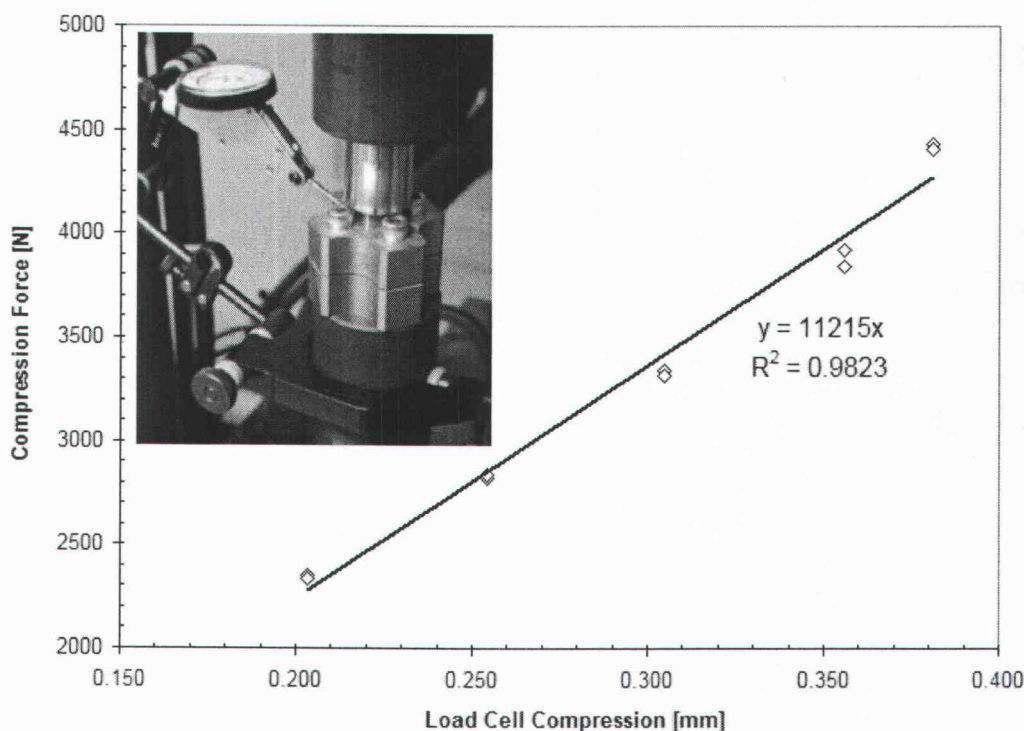
As discussed in previous chapters, incorrect timing of the bonding pressure can cause significant fin warpage and the prevention of deformed fins is crucial for microlaminated devices. The timing of bonding pressure with a bonding fixture based on thermal expansion is dependent on temperature and implies some difficulties. Unlike within a hot press the bonding pressure within a CTE-actuated clamp has to be applied some degrees before the final bonding temperature is reached to ensure proper contact. However, the temperature difference between contact and bonding temperature should be kept as minimal as possible to prevent significant fin warpage. The purpose of the experimental setup discussed here is to investigate a relationship between the point of pressure application during a bonding cycle and the resulting fin warpage. This would make it possible to adjust the appropriate timing of the thermal expansion fixture, since the amount of fin warpage is related to the temperature difference between contact and bonding temperature. Taking the thermal expansion potential of the fixture into account, the exact gap correction can be calculated to offset the contact point for an optimal pressure timing.

The experimental design for the pressure timing investigation was based on a multifactor categorical design with two experimental factors, bonding temperature and temperature of pressure application. The Pressmaster vacuum hot press was used for this experiment. Bonding temperature was handled on two levels, 600°C and 800°C. The temperature of pressure application was based on the bonding temperature and varied on three levels between 0%, 50% and 100% of the bonding temperature. Six fully randomized experimental runs with two samples per run were performed for a total of twelve test articles according to drawing A1-013. The bonding cycle was carried out in vacuum at  $10^{-4}$  torr with an applied bonding pressure of 8 MPa (1160 psi) for 30 minutes. A temperature ramp of 20°C/min was used for all experimental runs. The

resultant fin warpage was measured with the Dektak<sup>3</sup> profiler at three different positions (left, middle, right) for each fin. In addition to the experimental results the fin warpage of the test articles was investigated theoretically with a simple finite element model for direct comparison.

#### 4.7 LOAD CELL VALIDATION

Important for the correct setting of bonding pressure is the knowledge of the relationship between force and displacement, mainly given by the spring constant of the used springs. The used Inconel Belleville disc springs have an outside diameter of 0.625 inch, an inside diameter of 0.317 inch and a thickness of 0.032 inch. The vendor states a nominal load of 180 lbs (800 N) by a deflection of 0.0115 inch (292  $\mu\text{m}$ ) for this type of spring which relates to a theoretical spring constant of 2740 N/mm. The total spring constant for the load cell will be four times the value of a single spring and sums up to 10'960 N/mm.



**Figure 4-7: Load Cell Validation**

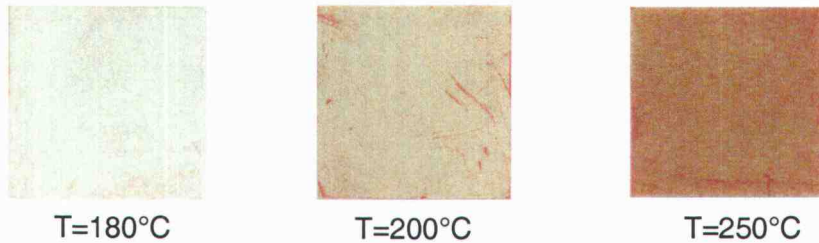
This theoretical result was validated by measuring the deflection of the load cell due to force application. The load cell was put between the hydraulic pushing rods of the

Pressmaster hot press and the applied force was read off the OMEGA high performance strain gauge indicator of the hot press. The deflection of the load cell was measured with a precise Mitutoyo dial gauge with an incremental resolution of 0.0005 inch (12.7  $\mu\text{m}$ ). The setup of the dial gauge can be seen in Figure 4-7. Loads and deflections were recorded and the slope of the linear regression equals the spring constant of the load cell. The linear fit showed good agreement with the theoretical spring constant and delivered a total spring constant for the load cell of 11'215 N/mm which is only 2.3% off. This value corresponds to a practical spring constant of 2804 N/mm for an individual disc spring in the load cell.

## **4.8 CALIBRATION OF THE $\Delta$ CTE-FIXTURE**

### **4.8.1 PRESSURE UNIFORMITY**

A uniform distributed pressure is essential for a constant bond quality across the entire substrate area. However, the pressure distribution is rather difficult to be quantified, especially in a closed furnace at elevated temperatures. The use of Fuji Prescale film has been found as a common measurement tool for the analysis of pressure uniformity in similar applications like embossing or general lamination procedures. Fuji Prescale film is a measurement film that can measure pressure and visualize its distribution according to different color densities for different pressure levels. For pressure levels below 50 MPa the film is a two-sheet type polyester based film where one sheet is coated with a layer of microencapsulated color forming material (A-film) and the other sheet with a layer of color developing material (C-film). When pressure is applied, the microcapsules break and the color forming material reacts with the color developing material and red patches appear on the film. The film thickness is 0.2 mm and has a pressure reading accuracy of  $\pm 10\%$ . Unfortunately, the recommended temperature for the film does not exceed 35°C. A method was experimentally investigated, which makes the use of Fuji Prescale film at elevated temperatures possible by sandwiching the film between Kapton<sup>TM</sup> film. With this method, the film remained functional up to temperatures of 190°C as shown in Figure 4-8.



**Figure 4-8: Temperature Limit of Fuji Pressure Sensitive Film**

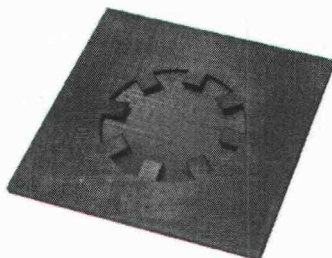
Above 190°C the two-type film started to interact with each other and the color forming material started to diffuse or evaporate to the developer film and a total discolorization of the film was the result. The film readings in Figure 4-8 were processed without any pressure (only self weight of top graphite plate) at the specified temperatures. Complete destruction of the film was observed at temperatures above 300°C.

Hence, the film was used for low temperature experiments to investigate and optimize the pressure uniformity and the timing of the prototype fixture. Type LW Fuji Prescale film with a detectable pressure range of 2.5 to 10 MPa was used for the experiments. The film was preliminary processed at different pressure levels in the hot press to produce reference samples. The bonding pressure was varied from 3 MPa up to 6 MPa in steps of 0.5 MPa. The film was processed between the bonding platens of the differential thermal expansion fixture shown in Figure 4-3 to guarantee equivalent conditions and for the validation of the pressure distribution based on the platens accuracy. The reference color densities for the pressure sensitive film can be found in Appendix E.

#### 4.8.2 TIMING OF THE BONDING PRESSURE

Since the Fuji Prescale film indicates the pressure transmitted in the fixture, conclusions can also be drawn regarding timing of the bonding pressure. The initial gap size was varied from zero up to the point where no contact between frame and load cell was established. The pre-load settings for the load cell were maintained constant at a resultant pressure of 4 MPa. More difficult is the validation of the contact condition at higher temperatures since the Fuji film was completely destroyed above temperatures of 300°C. Therefore, a test article made out of copper according to Figure 4-9 was developed for the pressure timing validation at higher temperatures. The test article shows a toothed structure, which are systematically bent-up after laser cutting. When

placed between platens with pressure the toothed features are pressed down onto the base layer and eventually bonded together, thus indicating transmitted pressure.



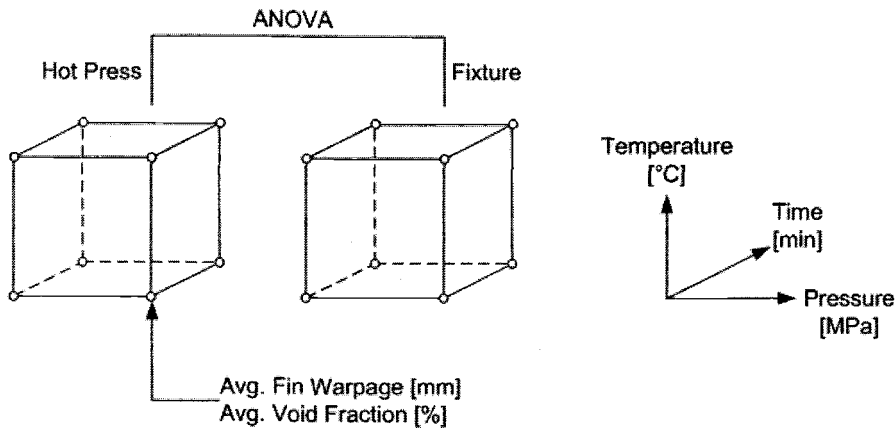
**Figure 4-9: Test Article with Bending Features for High Temperature Experiments**

A more precise validation can be made after the pressure cycle by examining the teeth with the surface profiler. Thus, these coupons can be used to investigate the timing of bonding pressure at high temperatures based on initial gap adjustments.

#### **4.9 EXPERIMENTAL DESIGN FOR $\Delta$ CTE-FIXTURE VALIDATION**

The final major experiment was designed to evaluate the functionality of the new proposed bonding method for the application in a microlamination procedure. A multifactor categorical design ( $2^4$ ) was chosen to evaluate if the coupons produced by a differential thermal expansion fixture were statistically different from those produced with a hot press. Mode, temperature, pressure and time were selected as the independent variables. The factor mode varied at two levels between “fixture” and “hot press”. Temperature was varied between 500 and 800°C and time between 30 and 60 minutes respectively. Pressure was handled at two levels, 3 MPa and 6 MPa. For hot press samples, the point of pressure application was at the end of the bonding ramp to prevent fin warpage. For the differential thermal expansion fixture, the point of pressure application was adjusted within 50°C before the final bonding temperature was reached. The experimental design was fully randomized with one replication for a total of 32 experimental runs. Since each run can process two samples, a total of 64 test articles according to drawing A1-013 were processed for measurements. Fin warpage and void fraction of the bond line were selected as the dependent variables of the experiment. Measurement of fin warpage followed the same procedure as used in the pressure timing experiment. After the measurement of fin warpage, test articles processed at same conditions were molded in epoxy for metallographic examination of the bond lines. The bond lines were inspected at various locations to generate an average value

of void fraction for each of the 8 bonding parameter combinations depending on the mode “hot press” or “fixture” as visualized in Figure 4-10.



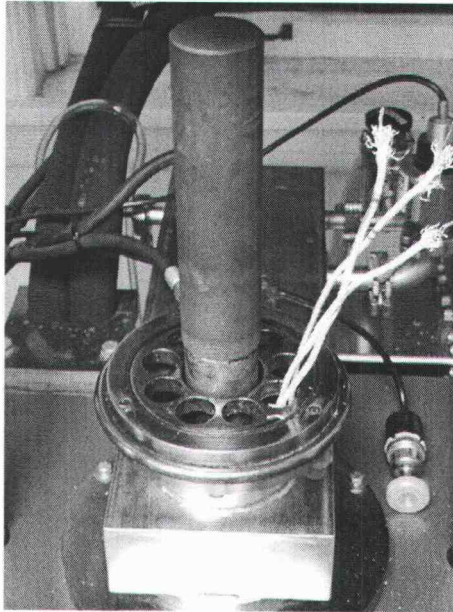
**Figure 4-10: Experimental Design of Comparison Experiment**

Finally, both dependent variables were analyzed in an ANOVA table to examine if the factor mode shows a statistically significant difference. If the p-value of the dependent variable fin warpage is greater than 0.05, a claim can be made that the pressure timing of the differential thermal expansion fixture is appropriate. Similar conclusions can be drawn for the dependent variable void fraction. If this p-value is greater than 0.05 also, a claim can be made that the pressure magnitude and sensitivity of the fixture is valid and no difference between the two bonding methods exists.

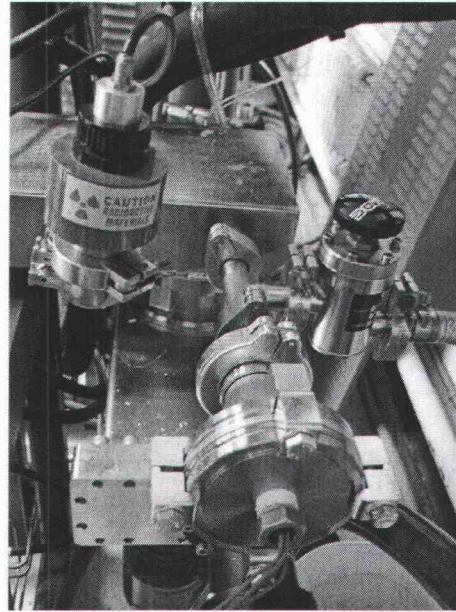
#### 4.10 THERMOCOUPLE SETUP AND MEASUREMENTS

Efforts were made to validate the temperature in the hot zone of the hot press. A preliminary melting experiment was conducted using a tin/lead solder of eutectic composition showing that there is a temperature difference of about 60°C between the thermocouple reading of the hot press and the actual temperature inside the hot zone. The eutectic melting point of the tin/lead solder is at 183°C and the reading of the hot press was 245°C when melting of the sample was observed. To prevent temperature overshooting, a low temperature ramp of 10°C/min was used. This is due primarily to the location of the type K thermocouple which is connected with the Eurotherm 2404 temperature control unit. The installed location of the thermocouple is behind the heating element to prevent interference with the hydraulic ram. Consequently, because of the proximity of the installed thermocouple being so close to the heating element and

so distant from the actual hot zone, the temperature reading is higher than the actual temperature in the working zone.



a) TC's entrance through vacuum chamber



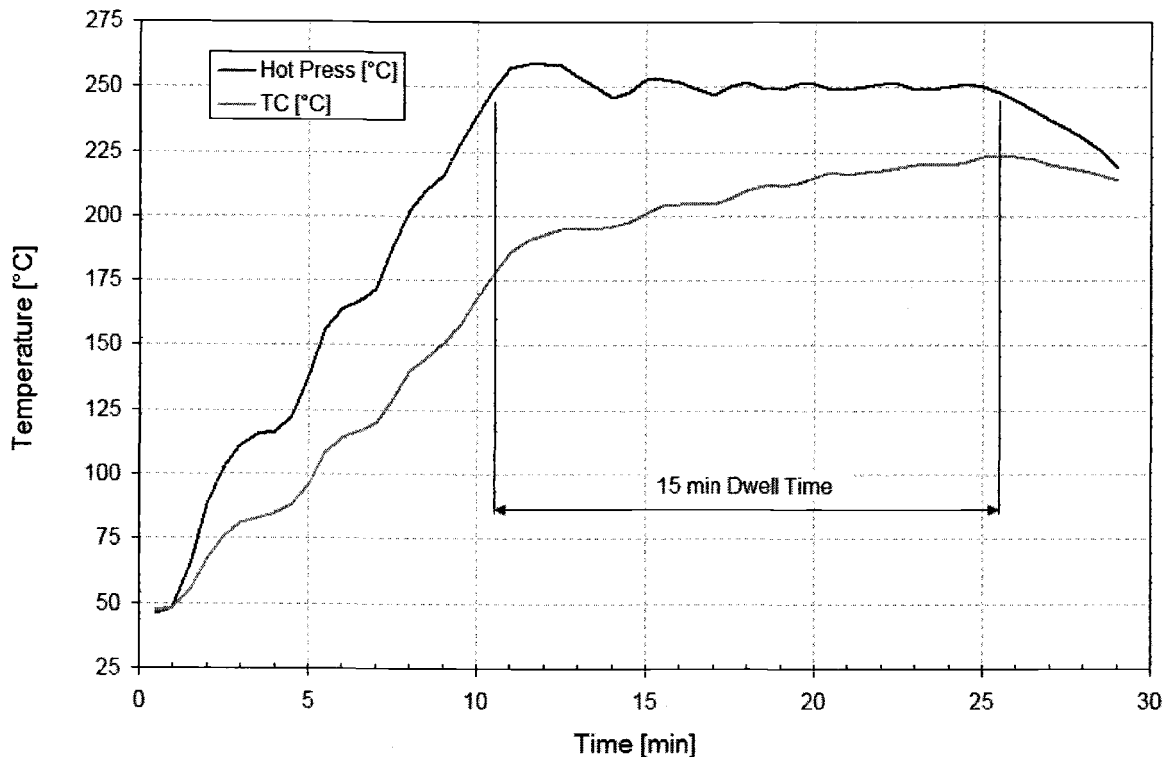
b) Installed TC vacuum port

**Figure 4-11: TC Setup on Pressmaster Vacuum Hot Press**

To circumvent these problems, additional thermocouples were installed to monitor the temperature of interest inside the hot zone. Flexible type K thermocouple wires were inserted through the vacuum manifold up into the hot zone as shown in Figure 4-11.

A 4-channel datalogging thermometer type 800024 from Sper Scientific Ltd. was used to record the temperature values. The temperature conversion of the instrument follows National Bureau of Standards and IEC584 temperature/voltage table for type K thermocouples. The measurement range of the digital thermometer goes from  $-200^{\circ}\text{C}$  up to  $1370^{\circ}\text{C}$  with a resolution of  $1^{\circ}\text{C}$  and an accuracy of  $\pm 0.2\%$  based on the reading. The internal memory of the datalogger can store 16,000 records per channel and is able to communicate bi-directionally over the RS232 interface to any PC using TestLink SE-309 software. A comparison of the temperatures recorded by the original and newly installed thermocouples is shown in Figure 4-12. The temperature was controlled by the original installed thermocouple near the heating elements. The additional thermocouple was fixed in a graphite block and measured the temperature in the center of the hot

zone. Temperature readings from the Eurotherm control unit and from the datalogger were recorded manually every 30 seconds and plotted in Figure 4-12.

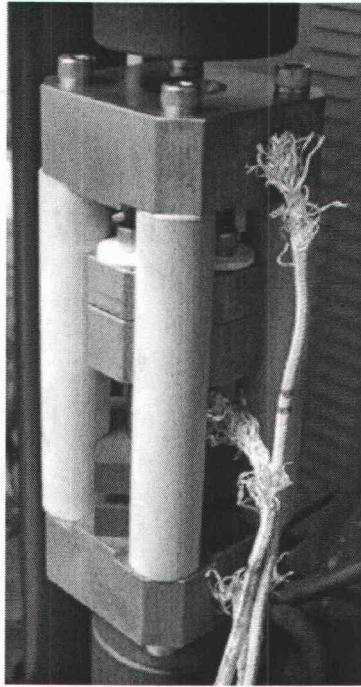


**Figure 4-12: Temperature Profile Hot Zone vs. Heating Elements**

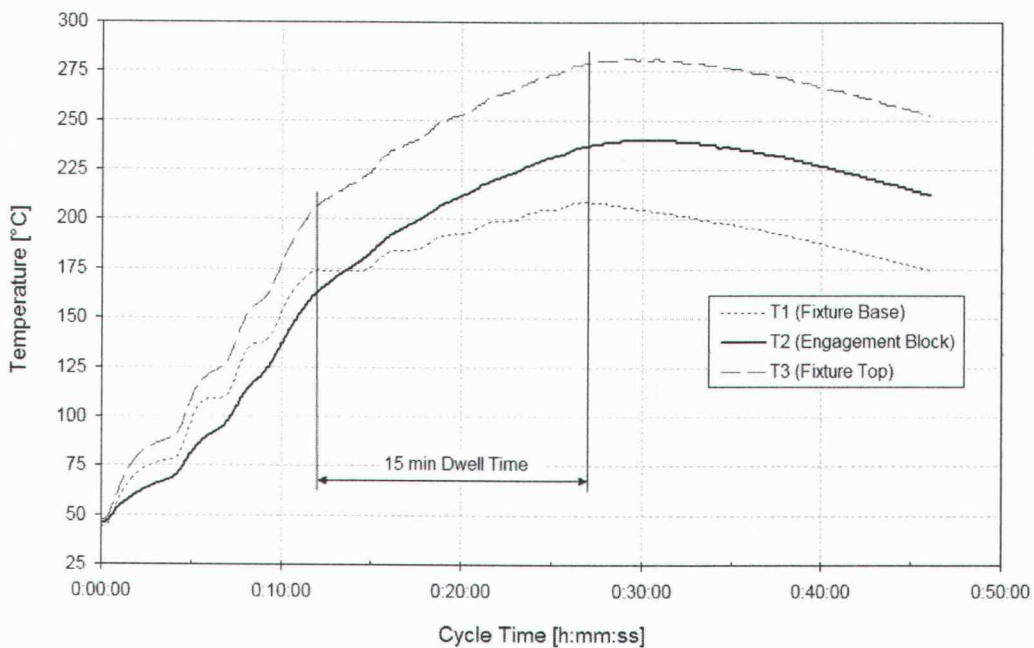
For this experiment a target temperature of 250°C was programmed with a 15 minute dwell time. The temperature ramp was defined to be 20°C/min and the test was run without vacuum. From the graph it can be seen that at the beginning of the dwell period a temperature difference of around 60°C exists which is in agreement with the earlier conducted tin/lead solder melting experiment. During the dwell time the temperature measured by the original thermocouple is still slightly increasing but never actually reaches the target temperature.

Connection of the thermocouples to the  $\Delta$ CTE fixture was made by drilling insert holes in the fixture base (molybdenum), the engagement block (SS 321) and the fixture top (molybdenum) as shown in Figure 4-13. The temperature of the engagement block was of most relevance to the experiments while the thermocouples in the fixture base and top provided some indication of the temperature gradient along the fixture. Figure 4-14

shows the temperature profiles measured at the three fixture locations using the same programmed temperature profile as was used in Figure 4-12.



**Figure 4-13: Thermocouple Setup of the  $\Delta$ CTE Fixture**



**Figure 4-14: Thermocouple Measurements on  $\Delta$ CTE Fixture (no vacuum)**

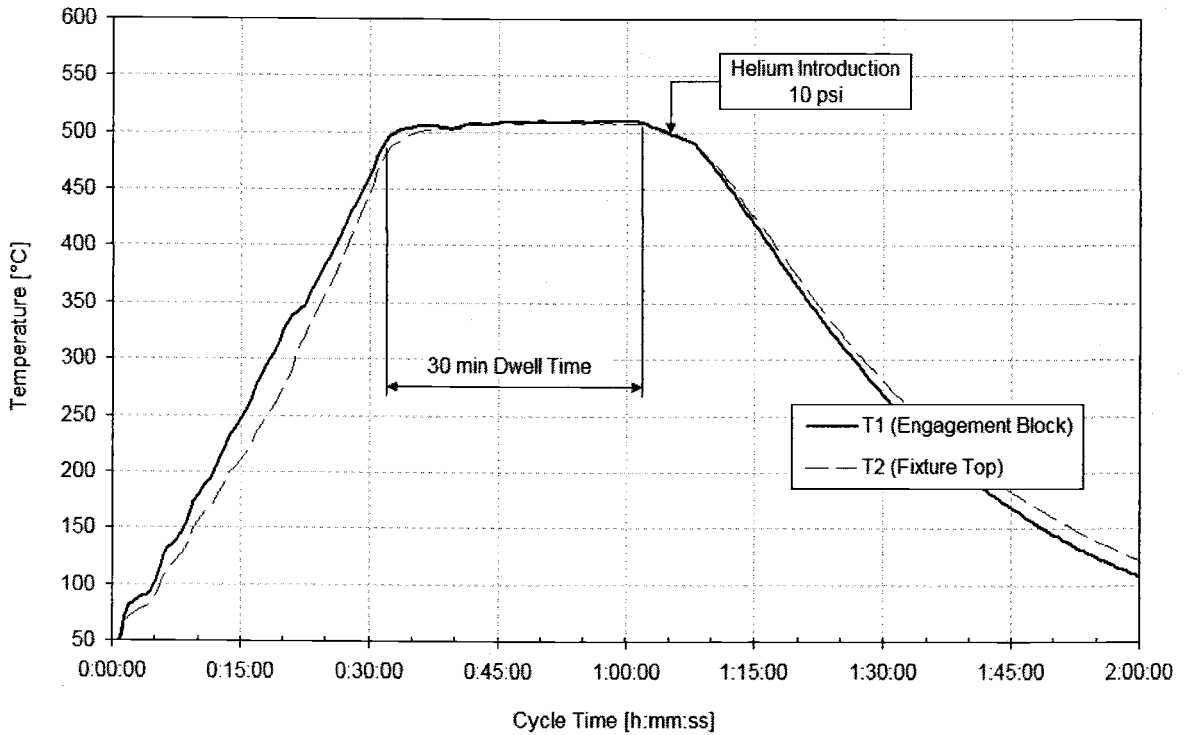
It should be noted that this test was run at atmospheric pressure. Consequently, after the 15 minute dwell period, thermal convection can be observed in the furnace cavity since the thermocouple readings are almost equally spaced (in both cases a temperature difference of about 40°C exists). These effects were not found to be present in vacuum (see below). Another observation of interest can be seen in the different thermal behavior of the molybdenum and stainless steel 321. The molybdenum frame responds much faster to temperature changes than the stainless steel engagement block which can be explained by the different thermal properties of the two materials as listed in Table 4-1.

**Table 4-1: Physical Properties of Molybdenum and SS 321**

	Density [kg/m <sup>3</sup> ]	Specific heat capacity [J/kg·K]	Thermal conductivity [W/m·K]
Molybdenum	10'220	255	138
Stainless Steel 321	8'000	500	16.1

To verify some of these findings, a second experiment was performed. For the purpose of producing more stable bonding pressure, it was decided that the temperature ramp should be set lower in order to achieve a more constant dwell temperature for the engagement block. Therefore, the temperature ramp was lowered to 15°C/min. Another improvement in the temperature profile was made by connecting the wire thermocouple located at the fixture engagement block directly to the Eurotherm 2404 temperature control unit of the hot press. Thus, a more precise temperature control of the hot zone was achieved (in vacuum) as can be seen in Figure 4-15. A second thermocouple was placed at the engagement block to record the temperature with the datalogger and to supervise the thermocouple which is connected to the temperature control unit. The third thermocouple was placed at the fixture top to observe any thermal gradients along the fixture.

For the temperature profile in Figure 4-15 a target temperature of 500°C was programmed with a dwell time of 30 minutes. The cycle was run in a vacuum of 10<sup>-4</sup> torr. The actual measured temperature slightly overshot to 508°C but no difference between the measured temperatures at the engagement block and at the fixture top was observed in vacuum. At the end of the dwell time, helium was introduced to the vacuum chamber to accelerate the cool down time.



**Figure 4-15: Improved Temperature Profile (in vacuum)**

#### 4.11 OPTIMIZATION OF THE FURNACE COOL DOWN TIME

As discussed in previous sections, the cool down time of the vacuum furnace is a major loss of time in the production cycle of a microlaminated device. Therefore, the influence of helium as a cooling gas was observed to cut down the cycle time during microlamination. Physical properties of popular gases used in furnace quenching [34][35] are illustrated in Table 4-2.

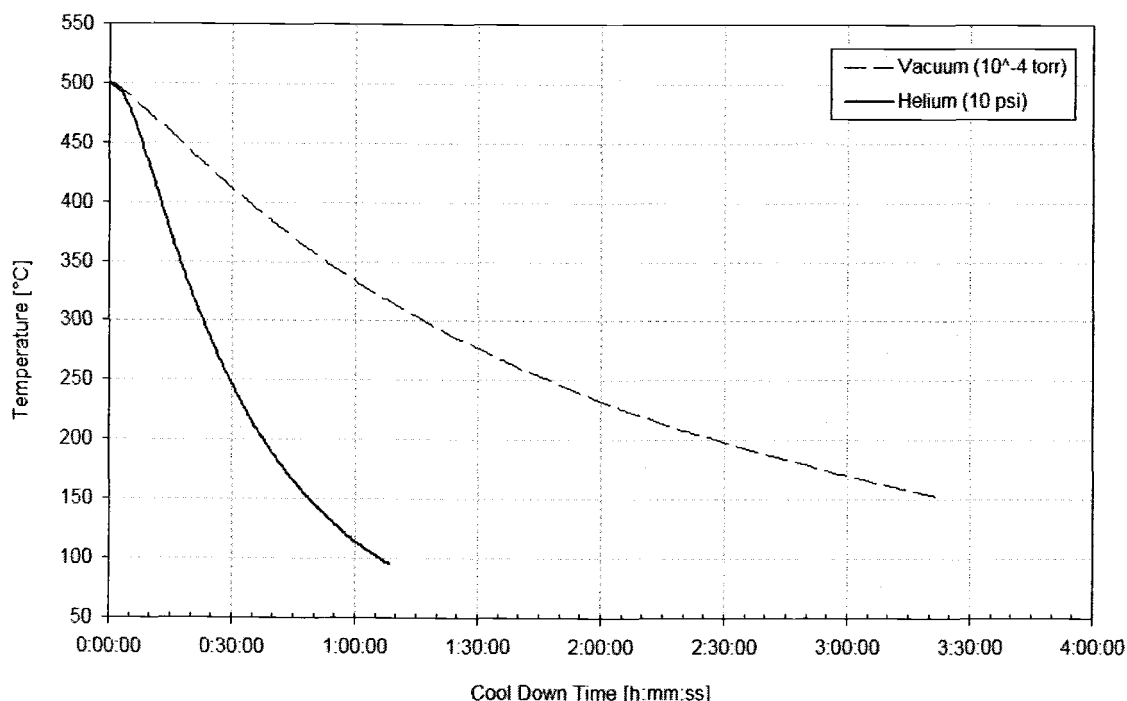
**Table 4-2: Physical Properties of Typical Furnace Quenching Gases**

	Density [kg/m <sup>3</sup> ]	Specific heat capacity [J/kg K]	Thermal conductivity [W/m K]
Argon	1.669	523	0.0173
Nitrogen	1.170	1'040	0.0255
Helium	0.167	5'190	0.1536
Hydrogen	0.084	14'300	0.1750

Listed properties at 15°C, 1bar

The low density of the helium gas results in an unusually high specific heat of helium compared with other noble gases. Therefore, it is a favorable gas for cooling as seen in

CO<sub>2</sub> laser systems, nuclear reactors and many other cooling applications. Only hydrogen would provide faster cooling rates but there are many critical safety issues to overcome with the use of hydrogen as a quench gas. The worst quench gas is argon based on the physical properties in Table 4-2.



**Figure 4-16: Cooling Curves in Helium vs. Vacuum**

As illustrated in Figure 4-15, quenching was accomplished by isolating the vacuum chamber of the Pressmaster hot press from the vacuum pump system (by closing the gate valve) and introducing slowly helium into the chamber at an over-pressure of 10 psi. The helium line continued to feed during the cool down to compensate for any leakage of the chamber. A comparison of the cool down from 500°C in vacuum (10<sup>-4</sup> torr) compared to helium can be seen in Figure 4-16.

The use of helium as a cooling assist during the cool down cycle in the diffusion bonding process can cut down the cycle time by more than 75% (increases the cooling rate by more than 4 times). The cool down time in vacuum (10<sup>-4</sup> torr) starting from 500°C down to 100°C takes over four hours. With the use of helium the cool down from 500°C to 100°C was achieved within one hour. The purity of the helium used for the cooling experiments was 99.5%. No visual oxidation was observed on the copper test

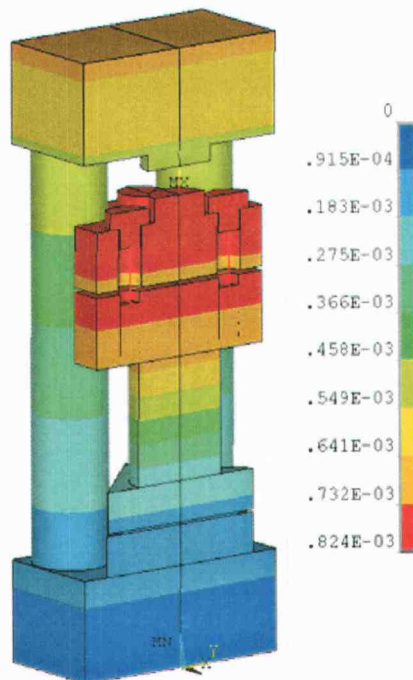
articles between the graphite bonding platens. The stainless steel engagement block and fasteners however showed indications of oxidations after a few runs. Consequently, they possibly serve a gettering function for the slight oxygen concentration in the chamber and hence protect the bonding specimens from oxidation. The next better purity level of helium would be 99.95% and is a factor of two times more expensive than the current grade.

## 5 RESULTS AND DISCUSSION

### 5.1 THEORETICAL RESULTS FE-MODEL

#### 5.1.1 THERMAL EXPANSION BEHAVIOR OF FIXTURE MODEL

The knowledge of the thermal expansion behavior of the fixture frame and inner parts is fundamental and essential for the predictability and usefulness of the fixture. Without this knowledge, the predictability of the contact point and initial gap size is not feasible. The thermal expansion behavior is the central and underlying driving force where fixture design, material properties and process parameters meet and define the functionality of the differential thermal expansion fixture. Modeling of the fixture in a finite element system allows addressing all of the above mentioned issues and makes it possible to study the expansion behavior of a particular fixture design.



**Figure 5-1: Thermal Expansion of Fixture in Z-Direction at 800°C (Units shown in m)**

Figure 5-1 shows a contour plot of the thermally expanded cross-section in z-direction of the current prototype developed in this thesis. The maximal service temperature of the fixture was defined to be 800°C due to the temperature limitation of the disc springs. Materials used in the prototype design are listed in Table 3-1 and Table 3-2.

Dimensions of the individual fixture parts can be found in Appendix A. The contour plot in Figure 5-1 shows clearly, that the inner parts reach a significant higher level of thermal expansion compared to the surrounding frame construction. Furthermore, the highest expansion gradient can be identified at the engagement block with the highest CTE in the system. Since all other used materials have significant lower CTE's, the expansion behavior can be fine tuned simply by either changing the length of the engagement block, or its material or both. The difference in thermal expansion between frame and inner parts is finally the important function which has to be tailored appropriately. A larger diversity in the expansion behavior between frame and inner parts results in a larger stroke which can be favorable for certain types of spring elements to reach enough compression or for the use of the fixture at even low temperatures. It should be noticed, that a larger difference also increases the sensitivity of the fixture according to Equation 14.

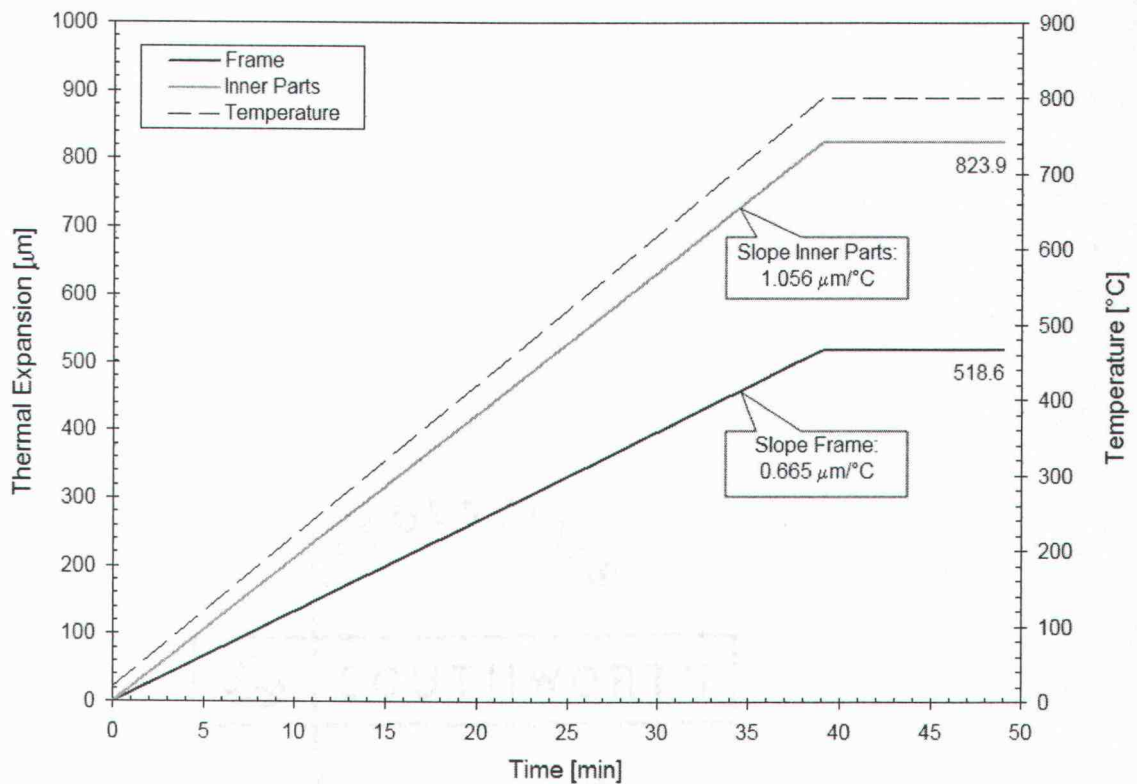


Figure 5-2: Thermal Expansion of Frame and Inner Parts

Hence, the differential thermal expansion should not be too large in order to keep the sensitivity low but also not too small to guarantee a working window over a wide temperature range. Figure 5-2 shows the results of thermal expansion from the ANSYS Time History Postprocessor (POST26) for the prototype fixture.

The end nodes of the compression-only LINK10 element (represents the set screw in the model) were selected as the points of observation in this plot. The temperature was ramped up from room temperature (20°C) to 800°C with a rate of 20°C/min which correlates to a ramping time of 39 minutes in Figure 5-2. The slope difference between frame and inner parts can be clearly identified and is representing the differential thermal expansion behavior of the fixture. The slope difference between inner parts and fixture frame is the important measure and is referred to as the gap closure function as shown in Equation 15.

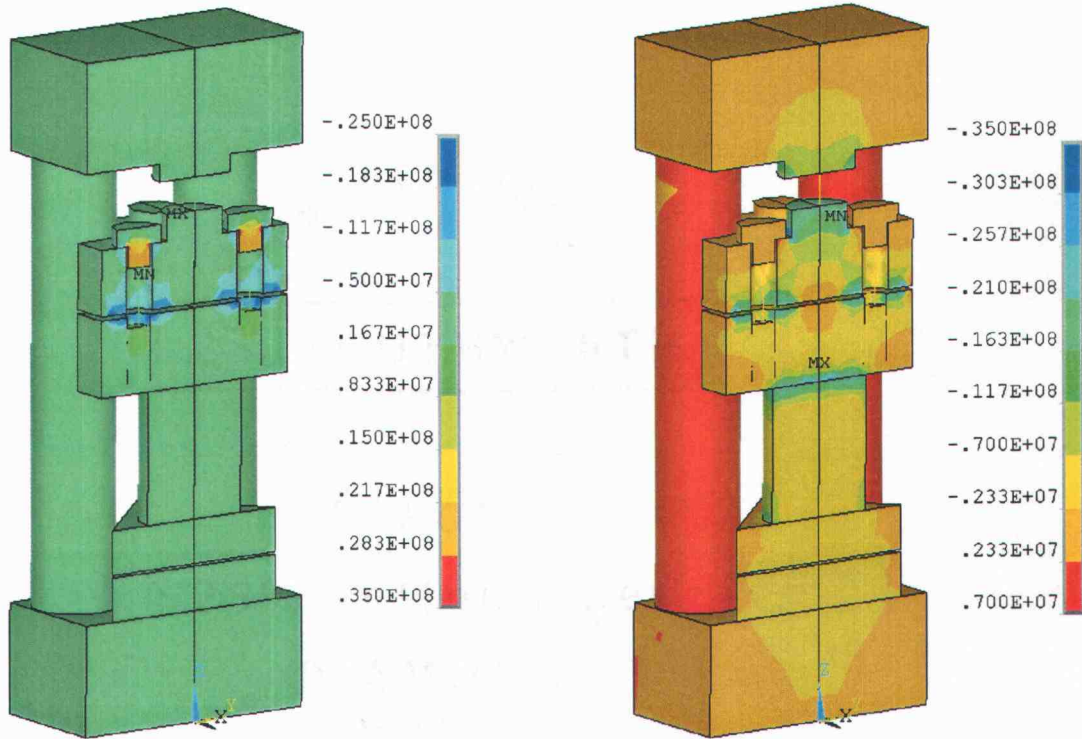
$$\Delta z_{gap} = \frac{\Delta z_e(T)}{\Delta T} - \frac{\Delta z_f(T)}{\Delta T} = 1.056 \mu m / ^\circ C - 0.665 \mu m / ^\circ C = 0.391 \mu m / ^\circ C \quad (24)$$

The gap closure function represents how much of an initial gap between load cell and frame is needed per °C change in temperature. The current design of the prototype fixture investigated in this thesis has an active stroke of 39.1 μm per 100°C change in temperature according to Figure 5-2 and Equation 24. With the knowledge of this function the fixture settings can be adjusted appropriately.

### 5.1.2 STRESS DISTRIBUTION IN THE FIXTURE MODEL

The primary purpose and application of the differential expansion fixture is to provide a desired level of bonding pressure to a stack of laminae. Thus, the study of pressure distribution throughout the fixture is certainly of interest. As mentioned earlier in the text, one of the main difficulties in building the FE-model was to establish the pre-loaded state of the load cell which is shown in Figure 5-3a. It can be seen, that besides the load cell platens and bolts the entire fixture is free of any stress. The level of initial strain in the LINK10 elements compresses the spring elements and puts a tensile load on the load cell bolts. Compression can be detected in the locations of the disc springs and tension along the bolts. The contour plots for Figure 5-3 implicated fixture settings for a resultant bonding pressure of 4 MPa. Figure 5-3b shows finally the stress

distribution in the fixture after the pre-loaded load cell released its stored force to the fixture frame upon contact.



a) at Room Temperature (pre-loaded)

b) at Bonding Temperature (released)

**Figure 5-3: Stress in Z-Direction (Values shown in Pa)**

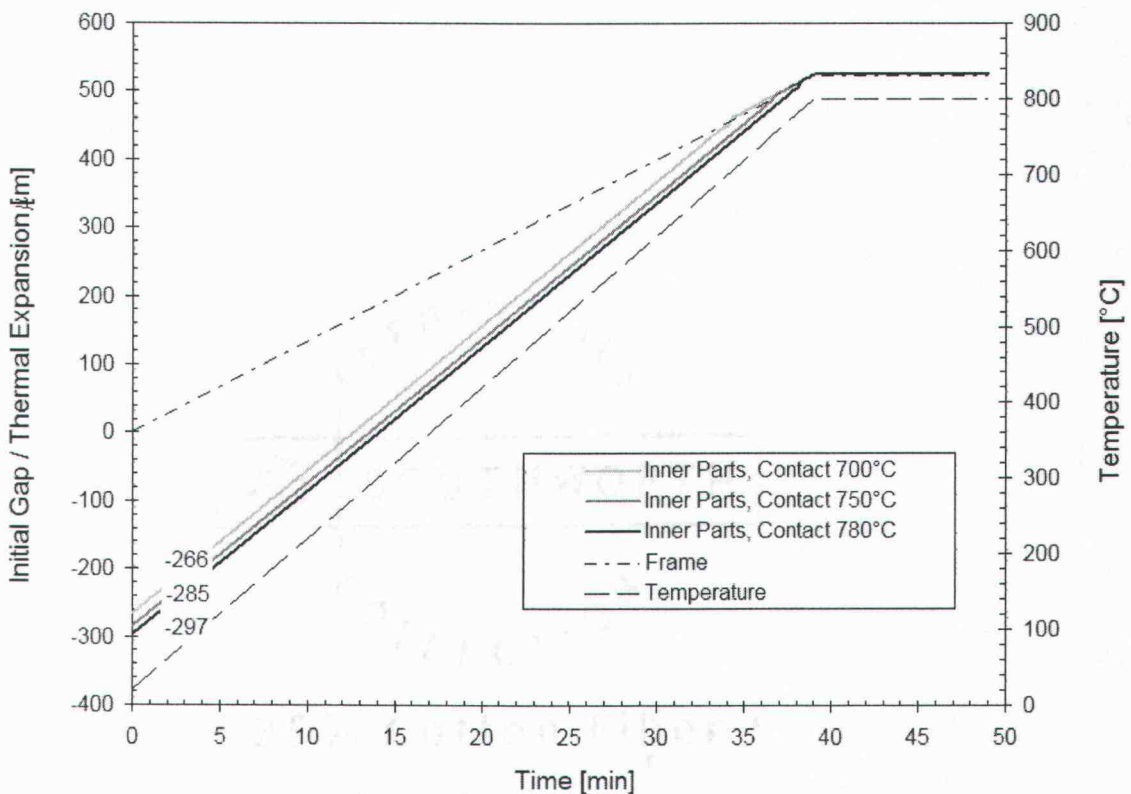
Now, the bolts of the load cell are free of stress since the force flow is established over the fixture frame. The level of pressure between the bonding platens can be identified between 2.3 and 7.0 MPa from the contour scale shown in Figure 5-3. More accurate pressure readings for the actual shim position between the bonding platens can be read off Figure 5-5.

### 5.1.3 INITIAL GAP AND PRESSURE TIMING ANALYSIS

The uniqueness of the differential thermal expansion fixture investigated in this thesis is the distinctive capability of being able to adjust independently the magnitude, timing and sensitivity of bonding pressure. The central relationship of each individual function is the differential thermal expansion behavior presented in Equation 24. In combination with the relationships established in Chapter 3, initial gap, load cell compression and pre-

load force calculations were necessary to establish experimental settings. Additionally, these results were necessary to calculate the real constant values for the initial strain of the LINK10 elements in the finite element model. Consequently, a spreadsheet was developed to perform all of these calculations simultaneously based on bonding conditions. An example of the values calculated for a set of bonding parameters can be found in Appendix C.

Figure 5-4 shows how the variation of the initial gap size affects the contact point of frame and inner parts. The simulations are based on a temperature ramp from room temperature up to 800°C with a ramp rate of 20°C per minute.



**Figure 5-4: Variation of Initial Gap and Effect on Contact Temperature**

The results show that increasing the initial gap size ( $g_0$ ) from 266 to 285 microns shifts the contact temperature 50°C upwards, and a further increase from 285 to 297 microns offsets the contact temperature an additional 30°C. In other words, increasing the initial gap by 1 micron shifts the contact temperature approximately 2.5°C which equals the

inverse function of Equation 24. The maximal initial gap size ( $g_{\max}$ ) will be reached if the contact temperature equals the bonding temperature according to Equation 25.

$$g_{\max} = \Delta z_{\text{gap}} \cdot (T_{\max} - T_R) = 0.391 \mu\text{m}/^{\circ}\text{C} \cdot (800 - 20)^{\circ}\text{C} = 305 \mu\text{m} \quad (25)$$

The amount of additional load cell compression due to thermal expansion from the point of contact up to the final bonding pressure equals the difference between the initial gap size and the maximal gap size.

$$\Delta z_{\text{add}} = |g_0| - g_{\max} \quad (26)$$

Therefore, the amount of additional load cell compression has to be considered by reducing the pre-loading of the load cell by that amount so that the correct bonding pressure is finally reached. Compensation for this effect can be seen in Figure 5-5. Again, the settings for the simulations can be found in Appendix C.

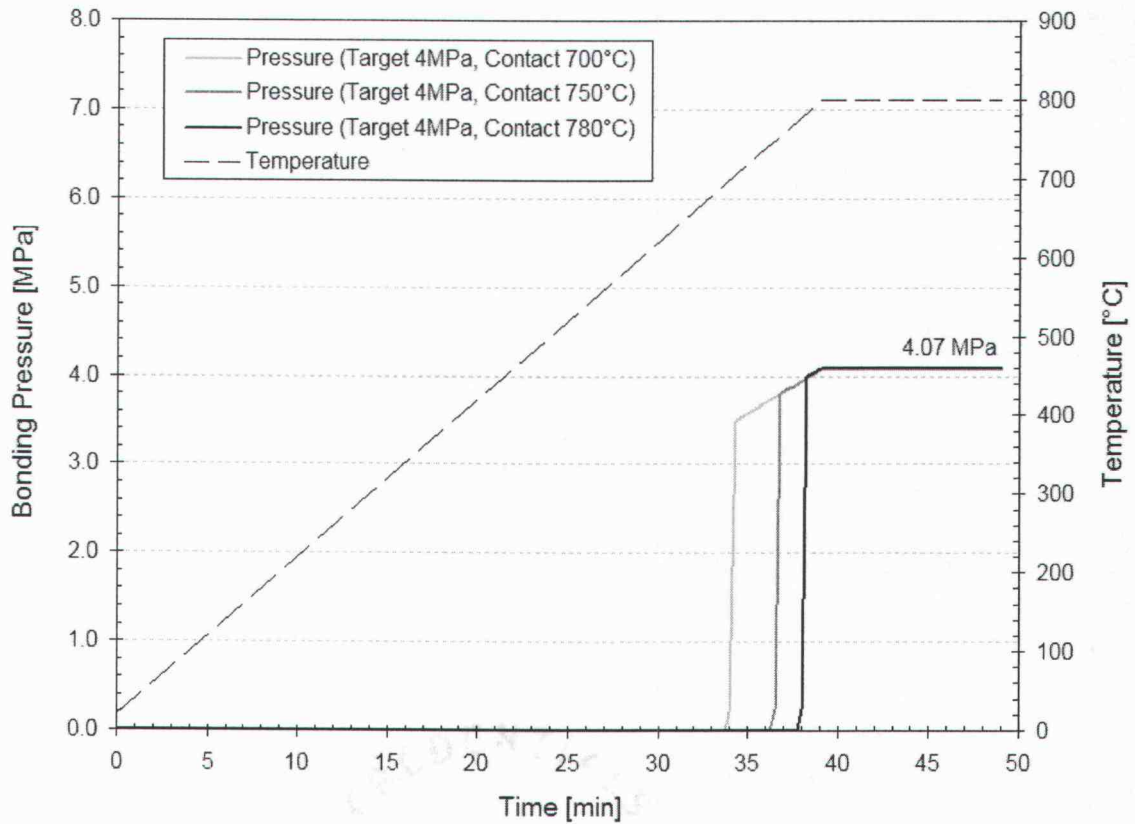


Figure 5-5: Effect of Contact Temperature on Pressure Timing

Based on the previous shifting of the contact temperature due to variations in the initial gap size the timing of the pressure can be controlled as shown in Figure 5-5. As soon as the load cell gets into contact with the fixture frame the bonding pressure kicks in with the pre-loaded force. The remaining portion of the target bonding pressure will be provided by the additional compression of the load cell depending on the difference between contact and bonding temperature shown in Equation 26. The slope of the additional pressure increase equals the pressure sensitivity stated in Equation 15 and is mainly depending on the total spring constant and the differential thermal expansion behavior. The finite element simulations reach a final pressure of 4.07 MPa which is only 1.75% off from the target pressure of 4 MPa.

#### 5.1.4 SENSITIVITY ANALYSIS

Within a  $\Delta CTE$  bonding unit, the bonding pressure depends on the temperature in the furnace. Therefore, slight swings in the bonding temperature can vary the pressure of the fixture over time. Thus, it is of interest to keep the pressure sensitivity of the fixture low so that once the pressure is released upon contact, temperature swings will have only a minimal effect on the resultant pressure. In the analysis of the simple differential thermal expansion unit based on a solid expansion block with no load cell and no disc springs, the sensitivity depends on the expansion block CTE and height and will be on the order of 0.5-1.0 MPa/°C. Thus, temperature fluctuations within a furnace of  $\pm 5^\circ\text{C}$  can change the bonding pressure by more than 100%, since common bonding pressures in microlamination are in the range of 2-8 MPa.

The pressure sensitivity for the  $\Delta CTE$  fixture developed in this thesis was stated theoretically in Equation 15. By introducing the values for the differential thermal expansion behavior of Equation 24 and the values for the spring constant and bonding area, the sensitivity for the fixture according to Equation 27 can be computed as 0.0069 MPa/°C which is around 150 times less sensitive as the case without disc springs.

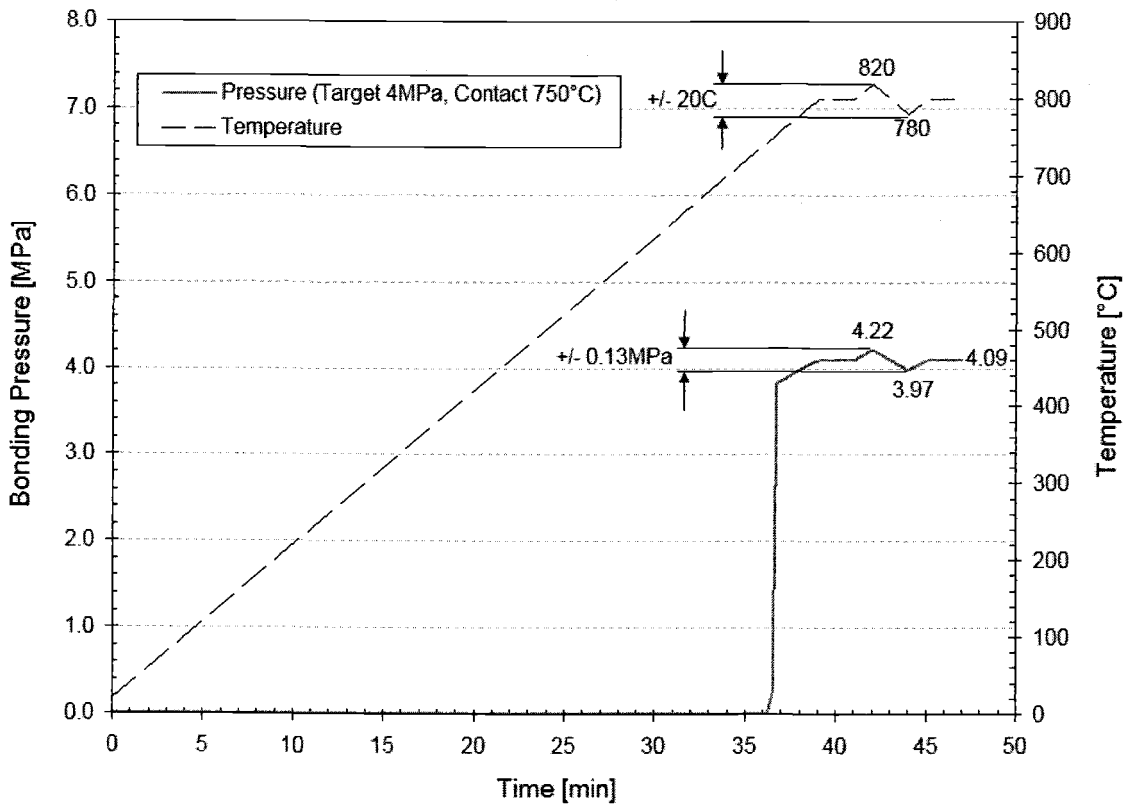
$$\Delta\sigma_{Theo}(T) = \frac{k_{total} \cdot \Delta z(T)}{A_B} = \frac{10960 \text{ N/mm} \cdot 0.391 \cdot 10^{-3} \text{ mm/}^\circ\text{C}}{625 \text{ mm}^2} = 0.0069 \text{ MPa/}^\circ\text{C} \quad (27)$$

Figure 5-6 illustrates simulation results of the finite element model where a temperature swing of  $\pm 20^\circ\text{C}$  at bonding temperature shows the effect on the resultant bonding

pressure. This temperature swing caused a change in the pressure of  $\pm 0.13$  MPa which represents about 3% of the target pressure. Therefore, the pressure sensitivity seen in the finite element model can be calculated according to Equation 28 and is in good agreement with the theoretical calculated pressure sensitivity of Equation 27.

$$\Delta\sigma_{FEM}(T) = \frac{\Delta p}{\Delta T} = \frac{\pm 0.13 \text{ MPa}}{\pm 20^\circ \text{C}} = 0.0065 \text{ MPa}/^\circ \text{C} \quad (28)$$

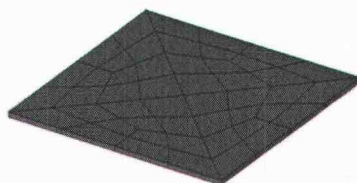
It should be noticed that the temperature difference between the contact temperature and the bonding temperature ( $\Delta T_{CB}$ ) has always to be larger than the maximal negative temperature fluctuation of the furnace. Otherwise, if the furnace temperature swings below the adjusted contact temperature of the fixture, the pressure will not be transmitted since the contact between frame and load cell will be lost. Obviously, this can only happen if the change in temperature is so slow that the fixture actually has the time to respond to the temperature change.



**Figure 5-6: Pressure Sensitivity Depending on Temperature Fluctuations**

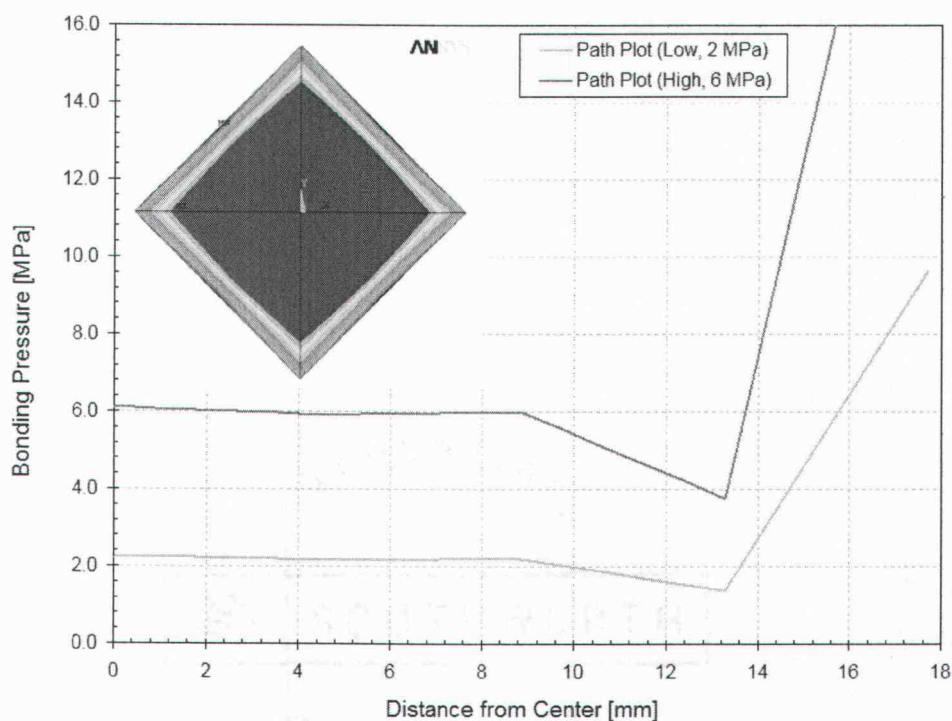
### 5.1.5 PRESSURE UNIFORMITY

The plotted pressure values in Figure 5-5 and Figure 5-6 are based on the nodal solution of the center node of the modeled substrate shown in Figure 5-7. For the application in diffusion bonding the pressure distribution over the whole area is certainly of interest and can be observed in the finite element model by selecting the elements based on the substrate material.



**Figure 5-7: Copper Substrate of the FE-Model (mapped mesh)**

With path plot operations nodal solutions can be plotted along a specific path defined by two nodes. The path is defined from the center node out to the corner of the substrate and is representing the half-diagonal across the 25x25 mm substrate. Path plots of the pressure along the half-diagonal can be seen in Figure 5-8 together with the contour plot of the substrate.



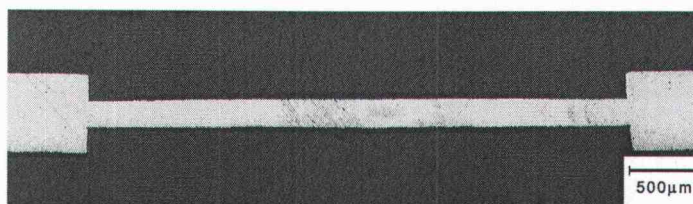
**Figure 5-8: Path Plots of Pressure Distribution at Substrate**

The pressure in the center region of the substrate (diameter 20 mm) is uniform and at the expected level of pressure. The boarder of the substrate however, shows a significant increase in stress. This phenomenon of stress localization at element boundaries has to do with the approach the model was made and actually is not representing the real stress situation. Such stress peaks are always the case on edges where two different materials interface each other and nodal movements are constrained by the same mesh since the structure is modeled as one solid piece. This is especially true, if the material properties ( $E, \nu$ ) are very different, as is the case for graphite (platens) and copper (substrate). A possible approach to solve this issue in future models is to consider a contact pair between the bonding platens and the substrate surfaces. A contact surface would allow different lateral movements for the different materials and hence the stress localization on edges should disappear. However, the modeling of a contact pair needs two surfaces facing each other and thus there has to be a gap introduced between the bonding platens and the substrate surface in order to create the contact pair. In most cases, this is not easy to do and requires major modeling efforts. A possible simpler method would be to apply orthotropic stress-strain relations [41] to calculate fictitious material properties in lateral directions. In the direction of the bonding pressure (z-direction), the orthotropic material property components are given by the isotropic material properties of the materials. Furthermore, the pressure on both material interfaces in the z-direction is equal and given by the bonding pressure. By applying orthotropic stress-strain relations fictitious material properties in the lateral direction can be expressed by assuming that the lateral stresses are zero and lateral strains of the two materials are equal. Once these fictive lateral material properties are found, interfacial stresses should disappear.

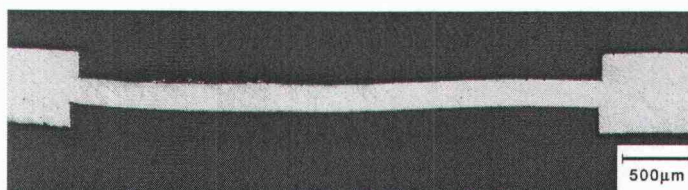
## 5.2 EFFECT OF PRESSURE TIMING ON FIN WARPAGE

Shifting the point of contact (i.e. pressure application) during the bonding cycle has shown significant influence on the magnitude of fin warpage. Metallographical cross-sections of the test article were made to illustrate the warpage effect of the fins due to pressure application during temperature ramping. The cuts through the test articles as shown in Figure 5-9a to Figure 5-9e represent the center sections of the 4mm wide fins. The thickness of the fins equals the shim thickness of 203  $\mu\text{m}$  (8 mil). The cross sections clearly show an increase in fin warpage with a decrease in the temperature at

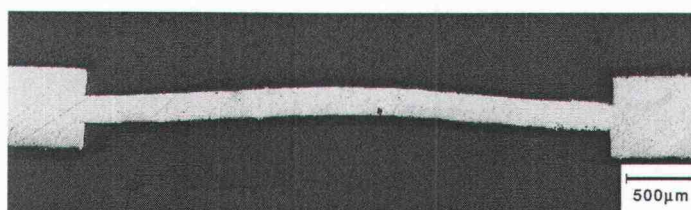
which pressure application was made. The fins buckled the most in the center sections and flattened out toward the ends.



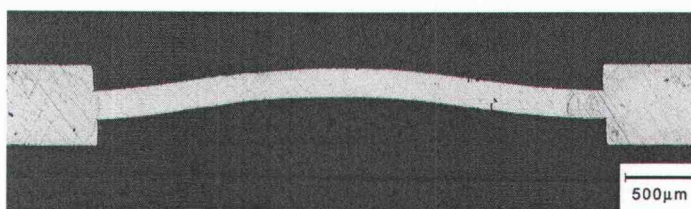
a) Pressure Application at the End of Ramp ( $\Delta T=0^{\circ}\text{C}$ )



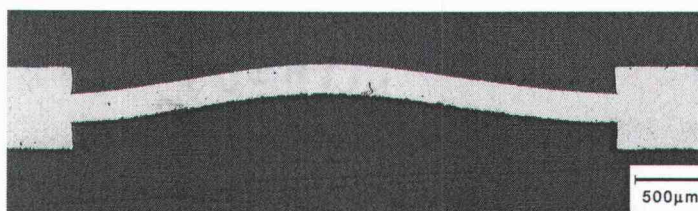
b) Pressure Application  $\Delta T=300^{\circ}\text{C}$  before the End of Ramp



c) Pressure Application  $\Delta T=400^{\circ}\text{C}$  before the End of Ramp



d) Pressure Application  $\Delta T=600^{\circ}\text{C}$  before the End of Ramp



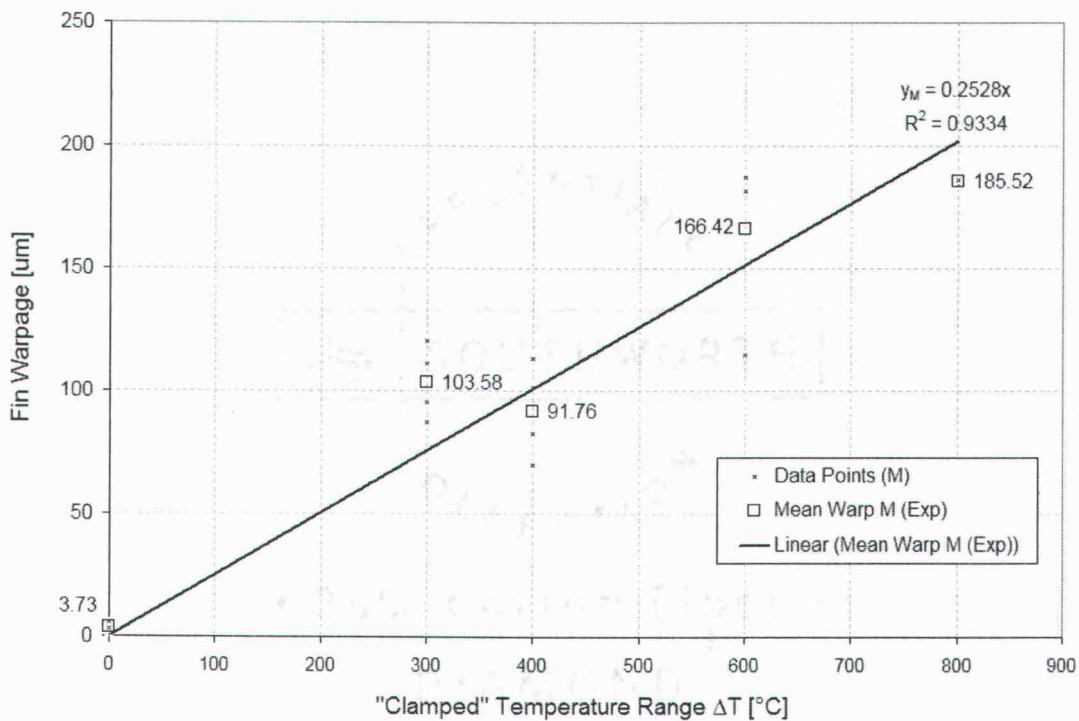
e) Pressure Application  $\Delta T=800^{\circ}\text{C}$  before the End of Ramp

**Figure 5-9: Metallographic Cross-Sections of Fin Warpage**

The warpage of the fins produced in the experiment was measured with the Veeco Dektak<sup>3</sup> profiler by scanning over the fin sections in the center and to the left and right end of the fin. The experimental results of the warpage in the middle (M) of the fins are shown in Figure 5-10. For each data set the mean warpage and standard deviation were calculated and the mean values at each temperature difference  $\Delta T$  (clamped temperature range) were fitted in good agreement with a linear regression. The experimental results are summarized in Table 5-1.

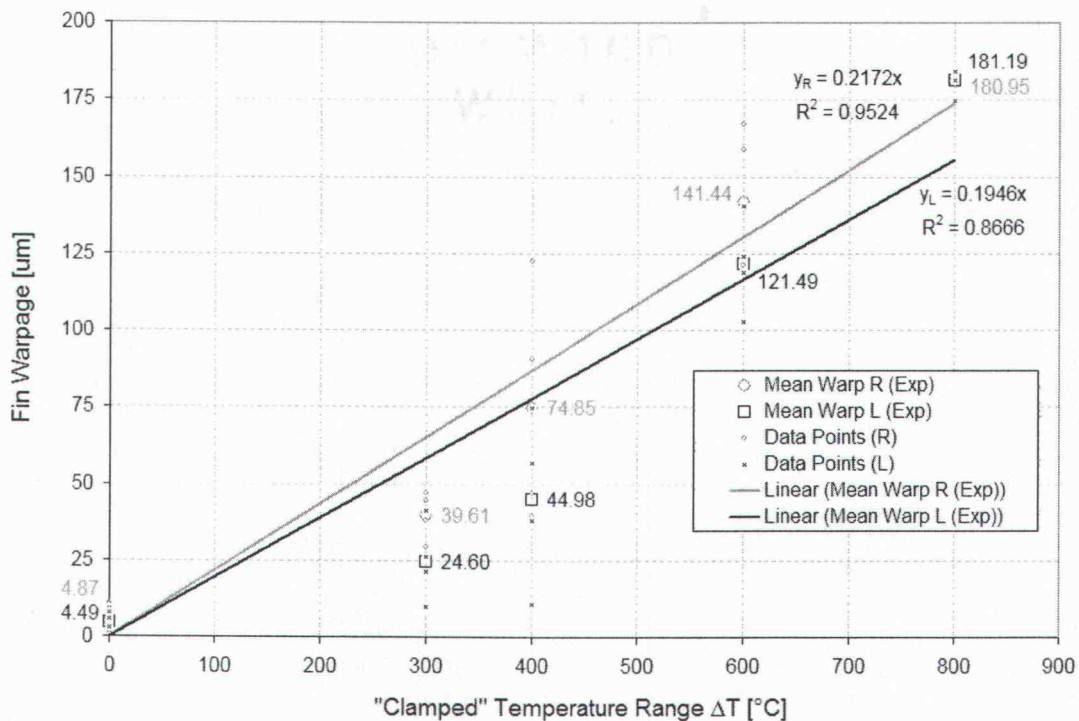
**Table 5-1: Experimental Results of Fin Warpage**

$\Delta T = T_B - T_C$ [°C]	Warpage L [ $\mu\text{m}$ ]	S.D. L [ $\mu\text{m}$ ]	Warpage M [ $\mu\text{m}$ ]	S.D. M [ $\mu\text{m}$ ]	Warpage R [ $\mu\text{m}$ ]	S.D. R [ $\mu\text{m}$ ]
0	4.49	2.77	3.73	1.41	4.87	3.48
300	24.60	11.31	103.58	12.83	39.61	6.84
400	44.98	23.76	91.76	16.64	74.85	33.78
600	121.49	13.35	166.42	29.96	141.44	21.61
800	181.19	3.99	185.52	1.48	180.95	0.76



**Figure 5-10: Experimental Fin Warpage Measured in the Center of the Fins**

It is observed that the fin warpage seems to reach the maximal possible fin deflection of roughly 185  $\mu\text{m}$  at  $\Delta T=800^\circ\text{C}$  and that the standard deviation under these conditions is very small. This is likely due to the fact that the buckled fin is constrained by the graphite bonding platens. Evidence for this can be seen in the metallographic cross-section of Figure 5-9e showing that the fin deflection has reached its maximal extent. However, theoretically the maximal deflection should equal the shim thickness of 203  $\mu\text{m}$ . The difference of the measured maximal deflection can be explained by the fact, that the conical profiler tip does not reach the lowest corner of the fin. Since the fins are buckled, the measurements already start with a small offset. The experimental results of the fin warpage for the left (L) and right (R) side of the fins are visualized in Figure 5-11.



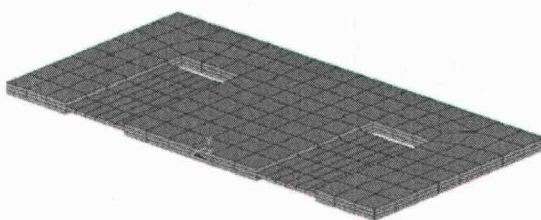
**Figure 5-11: Experimental Fin Warpage Measured to the Right and Left of the Fins**

The result of this study can be used as a calibration curve for the differential thermal expansion unit to re-adjust the initial gap size depending on the amount of measured fin warpage. Moreover, the significance of the appropriate timing of bonding pressure during a microlamination process was made evident by this experiment. If possible, the bonding pressure should always be applied when the laminae stack and the bonding

fixture have reached a uniform temperature and all components are fully expanded. It is expected that this would yield flatter and less deformed channel cross-sections.

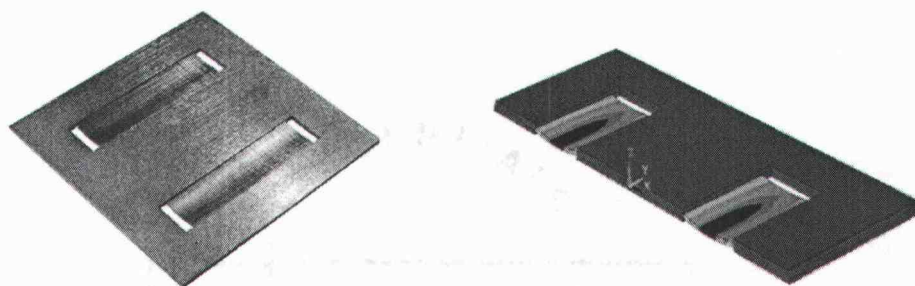
### 5.2.1 COMPARISON OF FIN WARPAGE WITH THE FINITE ELEMENT MODEL

The buckling behavior of the fins was also studied with the help of a finite element model of the test article. The three layered test article used in the warpage study (Figure 4-4) was modeled in ANSYS as shown in Figure 5-12.



**Figure 5-12: FE Model of the Test Article (half cut)**

The test article model was used to compare the theoretical fin warpage with the experimentally measured results. The model does not consider friction behavior between the layer interfaces and is modeled as a solid piece. A further assumption was made by fixing the displacement of the outer edges to simulate the expansion restraint of the fixture platens due to friction onto the layer stack. The active coefficient of thermal expansion was input as the difference between the substrate material and the fixture material. Qualitatively similar magnitudes of fin warpage can be observed between the physical test articles and the finite element model as shown in Figure 5-13.



**Figure 5-13: Real Test Article (left) and FE-Model Half Cut (right)**

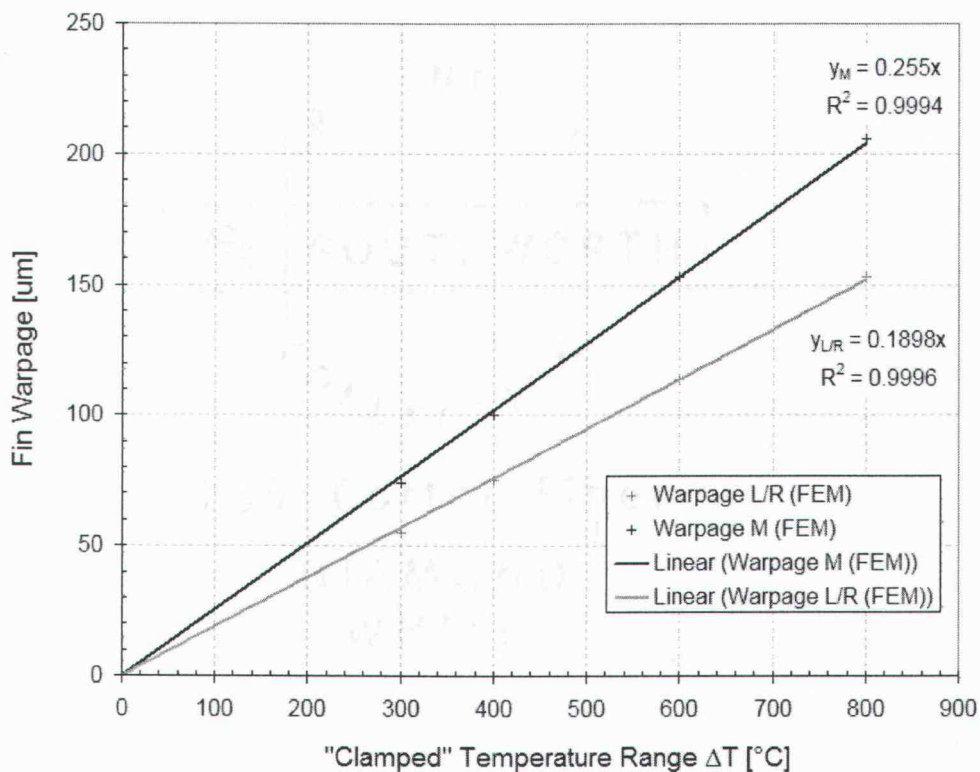
The fin warpage of the model was measured also in the center (M) of the fin and on the outside (L/R). Results of the simulations are summarized in

Table 5-2.

**Table 5-2: FE-Simulation Results of Fin Warpage**

$\Delta T = T_B - T_C$	Warpage Center [ $\mu\text{m}$ ]	Warpage Left/Right [ $\mu\text{m}$ ]
0°C	0	0
300°C	74	55
400°C	100	75
600°C	153	114
800°C	206	153

The linear regression for both, warpage at the center (M) and on the outside (L/R) of the fin is visualized in Figure 5-14.

**Figure 5-14: Theoretical Fin Warpage of Test Article based on FE-Analysis**

Comparable slope values for the linear regression models can be seen between the experimental and theoretical results. Fin warpage in the middle of the fin shows excellent agreement when compared with the experimentally-derived linear regressions. A larger divergence can be observed between measured and simulated warpage on the outside of the fin. The difference in these results can be clarified due to the fact that the fin warpage was not recorded at exactly the same positions. The values

for the finite element model compare to the outer most deflections on the edge of the fin. However, in the experimental examination, the warpage on the outside of the fin had to be scanned one to two millimeters away from the edge. Thus, the experimental values are slightly larger.

Based on the agreement between the experimental and theoretical investigations of the fin warpage behavior ( $w(T)$ ), the regression model for the fin center can be used as a valid calibration tool for the pressure timing of the fixture. If a certain initial gap setting shows significant fin warpage across the fin center then it can be related to the temperature difference ( $\Delta T_w$ ) that caused the warpage by introducing the measured fin warpage ( $w_M$ ) into Equation 29.

$$\Delta T_w = \frac{w_M}{w(T)} = \frac{w_M}{0.25 \mu m / ^\circ C} \quad (29)$$

Thus, the measured warpage value can be expressed as the amount of initial gap correction ( $\Delta g_{corr}$ ) according to Equation 30.

$$\Delta g_{corr} = \Delta z_{gap} \cdot \frac{w_M}{w(T)} = 0.391 \mu m / ^\circ C \cdot \frac{w_M}{0.25 \mu m / ^\circ C} \quad (30)$$

By adding the amount of gap correction ( $\Delta g_{corr}$ ) to the initial gap setting that caused the warpage, the contact temperature will be offset to the appropriate point where acceptable warpage results.

### 5.3 LOAD CELL DESIGN MODIFICATIONS

Extensive experimental testing revealed that the ceramic bolts of the original design did not withstand the tensile preloading of the load cell even though the preloaded force did not exceed the specified stress limit of the bolts. This is mainly due to the design of the bolt which permits stress concentration at the sharp corner where the bolt head meets the bolt thread. As an alternative, custom bolts were fabricated out of graphite ISO-63 as shown in Figure 5-15. The diameter of these bolts were increased to 8 mm (5/16"). Although calculations showed that the tensile strength of the graphite bolts should be sufficient for carrying the preload (safety factor of 2) the graphite bolts also cracked during experiments.

The cause of the failure can be explained by the procedure of how the bolts are tightened during the preloading of the load cell. The load cell is compressed at the desired preload level with the hydraulic ram of the hot press. Subsequently, the bolts are snugly tightened so that the hydraulic ram can be retracted to transmit the preload to the bolts. However, it is almost impossible to adjust the bolts in a manner that the load gets distributed uniformly among the four bolts. One bolt will potentially have more load than the others and due to the unequal force distribution, bending moments are set up in the bolts. As soon as the first bolt cracks, the forces increase for the remaining bolts and they subsequently fail in order.

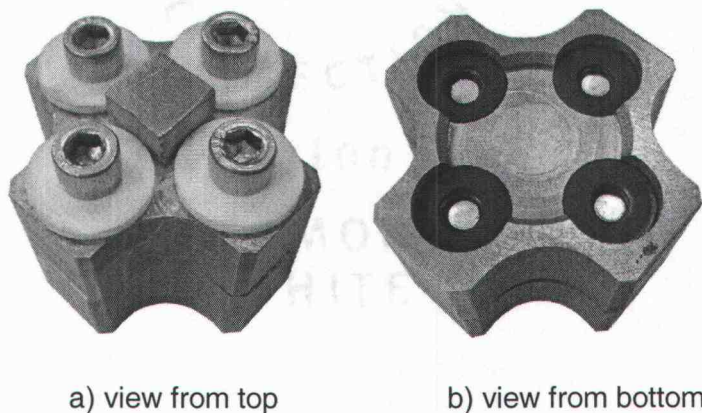


**Figure 5-15: Load Cell with Graphite Bolts**

The problem of the current load cell design can be found in the selection of the material for the load cell platens. Since the platens are made of a metallic high temperature material (molybdenum), a non-metallic material has to be selected for the bolts to prevent solid-state diffusion at high temperatures. For future fixture designs, the load cell platens should be made out of a machinable ceramic like Aremcolox 502-1100. This would allow the load cell bolts to be made out of a tough and low CTE material like molybdenum and the maximal possible pressure of the load cell would not be restricted by the stress limit of the bolts. However, such bolts can not be purchased and would have to be custom made.

The modification of the current load cell design to withstand the preload can be seen in Figure 5-16. Since only metallic bolts are tough enough to hold the preload, stainless steel 316 bolts were selected (max. service temperature 870°C). To prevent bonding to the load cell platens, threaded graphite sleeves were placed in the load cell base

(Figure 5-16b). The bolt head was protected with ceramic washers from bonding to the load cell top (Figure 5-16a). This modification with sleeves made the preloading possible and could also be of interest for future fixture designs especially since the ceramic threads experienced significant wear. Threaded sleeves could be simply replaced and provide better design modularity. Different thread sizes for different bolt diameters would be possible and interchangeable.



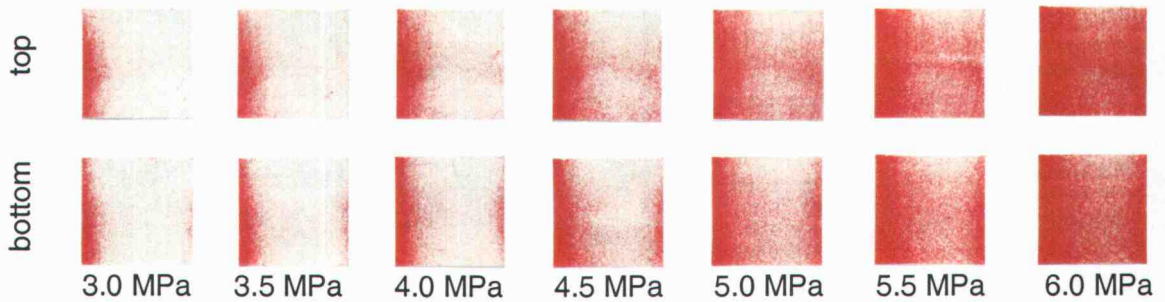
**Figure 5-16: Final Load Cell Design**

It should be noticed that the ceramic bolts used for the fixture frame had to be replaced also with stainless steel bolts.

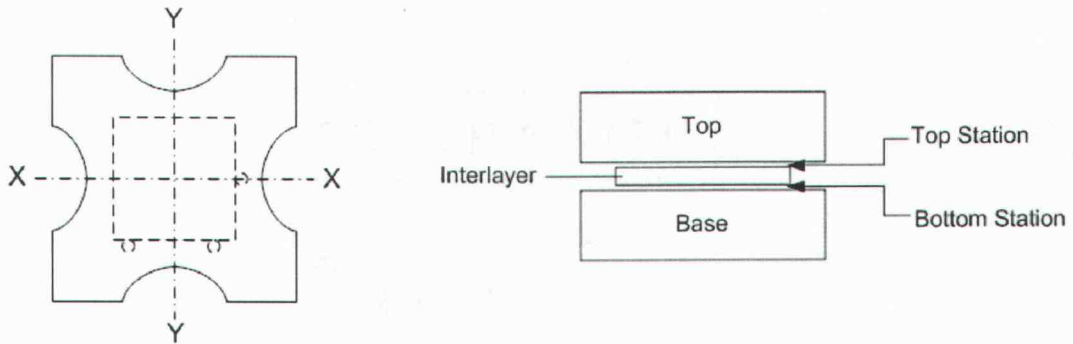
## **5.4 ANALYSIS OF PRESSURE UNIFORMITY WITH FUJI PRESSCALE FILM**

### **5.4.1 PRESSURE UNIFORMITY BASED ON BONDING PLATENS ACCURACY**

The resultant pressure uniformity is strongly dependent on the machining quality of the bonding platens, especially the flatness and the parallelism of the platens are important. Thus, the graphite bonding platens of the  $\Delta$ CTE-fixture (Figure 4-3) were tested on their ability to distribute the pressure uniformly. Pressure sensitive film (Fuji Prescale type LW) was used to test the pressure distribution at different pressure levels for the bottom and top bonding station of the bonding platens. The load was applied with the Pressmaster hot press and the film readings are summarized in Table 5-3. The film readings show that the pressure is localized the most at the left edge of the bonding area. With increased load the pressure localization can also be seen on the right edge which is an indication of a bowed shape in X-X direction in one or multiple fixture platens.

**Table 5-3: Initial Pressure Film Readings of Bonding Platens**

Therefore, the bonding platens were scanned with the Dektak<sup>3</sup> surface profiler for geometrical inaccuracy in X-X and Y-Y direction as visualized in Figure 5-17.

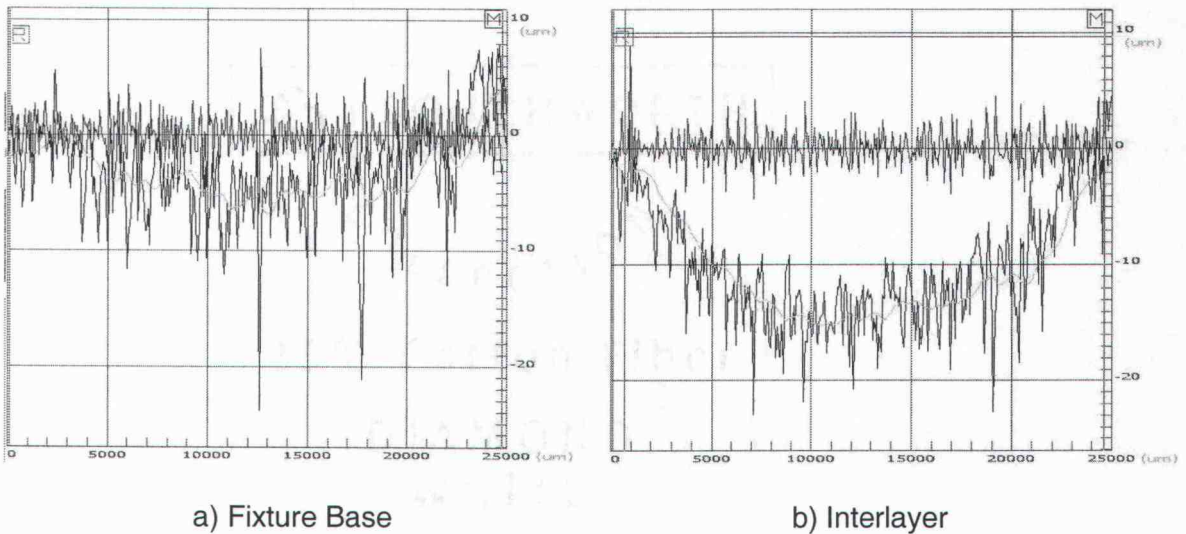
**Figure 5-17: Axis Definition of the Graphite Bonding Platens**

The Dektak<sup>3</sup> surface profiler is equipped with short pass and long pass digital filters for filtering out high and low frequencies to distinguish between roughness and waviness. The appropriate cutoff wavelength can vary from application to application. However, a general rule for selecting the appropriate cutoff filter values is to divide the scan length by 100 for the short pass filter (roughness) and to divide the scan length by 10 for the long pass filter (waviness). A scan length of 25 mm was selected in X-X and Y-Y direction to scan the bonding platens. The resulting plots show the raw measurement data and based on the filtering the surface roughness and the waviness of the scan. Values for the roughness and the waviness were calculated based on the arithmetic average surface roughness ( $R_a$ ) and the maximum peak to valley waviness ( $W_t$ ) respectively. The measured values for the initial state of the platens are summarized in Table 5-4. The fixture top does not show significant inaccuracy and the surface waviness is within machining tolerances.

**Table 5-4: Initial Bonding Platens Waviness and Roughness in X and Y-Direction**

	$R_{a,X-X} [\mu m]$	$W_{t,X-X} [\mu m]$	$R_{a,Y-Y} [\mu m]$	$W_{t,Y-Y} [\mu m]$
Base	1.35	10.97	1.38	4.11
Interlayer	1.17	14.77	1.24	6.51
Top	0.72	8.33	0.80	3.67

The waviness of the base and the interlayer however, shows significant waviness in X-X direction (Figure 5-18) which was expected based on the pressure film readings of Table 5-3. Also the thickness of the interlayer plate shows slight differences in X-X direction and the left side is actually slight thicker than the right side which results in the pressure distribution seen in Table 5-3.

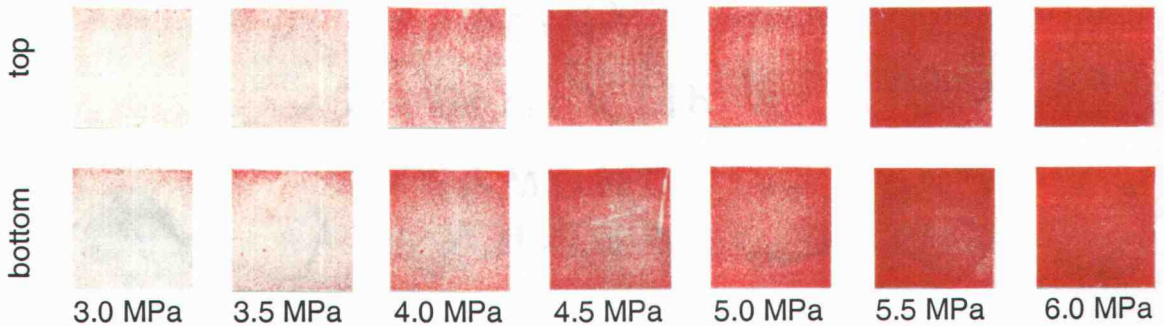
**Figure 5-18: Initial Surface Roughness and Waviness in X-X Direction**

Based on these measurements the bonding platens were re-machined in order to yield a more uniform pressure distribution. A precise vacuum chuck was fabricated to prevent any bowing of the platens due to clamping forces during machining. Then, the surfaces of all graphite bonding platens were re-machined with a fly-cutter. Measurements taken after the re-machining are summarized in Table 5-5.

**Table 5-5: Corrected Bonding Platens Waviness and Roughness in X and Y-Direction**

	$R_{a,X-X} [\mu m]$	$W_{t,X-X} [\mu m]$	$R_{a,Y-Y} [\mu m]$	$W_{t,Y-Y} [\mu m]$
Base	0.65	2.13	0.69	3.22
Interlayer	0.61	2.30	0.58	1.60
Top	0.52	2.27	0.50	1.61

The re-machining of the surfaces significantly reduced the peak to valley surface waviness to an average of 2.19  $\mu m$ , which is excellent considering the machining equipment used. A pressure distribution experiment with the pressure sensitive film was repeated to see the effects. Film readings for both the top and bottom bonding station are shown in Table 5-6 for different levels of pressure.

**Table 5-6: Final Film Readings of Bonding Platens**

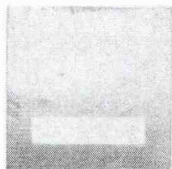
It can be seen that after re-machining the surface of the bonding platens, the pressure became evenly distributed across the bonding area for both the top and bottom bonding stations.

The evaluation of the pressure uniformity has shown that the machining quality of the bonding platens is critical in order to achieve a uniform pressure distribution. Based on this study, a surface waviness below 5  $\mu m$  is generally recommended in order to yield an acceptable pressure uniformity. It should be noted that for large substrate fixture designs, the surface waviness of the important contact surfaces will be very critical.

## 5.5 ANALYSIS OF PRESSURE TIMING AT LOW TEMPERATURES

Validation of the fixture timing concept was made by setting an initial gap with the feeler gauge and the use of the pressure sensitive film at temperatures of 180°C. To make reading of the pressure film easier, a copper channel layer from the test article was placed below the pressure sensitive film. The copper layer was flattened and its

parallelism verified to prevent false pressure readings due to a warped copper layer. An initial test run was performed at 180°C with an initial gap setting of zero (to make sure that pressure was transmitted). This run showed a non-uniform pressure distribution across the bonding area as seen on the film reading in Figure 5-19. The pressure was concentrated along the lower edge while the upper edge of the film showed only very light colorization.



**Figure 5-19: Non-uniform Pressure Distribution due to Expanded Frame Bolts**

By screwing off the top fixture plate, it was realized that the stainless steel frame bolts had loosened on the side where less pressure was detected. This was explained by the fact that the thermal expansion of the stainless steel bolts is much higher compared to the molybdenum plates. Consequently, during thermal cycling the bolts are loosening and the fixture frame rigidity is lost. Therefore, disc springs were also introduced in the frame construction of the fixture to preload the frame plates as shown in Figure 5-20.



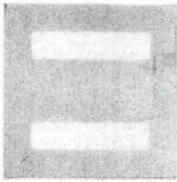

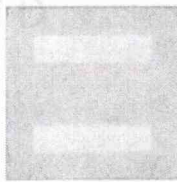
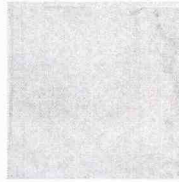
**Figure 5-20: Fixture Frame Fastening Modification with Disc Springs**

The disc springs located at the frame bolts guarantees that the molybdenum fixture plates are always pressed against the ceramic posts. During fastening of the plates on the posts, the disc springs were compressed until they had reached flat load. This level of compression is not reached within the load cell and hence, there is always a net force on the frame plates which will hold the frame construction in place. After the

modifying the frame with disc springs, the bolts remained tight after thermal cycling and the pressure uniformity was established as shown on the pressure film readings in Table 5-7.

A pressure timing experiment was conducted by varying the initial gap settings of the fixture. The temperature and the pressure were set to 180°C and 4 MPa respectively (fixture settings in Appendix E). The results of this experiment are visualized in Table 5-7.

**Table 5-7: Low Temperature Pressure Film Readings for Fixture Validation**

			
$g_0=0\ \mu\text{m}$ $T_C=20^\circ\text{C}$ $T_B=180^\circ\text{C}$	$g_0=30\ \mu\text{m}$ $T_C=100^\circ\text{C}$ $T_B=180^\circ\text{C}$	$g_0=50\ \mu\text{m}$ $T_C=150^\circ\text{C}$ $T_B=180^\circ\text{C}$	$g_0=70\ \mu\text{m}$ $T_C > 180^\circ\text{C}$ $T_B=180^\circ\text{C}$

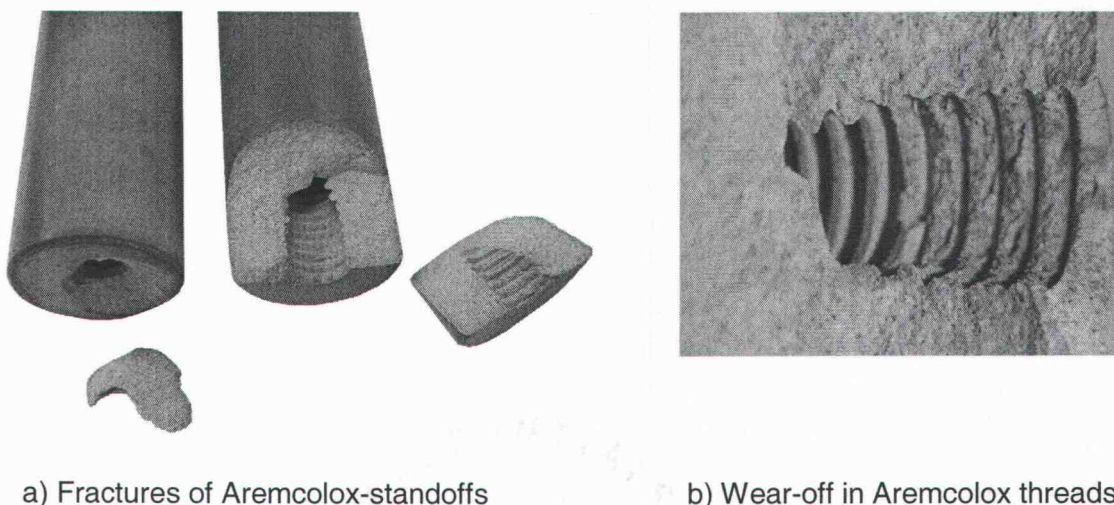
It can be seen that pressure was clearly transmitted in the first three film readings while the last sample does not show any pressure. Based on theoretical calculations (Appendix E), for an initial gap setting greater than 63  $\mu\text{m}$ , no contact will be established. This non-contact situation was experimentally confirmed by a gap setting of 70  $\mu\text{m}$  as it can be seen in Table 5-7. The color density of the first sample compared with reference samples of the hot press at 4 MPa shows an equivalent level of pressure. Furthermore, the pressure was uniform distributed across the bonding area. The film readings for the gap settings of 30 and 50  $\mu\text{m}$  however, show lower pressure reading. A possible source of error can be found in the relaxation of the load cell due to the use of high expanding stainless steel bolts although the additional expansion of the bolts was considered in the amount of preload of the load cell. Nevertheless, the physical functionality of the  $\Delta\text{CTE}$ -fixture was confirmed with this timing experiment and showed good agreement with theoretical fixture settings even at low temperatures.

## 5.6 FIXTURE VALIDATION AT HIGH TEMPERATURES

The  $\Delta$ CTE-fixture was shown to provide functionality at low temperatures (180°C). Further experiments were needed to confirm high temperature operation. Therefore, test runs were performed at 500°C and 800°C.

### 5.6.1 FAILURE OF AREMCOLOX 502-1100 CERAMIC FIXTURE POSTS

Experimental runs at elevated temperatures have shown fatal failure of the Aremcolox 502-1100 ceramic fixture posts at locations of the threads as shown in Figure 5-21a. This special type of machinable ceramic was selected due to its very low thermal expansion coefficient of  $5.2 \mu\text{m}/\text{m}^\circ\text{C}$ . Due to the significant CTE mismatch between the stainless steel 316 bolts ( $16.2 \mu\text{m}/\text{m}^\circ\text{C}$ ) major stresses within the threads were responsible for the failure during thermal cycling.



a) Fractures of Aremcolox-standoffs

b) Wear-off in Aremcolox threads

**Figure 5-21: Ceramic Post Failures and Thread Wear**

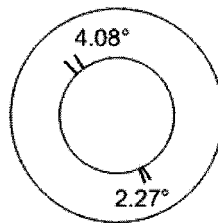
The porous structure of the Aremcolox 502-1100 ceramic posts also showed severe wear in the threads as shown in Figure 5-21b. It can be seen that the used teeth were almost sheared off after 25 to 30 fastening operations.

Although the Aremcolox 502-1100 ceramic posts provided an excellent  $\Delta$ CTE behavior ( $0.391 \mu\text{m}/^\circ\text{C}$ ), the continuous use of this posts in combination with the stainless steel bolts was not possible at higher temperatures. Thus, the posts were exchanged with the initial selected Steatite L-5 ceramic posts available from McMaster Carr (Part-# 94335A160). Unfortunately, the Steatite L-5 posts have a higher thermal expansion

coefficient of  $9.5 \mu\text{m}/\text{m}^\circ\text{C}$  and altered the  $\Delta\text{CTE}$  behavior to  $0.024 \mu\text{m}/^\circ\text{C}$  based on FEM calculations. Consequently, initial gap adjustments decreased to such small sizes, that the initial setting with the feeler gage was not possible anymore (smallest gauge thickness  $30 \mu\text{m}$ ). Therefore, a new method was used to adjust smaller gaps.

### 5.6.2 METHOD FOR INITIAL GAP ADJUSTMENT OF VERY SMALL GAPS

Due to the use of the higher expanding Steatite L-5 posts, initial gap sizes of 10 and  $18 \mu\text{m}$  have to be adjusted for achieving a  $\Delta T_{\text{CB}}$  of  $50^\circ\text{C}$  at bonding temperatures of  $500^\circ\text{C}$  and  $800^\circ\text{C}$  respectively (fixture settings Appendix F). The gap adjustment is made by an angular offset of the fine threaded set screw ( $3/4''$ -16 UNF) in the fixture top. The pitch of the set screw is  $1/16$  inch ( $1.5875 \text{ mm}$ ) per revolution. Hence, the angular offset for 10 and  $18 \mu\text{m}$  is  $2.27^\circ$  and  $4.08^\circ$  respectively. To assist in the process of setting the initial gap, a gauge ring with laser marks was laser machined as shown in Figure 5-22.



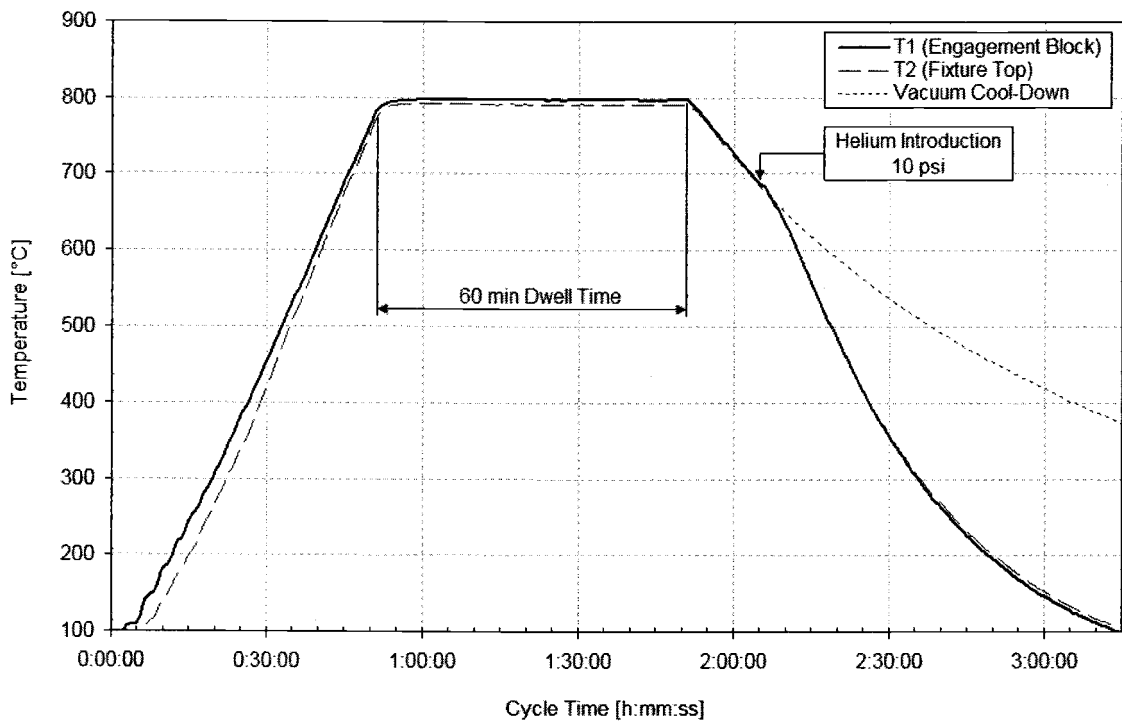
**Figure 5-22: Gauge Ring for Small Gap Adjustments**

After all parts are placed in the fixture and the fixture top is secured, the set screw was screwed down until it touches the load cell top. Subsequently, the gauge ring is placed with the appropriate laser mark aligned to the slot of the set screw. Finally, the set screw is rotated to the next laser mark setting the initial gap.

### 5.6.3 HIGH TEMPERATURE CYCLE TESTS WITH STEATITE L-5 POSTS

First test runs with the new Steatite L-5 posts were made at a temperature of  $500^\circ\text{C}$  with no problems. Test articles were successfully bonded and no major fin warpage was observed. Subsequently, the  $\Delta\text{CTE}$ -fixture was tested at a bonding temperature of  $800^\circ\text{C}$ . The  $\Delta\text{CTE}$ -fixture did not show any material failures due to high temperature cycling and showed full functionality. Test articles were also successfully bonded at  $800^\circ\text{C}$  without any major warpage effects. Furthermore, the Steatite L-5 posts showed less thread wear than observed on the Aremcolox posts. Some of the Steatite L-5 posts

however showed bubble creations on the glazed surface of the ceramic posts although the maximal service temperature is specified to be 930°C (1700 °F). Nevertheless, the posts were fully functional in spite of the bubbling issue in the glaze. Figure 5-23 shows high temperature measurements of the bonding cycle at 800°C with the implemented thermocouples. It can be seen that good control over the temperature profile is obtained by connecting the thermocouple at the engagement block directly to the temperature control unit.



**Figure 5-23: Temperature Profile of 800°C Bonding Cycle**

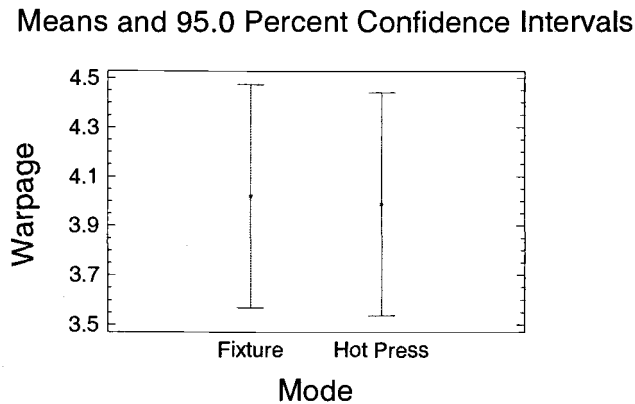
In addition, no significant temperature difference was detected between the temperature reading at the fixture top and at the engagement block. After completion of the cycle at 800°C, the introduction of helium was postponed until the cooling curve dropped below 700°C and started to flatten out to prevent severe oxidation effects (purity of used helium 99.5%) since the graphite heating elements were observed to glow at temperatures around 750°C. Hence, it is expected that quenching with room temperature helium could have a negative impact on the heating elements at temperatures above 750°C. Furthermore, by introducing helium at high temperatures,

the volumetric expansion of the quench gas could result in a high chamber pressure (i.e. > 10 psig).

## 5.7 VALIDATION OF THE $\Delta$ CTE-FIXTURE

### 5.7.1 RESULTS AND ANALYSIS OF FIN WARPAGE

After processing the 32 experimental runs the fin warpage was measured on the 64 test articles by scanning the channel fin with the Dektak<sup>3</sup> surface profiler. Since each test article had two fins a total of 128 measurements were taken. A multifactor analysis of variance (ANOVA) was performed to decompose the variability of the measured fin warpage into contributions due to the various factors (mode, temperature, pressure, time) and their interactions. The resulting ANOVA table with the calculated p-values can be seen in Appendix F. The analysis of variance has shown that there is no statistical significant difference between samples processed in the hot press or within the fixture on the basis of a p-value of 0.92 for the experimental factor mode. Figure 5-24 visualizes the mean warpage in  $\mu\text{m}$  for both methods with a 95% confidence interval.



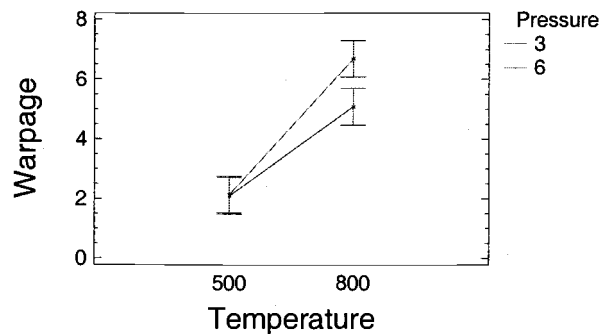
**Figure 5-24: Plot of Mean Fin Warpage based on the Experimental Mode**

The grand mean of the total 128 measurements processed at various bonding conditions is  $4.01 \mu\text{m}$  of fin warpage. This average fin warpage relates to a deviation in channel height of 2% and would not negatively affect the performance of a heat exchanger [24]. The mean fin warpage for specimens processed within the  $\Delta$ CTE-fixture was calculated as  $4.02 \mu\text{m}$  where the mean for specimens processed in the hot press was found to be  $3.99 \mu\text{m}$  as shown in Figure 5-24. Based on this study it can be

concluded that the diffusion bonding of devices within a  $\Delta$ CTE-fixture is not any different from processing devices in a hot press system. This is significant especially in light of the fact that the  $\Delta$ CTE-fixture has to engage prior to the bonding temperature inevitably resulting in warpage.

From the ANOVA table it can be seen that the factor temperature has clearly a statistically significant effect on fin warpage with a p-value of 0 since the fin buckling behavior is directly related to the coefficient of thermal expansion. Also pressure was found to significantly affect fin warpage with a p-value of 0.01. Similarly, it is very obvious that the interaction of temperature and pressure has a statistically significant effect on fin warpage as shown in Figure 5-25 (p-value of 0.014). No statistically significant effect on fin warpage was found for the experimental factor bonding time (p-value of 0.15).

Interactions and 95.0 Percent Confidence Intervals



**Figure 5-25: Interaction of Temperature and Pressure on Fin Warpage**

It can be seen that at lower temperatures the fin warpage is independent of the level of applied bonding pressure. However, at higher temperatures the application of a higher bonding pressure yields a significantly higher fin warpage than seen for a lower pressure. This can be explained by the fact that a certain misregistration in the layer stack creates a bending moment at the fin boundaries which is directly related to the level of pressure applied on the stack. Since the stiffness of the fin decreases with increased temperature the fin warpage will be more sensitive to the level of bonding pressure at higher temperatures.

An interesting relation can be seen by looking at the interaction plot of the experimental factors mode and pressure as illustrated in Figure 5-26. The p-value for the interaction of mode and pressure itself is statistically insignificant with a value of 0.092. However, it seems that the fin warpage observed within the  $\Delta$ CTE-fixture is less dependent on the level of pressure than seen for the hot press. The fin warpage for different levels of pressure is significantly different by using the hot press whereas the  $\Delta$ CTE-fixture does not show a significant difference of fin warpage for different levels of pressure. This could be due to either the fact that probably the level of pressure in the  $\Delta$ CTE-fixture was not comparable or that the more dynamic impact of pressure application within the hydraulic hot press. The examination of void fraction will show if the bonding conditions, especially the level of pressure, were similar for both bonding methods.

Interactions and 95.0 Percent Confidence Intervals

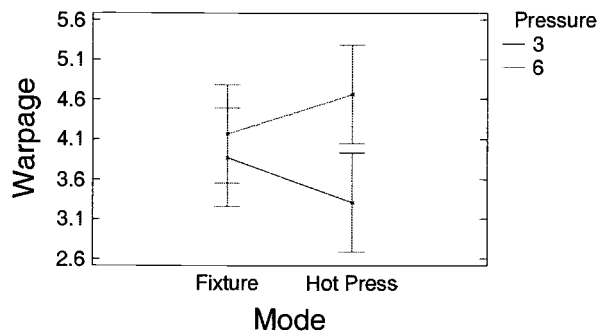


Figure 5-26: Interaction of Mode and Pressure on Fin Warpage

### 5.7.2 RESULTS AND ANALYSIS OF VOID FRACTION

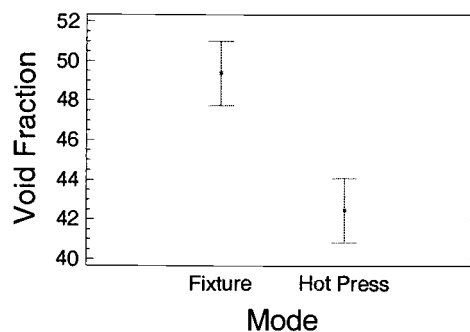
After measuring the fin warpage, samples bonded at similar conditions were molded in epoxy for metallurgical inspection of the bond lines. Eight different bonding conditions based on pressure, temperature and time resulted in 16 total samples across the two bonding platforms. Each sample contained four test articles and was cut through the center of the test articles with a diamond wafer blade. Subsequent polishing of the samples allowed the metallurgical inspection of the bond lines and determination of the void fractions at the different bonding conditions. Ten video images of the bond lines were taken for each sample for a total of 160 metallurgical pictures. An observation

length of 250  $\mu\text{m}$  for the determination of the void fractions was defined with the video measurement system (VIA-100) on a LEICA optical microscope. Voids at the bond lines were marked on a transparency foil on the computer screen at a magnification of 384X. The void fraction ( $v_f$ ) at the bond lines were calculated according to Equation 31.

$$v_f = \frac{\sum l_{\text{void}}}{l_0} \cdot 100\% \quad (31)$$

The micrographs of the bond lines with the determined void fraction for each bond line can be seen in Appendix F. Overall, the void fraction ranged from 8.0% to 100%. A multifactor analysis of variance (ANOVA) was performed to decompose the variability of the measured void fraction into contributions due to the various factors (mode, temperature, pressure, time) and their interactions. The resulting ANOVA table with the calculated p-values can be seen in Appendix F. The analysis of variance has shown that there is statistical significant difference between samples processed in the hot press or with the fixture for the experimental factor mode as seen in Figure 5-27. In addition, all experimental factors have a statistically significant influence on the resulting fraction of voids, where the factor temperature shows the strongest influence (highest F-ratio). This is not surprising as time, temperature and pressure were previously known to cause these effects. The main purpose of the experiment was to compare the different bonding platforms (mode) over a broad process design space.

Means and 95.0 Percent Confidence Intervals



**Figure 5-27: Mean Void Fraction for Experimental Factor Mode (see Appendix F)**

Where the hot press produced a void fraction of 43% overall, the  $\Delta\text{CTE}$ -fixture was found to have a significantly higher overall void fraction of 49% as listed in Table 5-8.

Experimental runs at 500°C/3MPa/30min did not show a sound bond and the layers were clearly separated although the layers seemed to be joined after processing. Such weak bonds are sometimes referred to as “kiss bonds” [32].

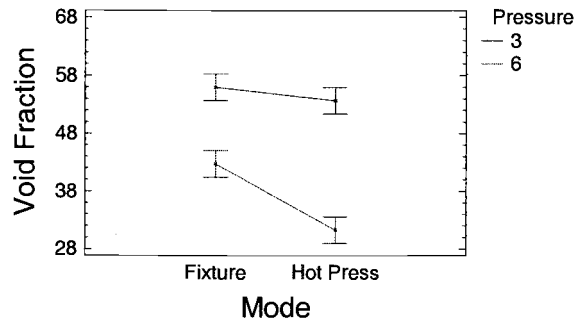
The comparison of the average void fractions in Table 5-8 for the different bonding conditions shows that the results obtained from the  $\Delta$ CTE-fixture are not greatly different from the hot press results and that the general trend is for the void fraction in the  $\Delta$ CTE-fixture to be higher. Although the experimental analysis shows that there is a statistically significant difference between samples bonded in the hot press compared to samples processed in the  $\Delta$ CTE-fixture, it can be seen that of all four main factors, the mode of the experiment matters slightest based on the smallest F-ratio observed.

**Table 5-8: Mean Void Fractions observed at Bonding Conditions**

Bonding Conditions	Void Fraction Hot Press	S.D.	Void Fraction $\Delta$ CTE-Fixture	S.D.
500°C/3MPa/30min	100.0%	0%	100.0%	0%
500°C/3MPa/60min	78.8%	8.4%	70.5%	8.7%
500°C/6MPa/30min	65.7%	10.3%	80.0%	6.2%
500°C/6MPa/60min	35.9%	12.0%	62.0%	7.3%
800°C/3MPa/30min	20.1%	6.9%	30.3%	10.3%
800°C/3MPa/60min	15.8%	9.5%	23.2%	4.2%
800°C/6MPa/30min	15.5%	3.7%	19.5%	8.5%
800°C/6MPa/60min	8.0%	2.4%	9.6%	2.8%
Overall	<b>42.5%</b>	<b>6.7%</b>	<b>49.4%</b>	<b>6.0%</b>

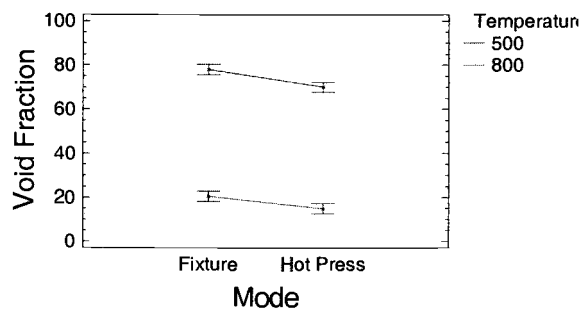
Major differences can be seen for the samples processed at 500°C with a bonding pressure of 6 MPa. The significant differences in the void fraction suggest that the preloading of the load cell was probably in error during these experiments. Since temperature and time for both experimental modes were equal, the source of variation has to be found in the level of pressure applied. From the interaction plot of the experimental mode and the level of pressure visualized in Figure 5-28 it can be seen that the level of pressure in the  $\Delta$ CTE-fixture was lower compared to the hot press.

Interactions and 95.0 Percent Confidence Intervals

**Figure 5-28: Interaction of Experimental Mode and Pressure on Void Fraction**

Considerably lower pressure in the  $\Delta$ CTE-fixture can be seen for samples processed at higher pressures (6 MPa) based on the significant difference in the mean amount of void fraction. At lower pressures (3 MPa) the difference in the average void fraction between the  $\Delta$ CTE-fixture and the hot press is less significant. The difference could be attributed to the fact that the stainless steel bolts used for fastening the load cell and fixture frame were highly expanding and therefore altered the expected level of pressure due to the loss of rigidity. Furthermore, it can be seen that the difference between the  $\Delta$ CTE-fixture and the hot press is less significant at higher temperatures as listed in Table 5-8 and as visualized in the interaction plot in Figure 5-29. Reasons for that could be found in the higher expansion rate during the high temperature bonding cycle and therefore the better elimination of initial tolerances and the proper release of the load cell preload. Of course, this could also suggest that the diffusion bonding process is simply more tolerant to pressure fluctuations at higher temperatures.

Interactions and 95.0 Percent Confidence Intervals

**Figure 5-29: Interaction of Mode and Temperature on Void Fraction**

It is believed that with some modifications to the fixture post design (see recommendations for future work) and the use of molybdenum fasteners in the load cell, the level of pressure within the  $\Delta$ CTE-fixture could be made more accurate and comparable. However, the  $\Delta$ CTE-fixture still yielded predictable and comparable bonding results especially at high temperatures as shown in the void fraction comparison in Table 5-9.

**Table 5-9: Void Fraction Comparison Hot Press vs.  $\Delta$ CTE-Fixture**

Hot Press 800°C / 6MPa / 60min	$\Delta$ CTE-Fixture 800°C / 6MPa / 60min
. . . . .	. . . . .
. . . . .	. . . . .
. . . . .	. . . . .
. . . . .	. . . . .
. . . . .	. . . . .
. . . . .	. . . . .
. . . . .	. . . . .
. . . . .	. . . . .
. . . . .	. . . . .
. . . . .	. . . . .
Avg. Void Fraction: 8.0%	Avg. Void Fraction: 9.6%

Functionality of the static fixture investigated in this thesis was demonstrated even at high temperatures of 800°C without any fin warpage effects and comparable bond quality as visualized in Table 5-9. Therefore, it can be concluded that this bonding approach is plausible for the microlamination of MECS devices.

## 6 CONCLUSIONS

### 6.1 THESIS SUMMARY

A new and unique thermal bonding device using differential thermal expansion has been presented in this thesis. It was shown that a controllable bonding pressure based on the difference in coefficients of thermal expansion ( $\Delta\text{CTE}$ ) requires control of not only the magnitude of bonding pressure but also the timing of bonding pressure application within the temperature profile. Further, it was shown that the use of disc springs can significantly reduce the pressure sensitivity of the bonding fixture compared with prior efforts to simply put a highly expanding material between a lower expanding frame construction [12].

A conceptual study of possible fixture designs was conducted and the feasibility of the final device concept was theoretically validated by a finite element model. Experimental investigations with a fixture prototype have proven the functionality of the proposed bonding device. This study has shown that the bonding pressure magnitude, timing and sensitivity in a diffusion bonding process can be controlled with the use of a static bonding fixture suggesting a plausible route towards the high-volume microlamination of diffusion-bonded MECS devices.

The recommended design of a  $\Delta\text{CTE}$  bonding device investigated in this thesis claims the use of high temperature spring elements (Belleville disc springs) to control the pressure magnitude and sensitivity of the bonding device. Further, it has been shown that the storage of a preloaded force in the spring elements can be used favorably to adjust exactly the desired level of pressure. Any further compression of the spring elements due to temperature swings has a minor influence on the magnitude of bonding pressure which makes the bonding device more robust.

The timing for applying bonding pressure within the temperature cycle was found to be a key factor for the prevention of fin warpage which is known to be an important consideration in microlaminated MECS devices. The timing of the pressure within the  $\Delta\text{CTE}$  bonding device was realized by setting an initial gap between the lower expanding frame construction and the higher expanding inner parts (platens, laminae, load cell and engagement block). Gap size was adjusted with a fine threaded set

screw. It was found that the use of a precise feeler gauge allows a simple and repeatable gap adjustment and yields a correct timing of pressure. Furthermore, the initial gap adjustment can also be performed adequately by calculating the angular offset of the fine threaded set screw depending on the thread pitch. An extensive experimental study (128 measurements) has shown that there is no statistically significant difference between the bonding pressure timing within the  $\Delta$ CTE-fixture or with the hot press based on the resulting fin warpage. Functionality of the  $\Delta$ CTE-fixture was also experimentally proved at low temperatures (180°C) with the use of pressure sensitive film (Fuji Prescale<sup>TM</sup>). The readings of the pressure sensitive film showed uniform pressure distribution within the bonding area of the  $\Delta$ CTE-fixture.

Thirty-two randomized bonding experiments at various bonding conditions were conducted to compare the bonding quality between samples bonded in the hot press and samples made within the  $\Delta$ CTE-fixture. The metallographic inspection of the void fractions for different bonding conditions has shown that the bonding quality of the  $\Delta$ CTE-fixture is comparable to samples bonded in the hot press although a statistically significant difference based on the void fraction readings was found. The difference can be attributed to the use of highly expanding stainless steel bolts which had to be used for securing the load cell and fixture frame which required the use of disc springs on the fixture frame and loss of frame rigidity. Based on the experimental investigations and “lessons learned” with the prototype fixture various recommendations and improvements have been proposed for future fixture designs. It is expected that solid engagement blocks and set screws could be replaced by a pneumatic or hydraulic engagement mechanism which would provide better pressure uniformity for large-substrate designs.

The  $\Delta$ CTE-fixture design investigated in this thesis has demonstrated several major advantages over existing designs in the patent literature. One major advantage involves the ability to decouple the pressure magnitude from the process temperature through the concept of preloading and force storage within a load cell. In other words, initial gap settings are independent of the pressure magnitude and, therefore, any level of bonding pressure can be achieved by processing at high as well as at low temperatures. In prior designs, changes in processing conditions and number of laminae would require changes in expansion block materials used which might limit the feasible set of bonding

process conditions achievable by the clamp. This flexibility makes the investigated  $\Delta$ CTE bonding device not only interesting for diffusion bonding, but also for any thermal bonding process. A second major advantage (as has already been described) is the ability to control the timing at which the bonding pressure is applied during the temperature cycle. A third major advantage (as has already been described) is that the fixture is much less sensitive to fluctuations in bonding temperature.

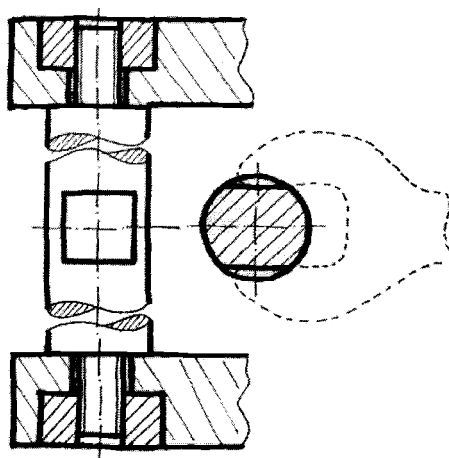
Major advantages also exist for the use of a  $\Delta$ CTE-fixture over existing vacuum hot press platforms. By replacing the solid engagement block in the  $\Delta$ CTE fixture with a pneumatic or hydraulic engagement mechanism, the first major advantage would be the ability to provide better pressure uniformity over the surface of large substrates. This will become increasingly more important as economics dictate the use of ever larger substrates for the microlamination of MECS devices. A second major advantage of the fixture is that it does not require dynamic loading at the bonding temperature. Loading of the bonding pressure in the CTE device is gradual. This may become important with heightened efforts to increase layer-to-layer registration precision and reduce fin warpage. And finally, like other differential CTE devices, the use of a  $\Delta$ CTE bonding device opens the possibility for the high-volume microlamination of MECS devices within a continuous furnace system which will permit the optimization of diffusion bonding (and ultimately any thermal bonding) cycles.

## **6.2 RECOMMENDATIONS FOR FUTURE WORK**

The investigations made in this thesis have shown the feasibility and functionality of a fixture concept for small substrate MECS applications. However, future fixtures must accomodate large-substrate MECS devices. It is believed that establishing a uniform pressure distribution will be one of the major difficulties in the design of a large-substrate  $\Delta$ CTE bonding unit. Therefore, extensive finite element studies should be carried out in order to evaluate an appropriate fixture design. Also, the role of thermal gradients throughout the bonding fixture will become more important as the fixture dimensions increase. Thus, thermal gradients could become a potential source of warpage in the microlamination of large-substrate devices. Consequently, the finite element model should be carried out with elements which have thermal analysis capabilities to study the effects of temperature distribution. The fixture modeling with

thermal elements would furthermore allow the complete simulation of the thermal bonding cycle with respect to heating-up and cooling-down of the fixture and the device. Such a model would allow process parameter selection within a conveyorized furnace system by defining the appropriate heating and cooling rates (i.e. temperature profile).

The prototype device used in this thesis was designed with ceramic posts in order to achieve a low expanding frame construction. During experimental investigations it was found that in the threaded regions of the ceramic posts, major wear and cracks negatively affected the continuous use of the fixture. For future fixture designs it is recommended to use molybdenum as a material for the fixture posts since molybdenum has a low CTE comparable to many low CTE ceramic materials. Although molybdenum has a high density, the post diameter can be reduced significantly compared to the ceramic posts used in this thesis since molybdenum allows much higher tensile loading. Furthermore, threads can be directly integrated at the ends of the molybdenum posts as shown in the conceptual design in Figure 6-1 and guarantee a long life.



**Figure 6-1: Design Recommendation for Future Fixture Post Design**

Machineable ceramic can be used as fixture platens and would significantly lower the overall weight of the fixture, especially for the design of a large-substrate fixture. The threaded connection between posts and platens can be done with the use of graphite sleeves. Hence, no wear would be experienced in the ceramic platens and the sleeves would provide an inexpensive solution to be replaced if necessary. By making a left and right-handed thread at the post ends the frame can be fastened by simply wrenching the posts as shown in Figure 6-1. This would provide a fast and simple approach to

fixture frame assembly. Similarly the design of the load cell can be modified. It is recommended that a machineable ceramic be used as the structural platens and that custom-made molybdenum bolts be used to fasten the platens together. Threaded graphite sleeves would also be recommended here to provide wear in the ceramic platens. Following these recommendations, a durable and robust large-substrate static fixture for high-volume production seems feasible.

## 7 REFERENCES

### Patent Documents

- [1] U.S. Patent No. 5,564,620, 1996, "Metal-Intermetallic or Metal-Ceramic Composites by Self-Propagating High-Temperature Reactions", J. C. Rawers, D. E. Alman, A. V. Petty
- [2] U.S. Patent No. 6,672,502 B1, 2004, "Method for Making Devices Having Intermetallic Structures and Intermetallic Devices Made Thereby" B. K. Paul, R. D. Wilson, D. E. Alman
- [3] U.S. Patent No. 5,611,214, 1997, "Microcomponent sheet architecture" R. S. Wegeng, K. M. Drost, C. E. McDonald
- [4] U.S. Patent No. 5,811,062, 1998, "Microcomponent chemical process sheet architecture" R. S. Wegeng, K. M. Drost, C. J. Call, J. G. Birmingham, C. E. McDonald, D. E. Kurath, M. Friedrich
- [5] U.S. Patent No. 4,636,149, 1987, "Differential Thermal Expansion Driven Pump", D. C. Brown
- [6] U.S. Patent No. 5,133,210, 1992, "Thermal Expansion Driven Indentation Stress-Strain System", J. J. Lesko, R. W. Armstrong
- [7] U.S. Patent No. 5,315,463, 1994, "Disk File Having Thermal Expansion Ring for Ensuring Disk/Hub Concentricity", G. N. Dew, A. R. Hearn, D. J. Sebborn, T. Young
- [8] U.S. Patent No. 5,439,306, 1995, "Device for Assembling Two Elements of Materials Having Different Coefficients of Thermal Expansion", J. C. N. Lhernould
- [9] U.S. Patent No. 5,460,703, 1995, "Low Thermal Expansion Clamping Mechanism", J. Nulman, R. E. Davenport
- [10] U.S. Patent No. 6,228,200, 2001, "Belt Press Using Differential Thermal Expansion", J. A. Willis, A. J. Willis
- [11] U.S. Patent No. 6,675,456, 2004, "Alignment Plate with Matched Thermal Coefficient of Expansion Method", R. J. Pommer
- [12] U.S. Patent Application Publication No. US2003/0221777 A1, 2003, "Method and Apparatus for Application of Pressure to a Workpiece by Thermal Expansion", D.C. McHerron, K. S. Patel, C. L. Tessler, J. A. Gorrell, J. E. Tersigni

### Journal and Conference Publications

- [13] B. K. Paul, R. B. Peterson, "Microlamination for Microtechnology-based Energy, Chemical, and Biological Systems," ASME International Mechanical Engineering Congress and Exposition, Nashville, Tennessee, AES Volume 39, November 15-20, 1999, pp 45-52

- [14] P. M. Martin, W. D. Bennett, J. W. Johnston, "Microchannel Heat Exchangers for Advanced Climate Control", Proceedings of SPIE, 1995, v. 2639, p. 82-88
- [15] P. M. Martin, D. W. Matson, W. D. Bennett, D. J. Hammerstrom, "Fabrication of Plastic Microfluidic Components", Proceedings of SPIE, 1998, v. 3515, p. 172-176
- [16] P. M. Martin, D. W. Matson, A. L. Tonkovich, G. L. Roberts, "Fabrication of a Stainless Steel Microchannel Microcombustor Using a Lamination Process", Proceedings of SPIE, 1998, v. 3514, p. 386-392
- [17] P. M. Martin, D. W. Matson, W. D. Bennett, D. C. Steward, Y. Lin, "Laser Micromachined and Laminated Microfluidic Components for Miniaturized Thermal, Chemical and Biological Systems", Proceedings of SPIE, 1999, v. 3680, p. 826-833
- [18] P. M. Martin, D. W. Matson, W. D. Bennett, D. C. Steward, C. C. Bonham, "Laminated Ceramic Components for Micro Fluidic Applications", Proceedings of SPIE, 1999, v. 3877, p. 95-100
- [19] B. K. Paul, T. Dewey, D. Alman, R. D. Wilson, "Intermetallic Microlamination for High Temperature Reactors", 4<sup>th</sup> Int. Conf. Microreaction Tech, Tennessee, November 15-20, 1999, pp. 45-52
- [20] B. K. Paul, J. S. Thomas, "Thermally-Enhanced Edge Registration for Aligning Metallic Microlaminated Devices", Society of Manufacturing Engineers, Dearborn, MI, 2002
- [21] W. Wattanuchariya, B. K. Paul, "Bonding Fixture Tolerances for High-Volume Metal Microlamination Based on Fin Buckling and Laminae Misalignment Behavior", Precision Engineering, 28(2), 2004, pp. 117-128
- [22] W. Wattanuchariya, B. K. Paul, "The Effect of Fixture Compliance on Thermally-Enhanced Edge Registration in Microlamination," in review JMfgSE, 2004
- [23] N. Sharma, J. D. Porter, B. K. Paul, "Understanding Cost Drivers in Microlamination Approaches to Microsystem Development", Industrial Engineering Research Conference, Portland, OR, May 18-20, 2003
- [24] W. Wattanuchariya, "Application of Buckling Behavior to Evaluate and Control Shape Variation in High-Temperature Microlamination," Ph.D. Dissertation, 2002, Oregon State University
- [25] K. Kanlayasiri, "Development of Nickelaluminide Microchannel Array Devices for High-Temperature Applications", Ph.D. Dissertation, 2003, Oregon State University
- [26] K. P. Kaemper, W. Ehrfeld, J. Doepper, V. Hessel, H. Lehr, H. Loewe, Th. Richter, A. Wolf, "Microfluidic Components for Biological and Chemical Microreactors", Proceedings IEEE Micro Electro Mechanical Systems, 1997, p. 338-343

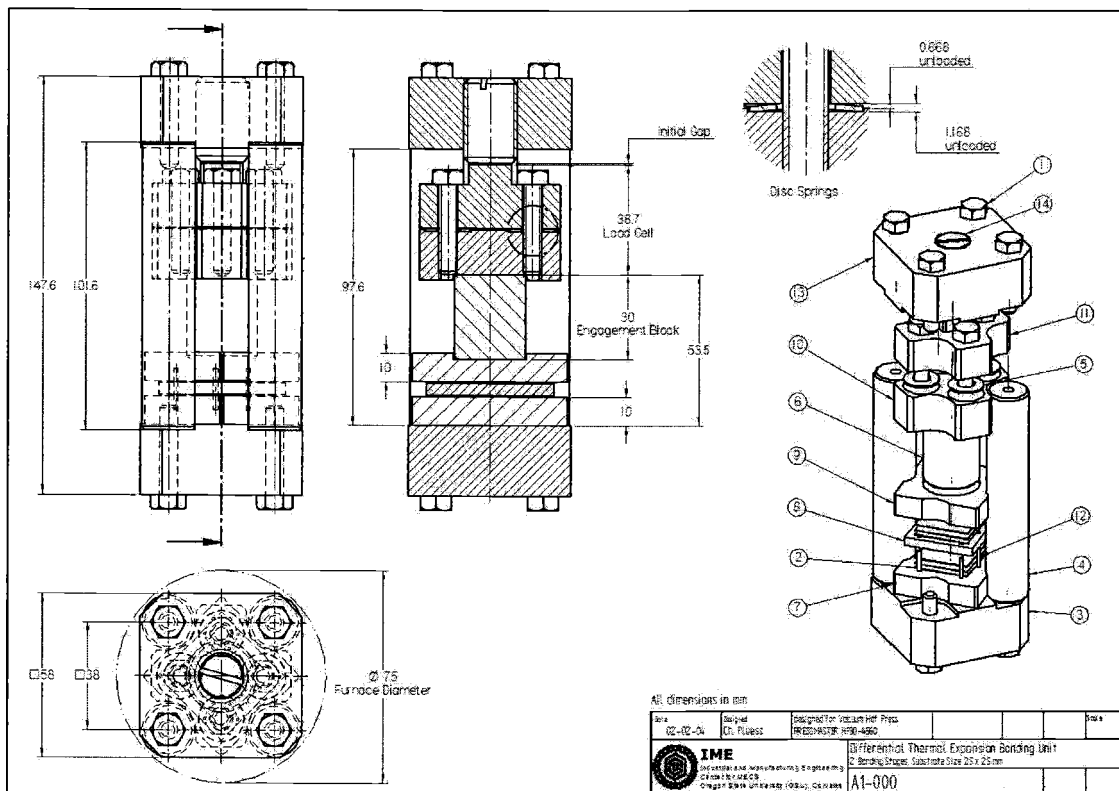
- [27] H. Loewe, W. Ehrfeld "State-of-the-Art in Microreaction Technology: Concepts, Manufacturing and Applications", *Electrochimica Acta*, 1998, v. 44, p. 3679-3689
- [28] M. Bachman, Y-M. Chiang, C. Chu, G. P. Li, "Laminated Microfluidic Structures Using a Micromolding Technique", *Proceedings of SPIE*, 1999, v. 3877, p. 139-146
- [29] S. Kiese-walter, "The Catalogue – Process Technology of Tomorrow", Institut für Mikrotechnologie Mainz (IMM), Germany, 2003
- [30] L. M. Pua, S. O. Rumbold, "Industrial Microchannel Devices – Where are we today?", 1<sup>st</sup> International Conference on Microchannels and Minichannels, April 24-25, 2003, Rochester, New York
- [31] S. B. Dunkerton, "Diffusion bonding – process and applications", *Welding and Metal Fabrication*, 1991, v. 59, p. 132,134-136
- [32] Z. C. Wang, N. Ridley, G. W. Lorimer, "Evaluation of diffusion bonds formed between superplastic sheet materials", *Journal of Materials Science*, 1996, v. 31, p. 5199-5206
- [33] I. Iswadi, H. Ogiyama, H. Tsukuda, "Solid State Diffusion Bonding of Superplastic Duplex Stainless Steel with Carbon Steel", *Materials Science Research International*, 2003, v. 9, p. 154-159
- [34] W. R. Jones, "Helium Gas Cooling Offers Cost Benefits", *Industrial Heating, International Journal of Thermal Technology*, 2002, [www.industrialheating.com](http://www.industrialheating.com)
- [35] R. Hill Jr., "High Gas Velocity: A New Frontier of Cooling Performance in Vacuum Furnaces", *Industrial Heating, International Journal of Thermal Technology*, 2004, [www.industrialheating.com](http://www.industrialheating.com)

#### Bibliography

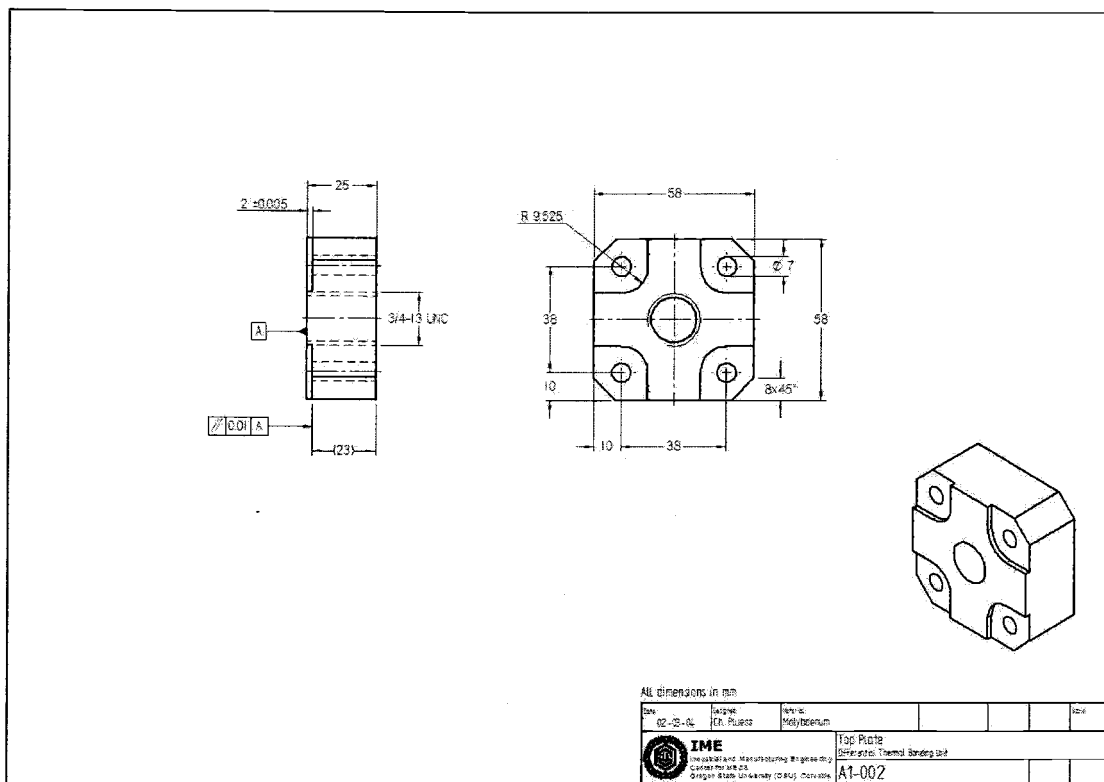
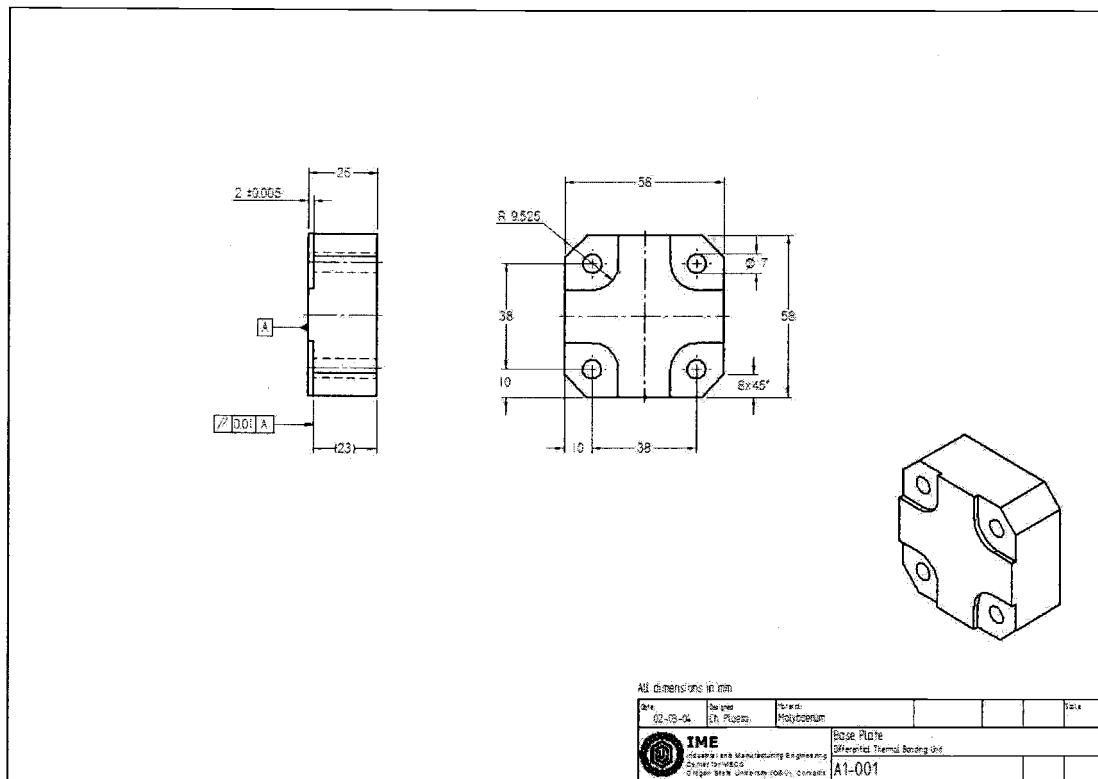
- [36] G. Kovacs, "Micromachined Transducers Sourcebook", McGraw-Hill, New York, NY, 1998
- [37] W. Ehrfeld, V. Hessel, H. Lowe, Chapter 2, "Modern Microfabrication Techniques for Microreactors", *New Technology for Modern Chemistry*, Wiley-VCH, New York, 2000, pp. 30-33
- [38] M. Koch, A. Evans, A. Brunnschweiler, "Microfluidic Technology and Applications", Research Studies Press Ltd., Hertfordshire, England, 2000
- [39] N. F. Kazakov, "Diffusion Bonding of Materials", Pergamon Press Inc., New York, NY, 1985
- [40] P. Kohnke, "ANSYS Theory Manual Release 5.7", ANSYS Inc., Canonsburg, PA, 2001
- [41] R. M. Jones, "Mechanics of Composite Materials", Taylor and Francis, Philadelphia, PA, 1999

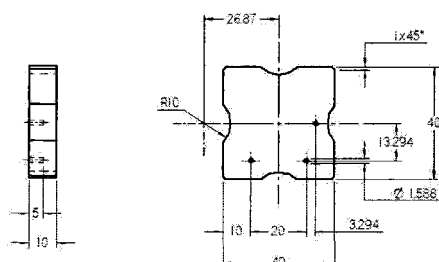
## 8 APPENDICES

## **APPENDIX A: FIXTURE DRAWINGS**



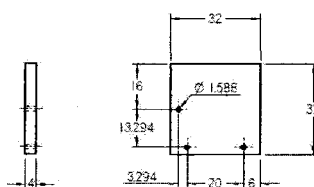
Pos	#	Name Drawing-Nr.	Material Dimensions	Vendor	Price per piece
1	12	Ceramic Screw	99.8% Al <sub>2</sub> O <sub>3</sub> 1/4"-20 x 1-1/4"	Ceramco Inc.	\$13.00
2	6	Substrate A1-013	Alloy 110 Copper Shim Stock 25 x 25mm, 0.008"	McMaster Carr Coil 6" x 50" Part-#: 9709K65	\$24.00
3	1	Base Plate A1-001	Molybdenum 60 x 60 x 30mm	Goodfellow Corp.	\$400.00
4	4	Frame Standoffs	Aremcolox 502-1100 Ø 3/4" x 4"	Aremco Inc.	\$72.50
5	4	Disc Springs	Inconel 718 0.317"x0.625"x0.046"	McMaster Carr Part-#: 97125K31	\$3.00
6	1	Engagement Block A1-006	SS 321 Ø2" x 12"	McMaster Carr Part-#: 86615K76	\$72.00
7	1	Bonding Platen A1-003	Graphite ISO-63		
8	1	Interlayer A1-004	Graphite ISO-63		
9	1	Bonding Platen A1-005	Graphite ISO-63		
10	1	Load Cell Bottom A1-007	Molybdenum 50 x 50 x 25mm	Goodfellow Corp.	\$300.00
11	1	Load Cell Top A1-008	Molybdenum 50 x 50 x 25mm	Goodfellow Corp.	\$300.00
12	3	Alignment Pin A1-011	Tungsten Ø1/16" x 15mm		
13	1	Top Plate A1-002	Molybdenum 60 x 60 x 30mm	Goodfellow Corp.	\$400.00
14	1	Set Screw A1-010	Graphite ISO-63		
Total Costs (w/o Machining Costs)					<b>\$1954.00</b>





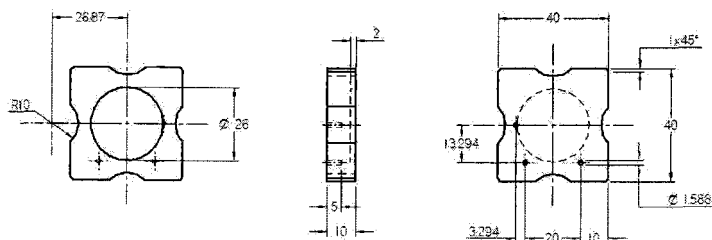
All dimensions in mm

Part	Design	Material	Side
02-03-04	On P. 003	Graphite	
<b>IME</b> Industrie e Macchine S.p.A. - Via S. Maria 10 - 20139 Milano (Italy) Graphite parts and components			
Bonding Piston Bottoms Graphite Thermal Binding Unit <b>A1-003</b>			



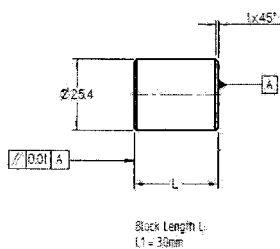
All dimensions in mm

Part	Design	Material	Side
02-03-04	On P. 003	Graphite	
<b>IME</b> Industrie e Macchine S.p.A. - Via S. Maria 10 - 20139 Milano (Italy) Graphite parts and components			
Interlayer Graphite Thermal Binding Unit <b>A1-004</b>			



All dimensions in mm

Rev.	Design	Drawn	Checked	By	Date
00-05-A	En. P. Rios	En. P. Rios	En. P. Rios		
<b>IME</b> Industrial and Manufacturing Engineering University of the Pacific Oregón State University (USA) - Oregón					
Bonding Plate (top) Differential Thermal Bonding Unit A1-005					

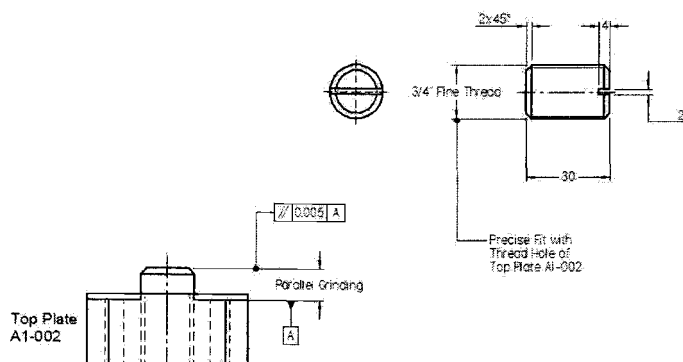


Block Length L:  
L1 = 30mm

All dimensions in mm

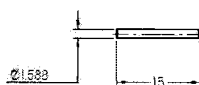
Rev.	Design	Drawn	Checked	By	Date
02-05-A	En. P. Rios	En. P. Rios	En. P. Rios		
<b>IME</b> Industrial and Manufacturing Engineering University of the Pacific Oregón State University (USA) - Oregón					
Engagement Block Differential Thermal Bonding Unit A1-006					





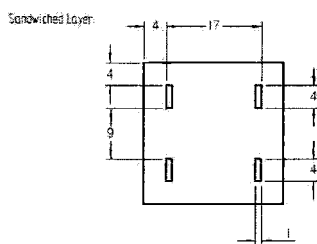
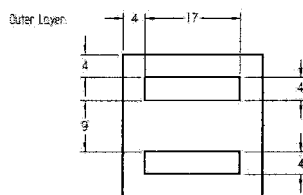
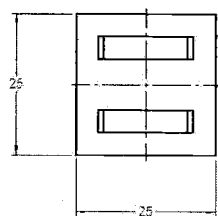
All dimensions in mm

Rev	Design	Ch. Process	Form	Graphical Id.	Rev	Rev
02-05-06				Graphical Id.: 70		
IME			Set Screw			
Industrial and Manufacturing Engineering			Differential Thermal Bonding Unit			
Centro de Investigación y Desarrollo en Ingeniería			A1-010			
Código de barras: 00000000000000						

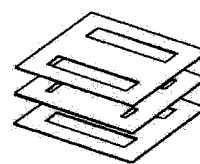


All dimensions in mm

Rev	Design	Ch. Process	Form	Graphical Id.	Rev	Rev
02-05-06				Graphical Id.		
IME			Alignment Pin			
Industrial and Manufacturing Engineering			Differential Thermal Bonding Unit			
Centro de Investigación y Desarrollo en Ingeniería			A1-011			
Código de barras: 00000000000000						



Stacking Order 3 Layer

Bonding Area: 685 mm<sup>2</sup>

All dimensions in mm

Rev	Design	Material				Rev
02-08-04	ON-FLUERS	Copper 6 mils (0.1524mm)				
IME INTEGRATED MANUFACTURING ENGINEERING CALIFORNIA MICROELECTRONICS DRAGON-TEAM UNIVERSITY (DTEAM) CENTER			Test Article "Timing Effect"			
			Differential Thermal Bonding Unit			
			A1-013			

## **APPENDIX B: APDL-MACRO FE-MODEL**

```

!-----APDL-Macro-----!
!-----CTE BONDING FIXTURE-----!
!-----!
!-----Copyright(C), 06/24/2004, Ch.Pluess-----!
!-----!

/SOLU                                     !Set initial conditions
ANTYPE,STATIC
NROPT,FULL
/PREP7
ESEL,ALL
EALIVE,ALL
FINISH
!
/SOLU
TREF,20                                  !Reference temperature 20°C
!-----

!Load Step 1:
NSEL,ALL
BFUNIF,TEMP,TR
T1=1E-6
TIME,T1
NSUBST,1
LSWRITE,1
!-----

!Load Step 2:
NSEL,ALL
TS=TC-10
BFUNIF,TEMP,TS
T2=(TS-TR)/R
TIME,T2
NSUBST,1
LSWRITE,2
!-----

!Load Step 3:
NSEL,ALL
BFUNIF,TEMP,TC
T3=(TC-TR)/R
TIME,T3
DELTIM,0.25
LSWRITE,3
!-----

!Load Step 4:
NSEL,ALL
BFUNIF,TEMP,TB
T4=(TB-TR)/R
TIME,T4
DELTIM,0.25
LSWRITE,4
!-----

```

!Load Step 5:

NSEL,ALL

BFUNIF,TEMP,TB

T5=T4+10

TIME,T5

DELTIM,OFF

NSUBST,1

LSWRITE,5

!-----

RESCONTROL,ALL,ALL

OUTRES,ALL,ALL

!Write every substep

\*DO,I,1,5,1

LSREAD,I

!Read-in LS files

\*IF,I,LE,3,THEN

SOLVE

\*ELSE

ESEL,S,ELEM,,8252,8253

!Select LINK10 elements

EKILL,ALL

!Deactivate LINK10 elements

ESEL,S,LIVE

!Select all active elements

NSEL,INVE

D,ALL,ALL,0

!Constrain floating nodes

NSEL,ALL

!Select all nodes

ESEL,ALL

!Select all elements

SAVE

SOLVE

\*ENDIF

\*ENDDO

FINISH

## **APPENDIX C: FE-MODEL SIMULATION SETTINGS**

# C1: Fixture Settings and Calculation of Initial Strain Values (ISTRN)

**Table C1-1:  $T_B=800^{\circ}\text{C}$  /  $T_C=700^{\circ}\text{C}$  /  $p_B=4\text{MPa}$**

Bonding Data Input			CTE Fixture Data Output: Preload Load Cell		
Room Temperature	20	$^{\circ}\text{C}$	Active Warpage Temperature Range	100	$^{\circ}\text{C}$
Bonding Temperature	800	$^{\circ}\text{C}$	Load Cell Force at Bonding Temperature	2500	N
Temperature of Contact	700	$^{\circ}\text{C}$	Load Cell Force at Contact Temperature	2072	N
Bonding Area (Test Article)	625	$\text{mm}^2$	Load Cell Force at Room Temperature	2341	N
Desired Bonding Pressure	4.0	MPa	Preload Force (Hot Press)	526	lbs
CTE Fixture Data Input			CTE Fixture Data Output: Initial Gap		
Gap Closure Function	0.391	$\mu\text{m}/^{\circ}\text{C}$	Additional Load Cell Compression	-25	$\mu\text{m}$
CTE Load Cell Fasteners	8.2	$10^{-6}/^{\circ}\text{C}$	Spring Constant per Stack	2740	N/mm
CTE Load Cell Platens	6.5	$10^{-6}/^{\circ}\text{C}$	Active Force per Spring Stack at Room T.	585	N
Active Expanding Bolt Length	16.7	mm	Active Force per Spring Stack at Contact	518	N
Thickness Load Cell Top	15.5	mm	Active Force per Spring Stack at Bonding T.	625	N
Tensile Stress Area Bolt	20.5	$\text{mm}^2$	Tensile Stress of Bolts at Room Temp.	29	MPa
Nominal Load Disc Spring	800	N	Tensile Stress of Bolts at Contact Temp.	25	MPa
Nominal Compression D.S.	0.292	mm	Load Cell Compression at Room Temp.	214	$\mu\text{m}$
Number of Springs per Stack	1		Load Cell Compression at Contact Temp.	189	$\mu\text{m}$
Number of Spring Stacks	4		Load Cell Compression at Bonding Temp.	228	$\mu\text{m}$
			Expansion Potential CTE Fixture	305	$\mu\text{m}$
			Active CTE Compression of Load Cell	39	$\mu\text{m}$
			Starting Pressure at Contact Temperature	3.3	MPa
			Pressure Sensitivity CTE Fixture in f(T)	0.0069	$\text{MPa}/^{\circ}\text{C}$
			Pressure Sensitivity CTE Fixture in f(z)	0.0175	$\text{MPa}/\mu\text{m}$
			Adjustable Initial Gap	266	$\mu\text{m}$
FEM Model Data Input			FEM Model Data Output: Real Constant Settings		
Element Length LINK10 (T.o.)	13.668	mm	ISTRN Value for LINK10 (Tension only)	0.01563	214
Element Length LINK10 (C.o.)	7.332	mm	ISTRN Value for LINK10 (Compr. only)	0.00713	52

**Table C1-2:  $T_B=800^{\circ}\text{C}$  /  $T_C=750^{\circ}\text{C}$  /  $p_B=4\text{MPa}$** 

Bonding Data Input			CTE Fixture Data Output: Preload Load Cell		
Room Temperature	20	$^{\circ}\text{C}$	Active Warpage Temperature Range	50	$^{\circ}\text{C}$
Bonding Temperature	800	$^{\circ}\text{C}$	Load Cell Force at Bonding Temperature	2500	N
Temperature of Contact	750	$^{\circ}\text{C}$	Load Cell Force at Contact Temperature	2286	N
Bonding Area (Test Article)	625	$\text{mm}^2$	Load Cell Force at Room Temperature	2575	N
Desired Bonding Pressure	4.0	MPa	Preload Force (Hot Press)	579	lbs
CTE Fixture Data Input			CTE Fixture Data Output: Initial Gap		
Gap Closure Function	0.391	$\mu\text{m}/^{\circ}\text{C}$	Additional Load Cell Compression	-26	$\mu\text{m}$
CTE Load Cell Fasteners	8.2	$10^{-6}/^{\circ}\text{C}$	Spring Constant per Stack	2740	N/mm
CTE Load Cell Platens	6.5	$10^{-6}/^{\circ}\text{C}$	Active Force per Spring Stack at Room T.	644	N
Active Expanding Bolt Length	16.7	mm	Active Force per Spring Stack at Contact	571	N
Thickness Load Cell Top	15.5	mm	Active Force per Spring Stack at Bonding T.	625	N
Tensile Stress Area Bolt	20.5	$\text{mm}^2$	Tensile Stress of Bolts at Room Temp.	31	MPa
Nominal Load Disc Spring	800	N	Tensile Stress of Bolts at Contact Temp.	28	MPa
Nominal Compression D.S.	0.292	mm	Load Cell Compression at Room Temp.	235	$\mu\text{m}$
Number of Springs per Stack	1		Load Cell Compression at Contact Temp.	209	$\mu\text{m}$
Number of Spring Stacks	4		Load Cell Compression at Bonding Temp.	228	$\mu\text{m}$
			Expansion Potential CTE Fixture	305	$\mu\text{m}$
			Active CTE Compression of Load Cell	20	$\mu\text{m}$
			Starting Pressure at Contact Temperature	3.7	MPa
			Pressure Sensitivity CTE Fixture in f(T)	0.0069	$\text{MPa}/^{\circ}\text{C}$
			Pressure Sensitivity CTE Fixture in f(z)	0.0175	$\text{MPa}/\mu\text{m}$
			Adjustable Initial Gap	285	$\mu\text{m}$
FEM Model Data Input			FEM Model Data Output: Real Constant Settings		
Element Length LINK10 (T.o.)	13.668	mm	ISTRN Value for LINK10 (Tension only)	0.01719	235
Element Length LINK10 (C.o.)	7.332	mm	ISTRN Value for LINK10 (Compr. only)	0.00688	50

**Table C1-3:  $T_B=800^{\circ}\text{C}$  /  $T_C=780^{\circ}\text{C}$  /  $p_B=4\text{MPa}$** 

Bonding Data Input			CTE Fixture Data Output: Preload Load Cell		
Room Temperature	20	$^{\circ}\text{C}$	Active Warpage Temperature Range	20	$^{\circ}\text{C}$
Bonding Temperature	800	$^{\circ}\text{C}$	Load Cell Force at Bonding Temperature	2500	N
Temperature of Contact	780	$^{\circ}\text{C}$	Load Cell Force at Contact Temperature	2414	N
Bonding Area (Test Article)	625	$\text{mm}^2$	Load Cell Force at Room Temperature	2716	N
Desired Bonding Pressure	4.0	MPa	Preload Force (Hot Press)	611	lbs
CTE Fixture Data Input			CTE Fixture Data Output: Initial Gap		
Gap Closure Function	0.391	$\mu\text{m}/^{\circ}\text{C}$	Additional Load Cell Compression	-28	$\mu\text{m}$
CTE Load Cell Fasteners	8.2	$10^{-6}/^{\circ}\text{C}$	Spring Constant per Stack	2740	N/mm
CTE Load Cell Platens	6.5	$10^{-6}/^{\circ}\text{C}$	Active Force per Spring Stack at Room T.	679	N
Active Expanding Bolt Length	16.7	mm	Active Force per Spring Stack at Contact	604	N
Thickness Load Cell Top	15.5	mm	Active Force per Spring Stack at Bonding T.	625	N
Tensile Stress Area Bolt	20.5	$\text{mm}^2$	Tensile Stress of Bolts at Room Temp.	33	MPa
Nominal Load Disc Spring	800	N	Tensile Stress of Bolts at Contact Temp.	29	MPa
Nominal Compression D.S.	0.292	mm	Load Cell Compression at Room Temp.	248	$\mu\text{m}$
Number of Springs per Stack	1		Load Cell Compression at Contact Temp.	220	$\mu\text{m}$
Number of Spring Stacks	4		Load Cell Compression at Bonding Temp.	228	$\mu\text{m}$
			Expansion Potential CTE Fixture	305	$\mu\text{m}$
			Active CTE Compression of Load Cell	8	$\mu\text{m}$
			Starting Pressure at Contact Temperature	3.9	MPa
			Pressure Sensitivity CTE Fixture in $f(T)$	0.0069	$\text{MPa}/^{\circ}\text{C}$
			Pressure Sensitivity CTE Fixture in $f(z)$	0.0175	$\text{MPa}/\mu\text{m}$
			Adjustable Initial Gap	297	$\mu\text{m}$
FEM Model Data Input			FEM Model Data Output: Real Constant Settings		
Element Length LINK10 (T.o.)	13.668	mm	ISTRN Value for LINK10 (Tension only)	0.01813	248
Element Length LINK10 (C.o.)	7.332	mm	ISTRN Value for LINK10 (Compr. only)	0.00673	49

## APPENDIX D: EXPERIMENTAL DATA

## D1: Experimental Data Laser Burrs

Wavelength: 532 nm

Power level: 100%

Cutting speed: 6 mm/s

Repetition rate: 3000 Hz

# of path repetitions: 25

**Table D1-1: Measurements of Burr Height after Laser Cutting**

10 randomly selected substrate, measured at 10 different positions

#	Burr [ $\mu\text{m}$ ]	#	Burr [ $\mu\text{m}$ ]	#	Burr [ $\mu\text{m}$ ]
1	19	2	17	3	25
4	13	5	6	6	13
7	20	8	6	9	18
10	2				
Mean burr height [ $\mu\text{m}$ ]					<b>14.2</b>
Standard deviation [ $\mu\text{m}$ ]					<b>7.3</b>

After deburring with Scotch Brite Ultra Fine no considerable burr was measurable and vanished in overall substrate surface roughness  $< 1 \mu\text{m}$ .

## D2: Experimental Data Substrate Flattening

Equipment used: Dektak<sup>3</sup> surface profiler

Scan length: 20 mm (between fin area)

Read out: peak-to-valley P-V computation of substrate waviness (band width flatness)

**Table D2-1: Measurements of Initial Substrate Flatness after Laser Cutting**

#	P-V [ $\mu\text{m}$ ]	#	P-V [ $\mu\text{m}$ ]	#	P-V [ $\mu\text{m}$ ]
1	60	2	155	3	197
4	133	5	157	6	54
7	121	8	11	9	140
10	17				
Mean substrate flatness [ $\mu\text{m}$ ]					<b>104.5</b>
Standard deviation [ $\mu\text{m}$ ]					<b>64.2</b>

**Table D2-2: Measurements of Substrate Flatness after Deburring**

#	P-V [ $\mu\text{m}$ ]	#	P-V [ $\mu\text{m}$ ]	#	P-V [ $\mu\text{m}$ ]
1	20.74	2	56.99	3	57.22
4	18.10	5	28.67	6	52.21
7	14.53	8	40.54	9	20.84
10	93.46	11	19.61	12	44.33
13	9.11	14	56.25	15	37.94
16	30.75	17	18.32	18	22.46
19	16.32	20	36.17	21	35.00
22	16.84	23	33.18	24	77.47
Mean substrate flatness [ $\mu\text{m}$ ]					<b>35.72</b>
Standard deviation [ $\mu\text{m}$ ]					<b>21.13</b>

**Table D2-3: Measurements of Substrate Flatness after Flattening**

#	P-V [ $\mu\text{m}$ ]	#	P-V [ $\mu\text{m}$ ]	#	P-V [ $\mu\text{m}$ ]
1	2.80	2	8.06	3	7.91
4	4.34	5	8.02	6	8.99
7	5.62	8	6.16	9	5.49
10	5.12	11	5.24	12	4.70
13	3.12	14	2.31	15	4.20
16	2.70	17	3.44	18	5.63
19	3.18	20	4.31	21	4.38
22	3.56	23	4.80	24	4.96
Mean substrate flatness [ $\mu\text{m}$ ]					<b>4.96</b>
Standard deviation [ $\mu\text{m}$ ]					<b>1.82</b>

### D3: Experimental Data Substrate Surface Roughness

Equipment used: Mitutoyo Surftest 212

Surface roughness of reference specimen:  $R_a=2.95\ \mu\text{m}$

**Table D3-1: Measurements on Reference Specimen**

#	$R_a\ [\mu\text{m}]$	#	$R_a\ [\mu\text{m}]$	#	$R_a\ [\mu\text{m}]$
1	2.91	2	2.88	3	2.78
4	2.94	5	2.75	6	3.01
7	2.73	8	2.80	9	2.95
10	2.83	11	2.87	12	2.73
Mean surface roughness $R_a\ [\mu\text{m}]$					<b>2.850</b>
Standard deviation $[\mu\text{m}]$					<b>0.094</b>

**Table D3-2: Measurements Test Article Substrates**

12 randomly selected substrates, 2 measurements taken perpendicular to each other

#	$R_a\ [\mu\text{m}]$	#	$R_a\ [\mu\text{m}]$	#	$R_a\ [\mu\text{m}]$
1	0.23	2	0.17	3	0.35
4	0.22	5	0.33	6	0.35
7	0.35	8	0.24	9	0.37
10	0.36	11	0.24	12	0.21
13	0.32	14	0.25	15	0.30
16	0.36	17	0.31	18	0.22
19	0.24	20	0.32	21	0.22
22	0.36	23	0.24	24	0.26
Mean surface roughness $R_a\ [\mu\text{m}]$					<b>0.284</b>
Standard deviation $[\mu\text{m}]$					<b>0.061</b>

#### D4: Experimental Data Bonding Fixture Evaluation

Equipment used: Dektak<sup>3</sup> surface profiler

Scan length: 5 mm (over fin window)

Read out: peak-to-valley P-V computation of fin waviness (band width fin warpage)

**Table D4-1: Measurements Test Article Orientation Test**

Run	Orientation	Fin	Position	P-V (1) [ $\mu\text{m}$ ]	P-V (2) [ $\mu\text{m}$ ]
1	0°	left	left	8.75	7.36
			middle	10.17	10.19
			right	4.37	4.22
		right	left	3.14	3.23
			middle	2.72	3.17
			right	2.33	1.60
	90°	left	left	1.27	1.28
			middle	2.74	3.28
			right	2.84	2.60
		right	left	1.87	1.98
			middle	2.40	2.61
			right	2.01	2.66
2	90°	left	left	1.79	2.67
			middle	6.42	6.71
			right	7.15	8.20
		right	left	1.89	2.68
			middle	4.29	4.03
			right	2.72	3.36
	0°	left	left	2.11	3.06
			middle	6.66	6.30
			right	1.71	3.11
		right	left	1.83	2.44
			middle	3.97	3.74
			right	2.72	3.36

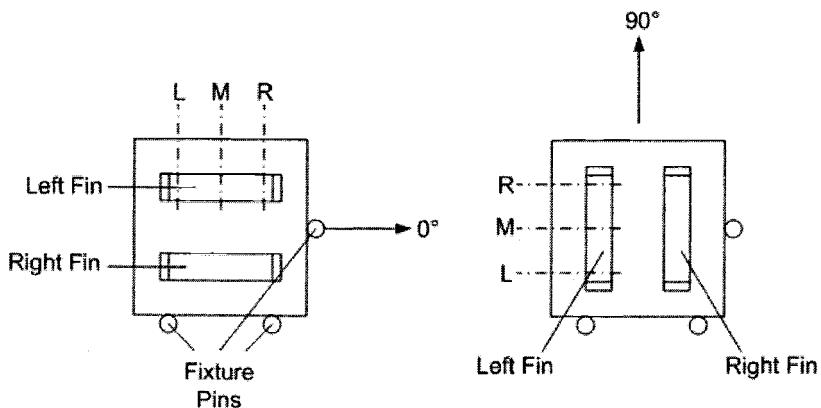


Figure D4-1: Test Article Measurement Configuration

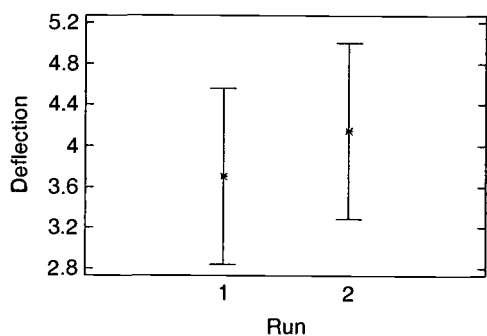
Table D4-2: Multifactor ANOVA

Analysis of Variance for Deflection - Type III Sums of Squares

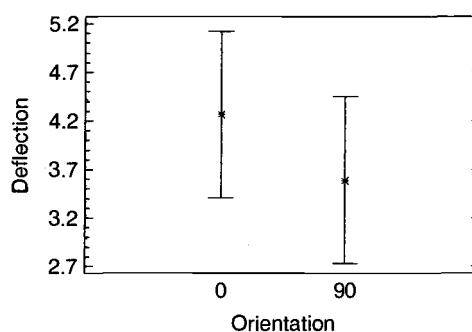
Source	Sum of Squares	Df	Mean Square	F-Ratio	P-Value
MAIN EFFECTS					
A:Run	2.41203	1	2.41203	0.55	0.4606
B:Fin	36.0187	1	36.0187	8.28	0.0063
C:Orientation	5.45401	1	5.45401	1.25	0.2692
D:Location	32.2328	2	16.1164	3.70	0.0330
RESIDUAL	182.699	42	4.34998		
TOTAL (CORRECTED)	258.817	47			

All F-ratios are based on the residual mean square error.

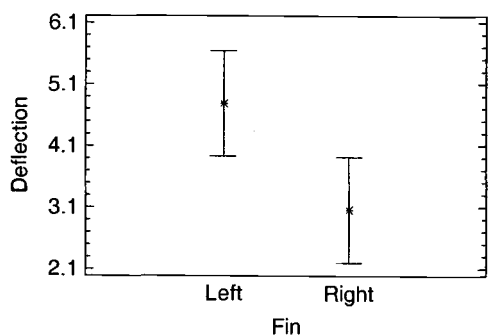
Means and 95.0 Percent Confidence Intervals



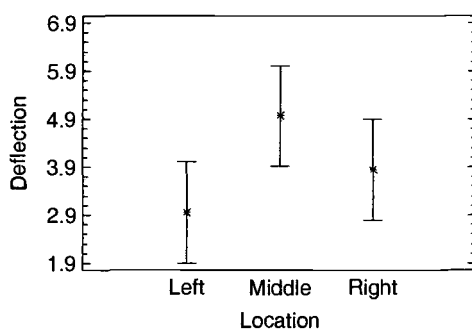
Means and 95.0 Percent Confidence Intervals



Means and 95.0 Percent Confidence Intervals



Means and 95.0 Percent Confidence Intervals



### D5: Experimental Data Pressure Timing Effect on Fin Warpage

Equipment used: Dektak<sup>3</sup> surface profiler, scan length 5 mm

Read out: peak-to-valley P-V computation of fin waviness (band width fin warpage)

**Table D5-1: Measurements Timing Effect of Bonding Pressure on Fin Warpage**

Run	Bonding Temp. $T_B$ [°C]	Pressure Application at % of $T_B$	Fin	Position	P-V [ $\mu\text{m}$ ]
1	600	0% (room temperature)	left	left	103.01
				middle	187.31
				right	118.95
			right	left	140.38
				middle	181.86
				right	158.95
2	800	100% (800°C)	left	left	6.43
				middle	4.11
				right	4.63
			right	left	8.80
				middle	4.13
				right	5.41
3	600	100% (600°C)	left	left	1.56
				middle	1.64
				right	3.61
			right	left	1.60
				middle	2.43
				right	1.59
4	600	50% (300°C)	left	left	41.26
				middle	120.17
				right	44.48
			right	left	21.03
				middle	87.47
				right	29.22
5	800	0% (room temperature)	left	left	184.85
				middle	184.06
				right	180.86
			right	left	184.13
				middle	187.68
				right	180.20
6	600	100% (600°C)	left	left	1.67
				middle	2.83
				right	1.23
			right	left	2.69
				middle	3.14
				right	1.69

Table D5-1 (Continued):

Run	Bonding Temp. $T_B$ [°C]	Pressure Application at % of $T_B$	Fin	Position	P-V [ $\mu\text{m}$ ]
7	800	0% (room temperature)	left	left	181.03
				middle	184.23
				right	182.20
			right	left	174.74
				middle	186.09
				right	180.53
8	800	50% (400°C)	left	left	38.10
				middle	113.15
				right	122.57
			right	left	10.49
				middle	70.07
				right	46.82
9	600	0% (room temperature)	left	left	118.63
				middle	181.83
				right	166.77
			right	left	123.93
				middle	114.68
				right	121.10
10	800	100% (800°C)	left	left	5.52
				middle	5.83
				right	10.41
			right	left	7.63
				middle	5.71
				right	10.37
11	600	50% (300°C)	left	left	9.83
				middle	111.20
				right	46.86
			right	left	26.27
				middle	95.49
				right	37.88
12	800	50% (400°C)	left	left	74.47
				middle	101.39
				right	90.58
			right	left	56.59
				middle	82.41
				right	39.42

**D6: Experimental Data Load Cell Validation**

Load Cell Compression [mil]	Force (1) [lbf]	Force (2) [lbf]
3	371	362
4	402	397
5	437	433
6	465	457
8	529	525
10	634	638
12	751	745
14	864	882
15	996	1002

## D7: Surface Roughness and Waviness of Bonding Platens

Equipment used: Dektak<sup>3</sup> surface profiler

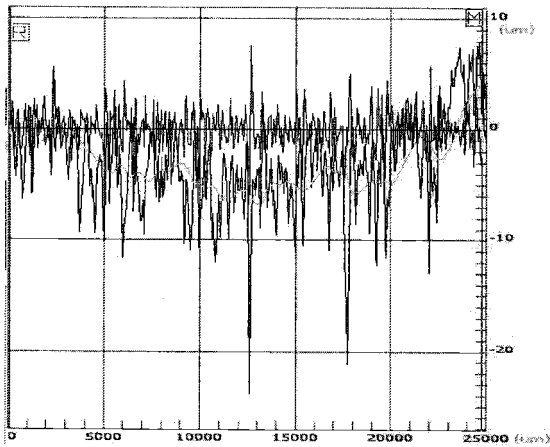
Scan length: 25 mm (over bonding area in x- and y-direction)

Short pass filter cutoff (roughness): 250

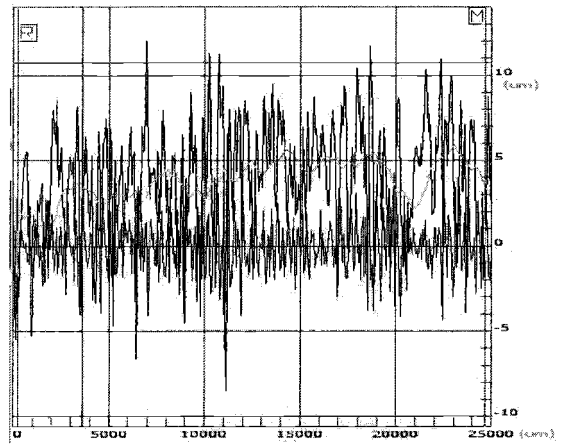
Long pass filter cutoff (waviness): 3000

### D7-1: Fixture Base (before re-machining):

X-X

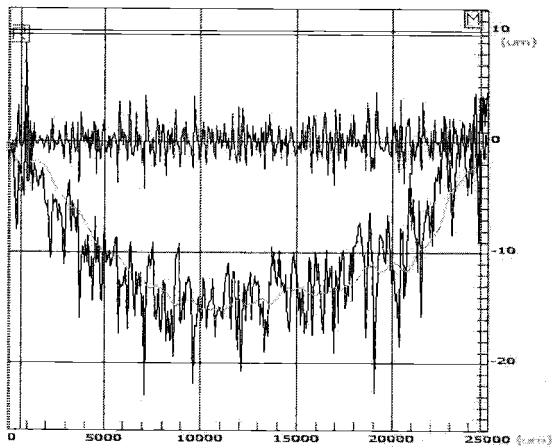


Y-Y

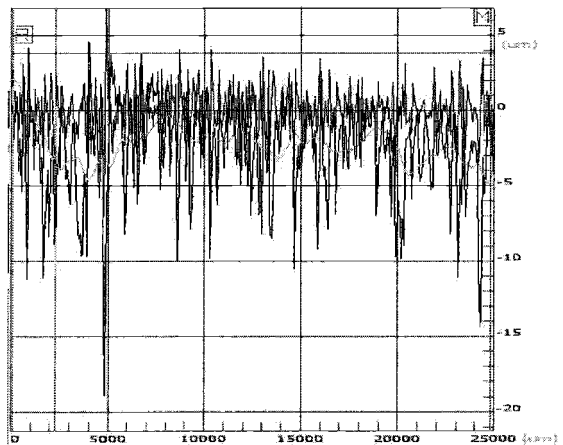


### D7-2: Interlayer (before re-machining):

X-X

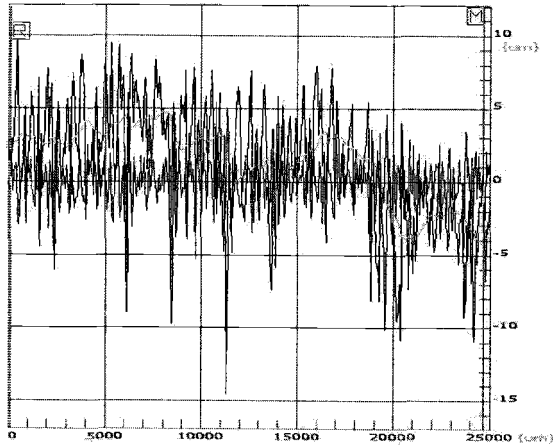


Y-Y

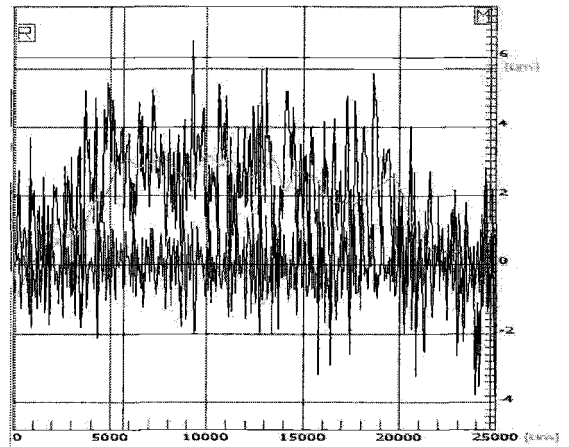


**D7-3: Fixture Top (before re-machining):**

X-X

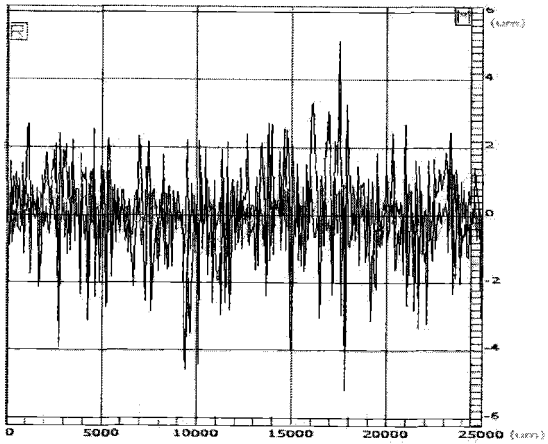


Y-Y

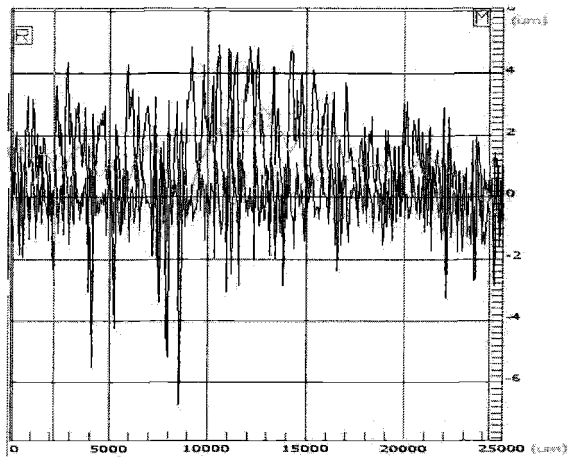


**D7-4: Fixture Base (after re-machining):**

X-X

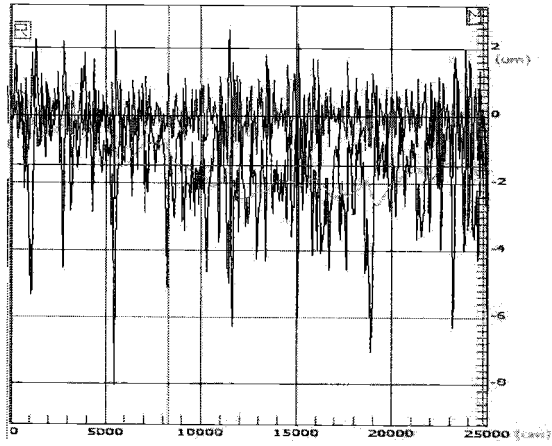


Y-Y

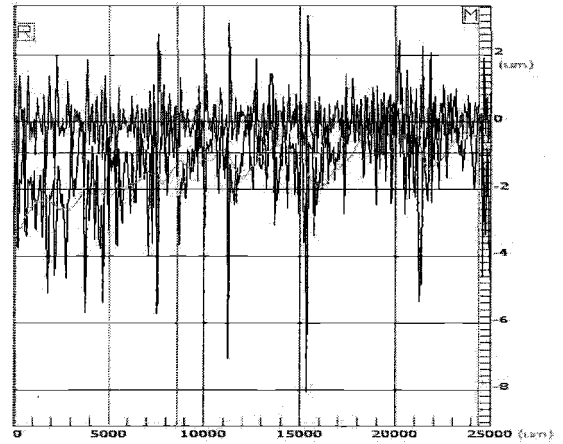


**D7-5: Interlayer (after re-machining):**

X-X

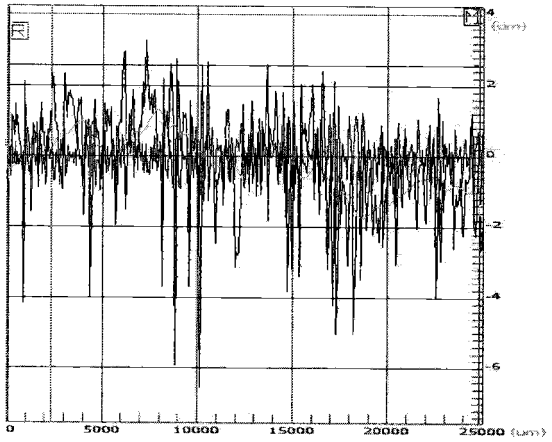


Y-Y

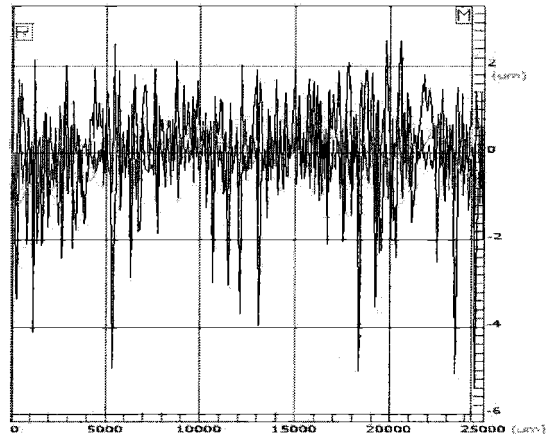


**D7-6: Fixture Top (after polishing):**

X-X



Y-Y



## **APPENDIX E: FIXTURE TIMING WITH FUJI FILM**

# E1: Colorization Chart Pressure Sensitive Film

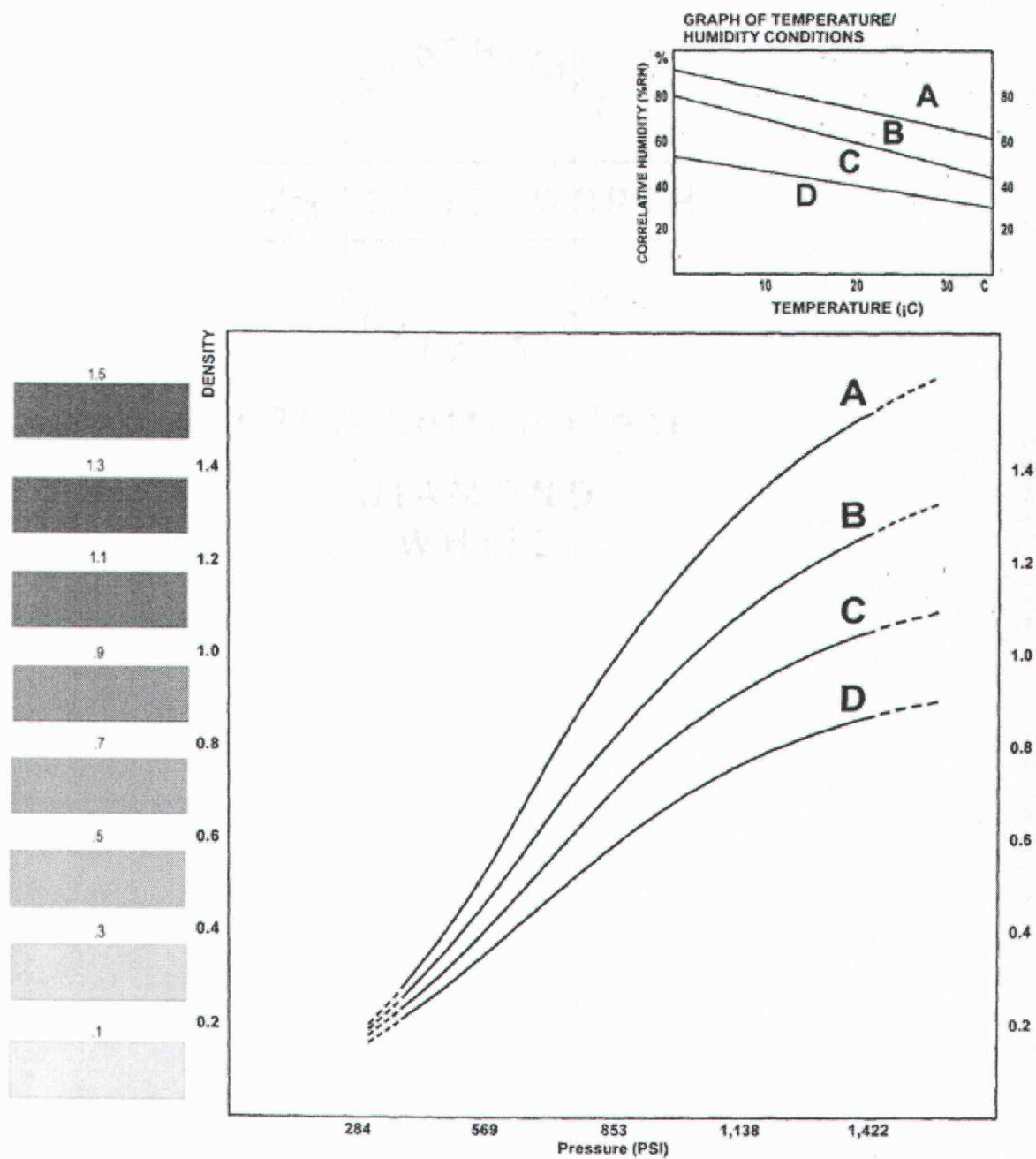


Figure E-1: Color Density Chart Pressure Sensitive Film Type LW

## E2: Fixture Settings for Timing Experiments at 180°C

**Table E2-1:  $T_B=180^\circ\text{C}$  /  $T_C=20^\circ\text{C}$  /  $p_B=4\text{MPa}$**

Bonding Data Input			CTE Fixture Data Output: Preload Load Cell		
Room Temperature	20	°C	Active Warpage Temperature Range	160	°C
Bonding Temperature	180	°C	Load Cell Force at Bonding Temperature	1956	N
Temperature of Contact	20	°C	Load Cell Force at Contact Temperature	1270	N
Bonding Area (Test Article)	489	mm <sup>2</sup>	Load Cell Force at Room Temperature	1270	N
Desired Bonding Pressure	4.0	MPa	Preload Force (Hot Press)	286	lbs
CTE Fixture Data Input			CTE Fixture Data Output: Initial Gap		
Gap Closure Function	0.391	μm/°C	Additional Load Cell Compression	0	μm
CTE Load Cell Fasteners	16.2	10 <sup>-6</sup> /°C	Spring Constant per Stack	2740	N/mm
CTE Load Cell Platens	6.5	10 <sup>-6</sup> /°C	Active Force per Spring Stack at Room T.	318	N
Active Expanding Bolt Length	16.7	mm	Active Force per Spring Stack at Contact	318	N
Thickness Load Cell Top	15.5	mm	Active Force per Spring Stack at Bonding T.	489	N
Tensile Stress Area Bolt	20.5	mm <sup>2</sup>	Tensile Stress of Bolts at Room Temp.	15	MPa
Nominal Load Disc Spring	800	N	Tensile Stress of Bolts at Contact Temp.	15	MPa
Nominal Compression D.S.	0.292	mm	Load Cell Compression at Room Temp.	116	μm
Number of Springs per Stack	1		Load Cell Compression at Contact Temp.	116	μm
Number of Spring Stacks	4		Load Cell Compression at Bonding Temp.	178	μm
			Expansion Potential CTE Fixture	63	μm
			Active CTE Compression of Load Cell	63	μm
			Starting Pressure at Contact Temperature	2.6	MPa
			Pressure Sensitivity CTE Fixture in f(T)	0.0088	MPa/°C
			Pressure Sensitivity CTE Fixture in f(z)	0.0224	MPa/μm
			Adjustable Initial Gap	0	μm

**Table E2-2:  $T_B=180^\circ\text{C}$  /  $T_C=100^\circ\text{C}$  /  $p_B=4\text{MPa}$**

Bonding Data Input			CTE Fixture Data Output: Preload Load Cell		
Room Temperature	20	°C	Active Warpage Temperature Range	80	°C
Bonding Temperature	180	°C	Load Cell Force at Bonding Temperature	1956	N
Temperature of Contact	100	°C	Load Cell Force at Contact Temperature	1613	N
Bonding Area (Test Article)	489	mm <sup>2</sup>	Load Cell Force at Room Temperature	1762	N
Desired Bonding Pressure	4.0	MPa	Preload Force (Hot Press)	396	lbs
CTE Fixture Data Input			CTE Fixture Data Output: Initial Gap		
Gap Closure Function	0.391	μm/°C	Additional Load Cell Compression	-14	μm
CTE Load Cell Fasteners	16.2	10 <sup>-6</sup> /°C	Spring Constant per Stack	2740	N/mm
CTE Load Cell Platens	6.5	10 <sup>-6</sup> /°C	Active Force per Spring Stack at Room T.	441	N
Active Expanding Bolt Length	16.7	mm	Active Force per Spring Stack at Contact	403	N
Thickness Load Cell Top	15.5	mm	Active Force per Spring Stack at Bonding T.	489	N
Tensile Stress Area Bolt	20.5	mm <sup>2</sup>	Tensile Stress of Bolts at Room Temp.	21	MPa
Nominal Load Disc Spring	800	N	Tensile Stress of Bolts at Contact Temp.	20	MPa
Nominal Compression D.S.	0.292	mm	Load Cell Compression at Room Temp.	161	μm
Number of Springs per Stack	1		Load Cell Compression at Contact Temp.	147	μm
Number of Spring Stacks	4		Load Cell Compression at Bonding Temp.	178	μm
			Expansion Potential CTE Fixture	63	μm
			Active CTE Compression of Load Cell	31	μm
			Starting Pressure at Contact Temperature	3.3	MPa
			Pressure Sensitivity CTE Fixture in f(T)	0.0088	MPa/°C
			Pressure Sensitivity CTE Fixture in f(z)	0.0224	MPa/μm
			Adjustable Initial Gap	31	μm

**Table E2-3:  $T_B=180^{\circ}\text{C}$  /  $T_C=150^{\circ}\text{C}$  /  $p_B=4\text{MPa}$** 

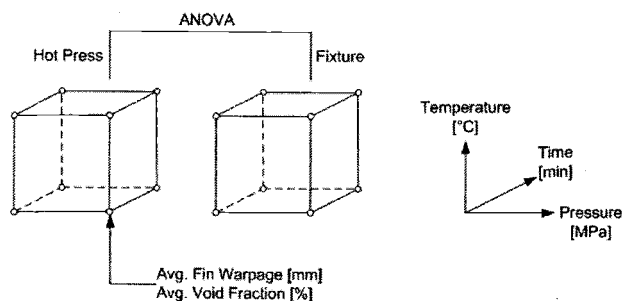
Bonding Data Input			CTE Fixture Data Output: Preload Load Cell		
Room Temperature	20	$^{\circ}\text{C}$	Active Warpage Temperature Range	30	$^{\circ}\text{C}$
Bonding Temperature	180	$^{\circ}\text{C}$	Load Cell Force at Bonding Temperature	1956	N
Temperature of Contact	150	$^{\circ}\text{C}$	Load Cell Force at Contact Temperature	1827	N
Bonding Area (Test Article)	489	$\text{mm}^2$	Load Cell Force at Room Temperature	2069	N
Desired Bonding Pressure	4.0	MPa	Preload Force (Hot Press)	465	lbs
CTE Fixture Data Input			CTE Fixture Data Output: Initial Gap		
Gap Closure Function	0.391	$\mu\text{m}/^{\circ}\text{C}$	Additional Load Cell Compression	-22	$\mu\text{m}$
CTE Load Cell Fasteners	16.2	$10^{-6}/^{\circ}\text{C}$	Spring Constant per Stack	2740	N/mm
CTE Load Cell Platens	6.5	$10^{-6}/^{\circ}\text{C}$	Active Force per Spring Stack at Room T.	517	N
Active Expanding Bolt Length	16.7	mm	Active Force per Spring Stack at Contact	457	N
Thickness Load Cell Top	15.5	mm	Active Force per Spring Stack at Bonding T.	489	N
Tensile Stress Area Bolt	20.5	$\text{mm}^2$	Tensile Stress of Bolts at Room Temp.	25	MPa
Nominal Load Disc Spring	800	N	Tensile Stress of Bolts at Contact Temp.	22	MPa
Nominal Compression D.S.	0.292	mm	Load Cell Compression at Room Temp.	189	$\mu\text{m}$
Number of Springs per Stack	1		Load Cell Compression at Contact Temp.	167	$\mu\text{m}$
Number of Spring Stacks	4		Load Cell Compression at Bonding Temp.	178	$\mu\text{m}$
			Expansion Potential CTE Fixture	63	$\mu\text{m}$
			Active CTE Compression of Load Cell	12	$\mu\text{m}$
			Starting Pressure at Contact Temperature	3.7	MPa
			Pressure Sensitivity CTE Fixture in f(T)	0.0088	$\text{MPa}/^{\circ}\text{C}$
			Pressure Sensitivity CTE Fixture in f(z)	0.0224	$\text{MPa}/\mu\text{m}$
			Adjustable Initial Gap	51	$\mu\text{m}$

**Table E2-4:  $T_B=180^{\circ}\text{C}$  /  $T_C=180^{\circ}\text{C}$  /  $p_B=4\text{MPa}$** 

Bonding Data Input			CTE Fixture Data Output: Preload Load Cell		
Room Temperature	20	$^{\circ}\text{C}$	Active Warpage Temperature Range	0	$^{\circ}\text{C}$
Bonding Temperature	180	$^{\circ}\text{C}$	Load Cell Force at Bonding Temperature	1956	N
Temperature of Contact	180	$^{\circ}\text{C}$	Load Cell Force at Contact Temperature	1956	N
Bonding Area (Test Article)	489	$\text{mm}^2$	Load Cell Force at Room Temperature	2254	N
Desired Bonding Pressure	4.0	MPa	Preload Force (Hot Press)	507	lbs
CTE Fixture Data Input			CTE Fixture Data Output: Initial Gap		
Gap Closure Function	0.391	$\mu\text{m}/^{\circ}\text{C}$	Additional Load Cell Compression	-27	$\mu\text{m}$
CTE Load Cell Fasteners	16.2	$10^{-6}/^{\circ}\text{C}$	Spring Constant per Stack	2740	N/mm
CTE Load Cell Platens	6.5	$10^{-6}/^{\circ}\text{C}$	Active Force per Spring Stack at Room T.	563	N
Active Expanding Bolt Length	16.7	mm	Active Force per Spring Stack at Contact	489	N
Thickness Load Cell Top	15.5	mm	Active Force per Spring Stack at Bonding T.	489	N
Tensile Stress Area Bolt	20.5	$\text{mm}^2$	Tensile Stress of Bolts at Room Temp.	27	MPa
Nominal Load Disc Spring	800	N	Tensile Stress of Bolts at Contact Temp.	24	MPa
Nominal Compression D.S.	0.292	mm	Load Cell Compression at Room Temp.	206	$\mu\text{m}$
Number of Springs per Stack	1		Load Cell Compression at Contact Temp.	178	$\mu\text{m}$
Number of Spring Stacks	4		Load Cell Compression at Bonding Temp.	178	$\mu\text{m}$
			Expansion Potential CTE Fixture	63	$\mu\text{m}$
			Active CTE Compression of Load Cell	0	$\mu\text{m}$
			Starting Pressure at Contact Temperature	4.0	MPa
			Pressure Sensitivity CTE Fixture in f(T)	0.0088	$\text{MPa}/^{\circ}\text{C}$
			Pressure Sensitivity CTE Fixture in f(z)	0.0224	$\text{MPa}/\mu\text{m}$
			Adjustable Initial Gap	63	$\mu\text{m}$

## **APPENDIX F: DATA COMPARISON EXPERIMENT**

## F1: Experimental Design



**Table F1-1: Randomized Experimental Runs (2<sup>4</sup> Full Factorial Design, 1 Replicate)**

Run	Mode	Temperature [°C]	Pressure [MPa]	Time [min]
1	Hot Press	800	3	60
2	Fixture	500	3	30
3	Hot Press	800	3	60
4	Hot Press	500	6	30
5	Fixture	500	6	30
6	Hot Press	800	6	30
7	Fixture	500	3	30
8	Hot Press	800	6	60
9	Fixture	800	3	60
10	Fixture	500	3	60
11	Hot Press	800	3	30
12	Hot Press	500	6	60
13	Hot Press	800	3	30
14	Hot Press	800	6	30
15	Hot Press	500	3	30
16	Fixture	800	3	30
17	Fixture	800	3	30
18	Fixture	800	3	60
19	Hot Press	500	6	60
20	Fixture	500	6	60
21	Hot Press	800	6	60
22	Fixture	500	3	60
23	Fixture	500	6	60
24	Fixture	800	6	30
25	Fixture	800	6	60
26	Fixture	800	6	60
27	Hot Press	500	3	60
28	Hot Press	500	3	60
29	Fixture	500	6	30
30	Hot Press	500	6	30
31	Hot Press	500	3	30
32	Fixture	800	6	30

## F2: Fixture Settings for Comparison Experiment

**Table F2-1:  $T_B=500^{\circ}\text{C}$  /  $T_C=450^{\circ}\text{C}$  /  $p_B=3\text{MPa}$**

Bonding Data Input			CTE Fixture Data Output: Preload Load Cell		
Room Temperature	20	$^{\circ}\text{C}$	Active Warpage Temperature Range	50	$^{\circ}\text{C}$
Bonding Temperature	500	$^{\circ}\text{C}$	Load Cell Force at Bonding Temperature	1467	N
Temperature of Contact	450	$^{\circ}\text{C}$	Load Cell Force at Contact Temperature	1454	N
Bonding Area (Test Article)	489	$\text{mm}^2$	Load Cell Force at Room Temperature	2254	N
Desired Bonding Pressure	3.0	MPa	Preload Force (Hot Press)	507	lbs
CTE Fixture Data Input			CTE Fixture Data Output: Initial Gap		
Gap Closure Function	0.024	$\mu\text{m}/^{\circ}\text{C}$	Additional Load Cell Compression	-73	$\mu\text{m}$
CTE Load Cell Fasteners	16.2	$10^{-6}/^{\circ}\text{C}$	Spring Constant per Stack	2740	N/mm
CTE Load Cell Platens	6.5	$10^{-6}/^{\circ}\text{C}$	Active Force per Spring Stack at Room T.	563	N
Active Expanding Bolt Length	16.7	mm	Active Force per Spring Stack at Contact	363	N
Thickness Load Cell Top	15.5	mm	Active Force per Spring Stack at Bonding T.	367	N
Tensile Stress Area Bolt	20.5	$\text{mm}^2$	Tensile Stress of Bolts at Room Temp.	27	MPa
Nominal Load Disc Spring	800	N	Tensile Stress of Bolts at Contact Temp.	18	MPa
Nominal Compression D. S.	0.292	mm	Load Cell Compression at Room Temp.	206	$\mu\text{m}$
Number of Springs per Stack	1		Load Cell Compression at Contact Temp.	133	$\mu\text{m}$
Number of Spring Stacks	4		Load Cell Compression at Bonding Temp.	134	$\mu\text{m}$
			Expansion Potential CTE Fixture	12	$\mu\text{m}$
			Active CTE Compression of Load Cell	1	$\mu\text{m}$
			Starting Pressure at Contact Temperature	3.0	MPa
			Pressure Sensitivity CTE Fixture in f(T)	0.0005	$\text{MPa}/^{\circ}\text{C}$
			Pressure Sensitivity CTE Fixture in f(z)	0.0224	$\text{MPa}/\mu\text{m}$
			Adjustable Initial Gap	10	$\mu\text{m}$

**Table F2-2:  $T_B=500^{\circ}\text{C}$  /  $T_C=450^{\circ}\text{C}$  /  $p_B=6\text{MPa}$**

Bonding Data Input			CTE Fixture Data Output: Preload Load Cell		
Room Temperature	20	$^{\circ}\text{C}$	Active Warpage Temperature Range	50	$^{\circ}\text{C}$
Bonding Temperature	500	$^{\circ}\text{C}$	Load Cell Force at Bonding Temperature	2934	N
Temperature of Contact	450	$^{\circ}\text{C}$	Load Cell Force at Contact Temperature	2921	N
Bonding Area (Test Article)	489	$\text{mm}^2$	Load Cell Force at Room Temperature	3721	N
Desired Bonding Pressure	6.0	MPa	Preload Force (Hot Press)	836	lbs
CTE Fixture Data Input			CTE Fixture Data Output: Initial Gap		
Gap Closure Function	0.024	$\mu\text{m}/^{\circ}\text{C}$	Additional Load Cell Compression	-73	$\mu\text{m}$
CTE Load Cell Fasteners	16.2	$10^{-6}/^{\circ}\text{C}$	Spring Constant per Stack	2740	N/mm
CTE Load Cell Platens	6.5	$10^{-6}/^{\circ}\text{C}$	Active Force per Spring Stack at Room T.	930	N
Active Expanding Bolt Length	16.7	mm	Active Force per Spring Stack at Contact	730	N
Thickness Load Cell Top	15.5	mm	Active Force per Spring Stack at Bonding T.	734	N
Tensile Stress Area Bolt	20.5	$\text{mm}^2$	Tensile Stress of Bolts at Room Temp.	45	MPa
Nominal Load Disc Spring	800	N	Tensile Stress of Bolts at Contact Temp.	36	MPa
Nominal Compression D. S.	0.292	mm	Load Cell Compression at Room Temp.	340	$\mu\text{m}$
Number of Springs per Stack	1		Load Cell Compression at Contact Temp.	267	$\mu\text{m}$
Number of Spring Stacks	4		Load Cell Compression at Bonding Temp.	268	$\mu\text{m}$
			Expansion Potential CTE Fixture	12	$\mu\text{m}$
			Active CTE Compression of Load Cell	1	$\mu\text{m}$
			Starting Pressure at Contact Temperature	6.0	MPa
			Pressure Sensitivity CTE Fixture in f(T)	0.0005	$\text{MPa}/^{\circ}\text{C}$
			Pressure Sensitivity CTE Fixture in f(z)	0.0224	$\text{MPa}/\mu\text{m}$
			Adjustable Initial Gap	10	$\mu\text{m}$

**Table F2-3:  $T_B=800^{\circ}\text{C}$  /  $T_C=750^{\circ}\text{C}$  /  $p_B=3\text{MPa}$** 

Bonding Data Input			CTE Fixture Data Output: Preload Load Cell		
Room Temperature	20	$^{\circ}\text{C}$	Active Warpage Temperature Range	50	$^{\circ}\text{C}$
Bonding Temperature	800	$^{\circ}\text{C}$	Load Cell Force at Bonding Temperature	1467	N
Temperature of Contact	750	$^{\circ}\text{C}$	Load Cell Force at Contact Temperature	1454	N
Bonding Area (Test Article)	489	$\text{mm}^2$	Load Cell Force at Room Temperature	2812	N
Desired Bonding Pressure	3.0	MPa	Preload Force (Hot Press)	632	lbs
CTE Fixture Data Input			CTE Fixture Data Output: Initial Gap		
Gap Closure Function	0.024	$\mu\text{m}/^{\circ}\text{C}$	Additional Load Cell Compression	-124	$\mu\text{m}$
CTE Load Cell Fasteners	16.2	$10^{-6}/^{\circ}\text{C}$	Spring Constant per Stack	2740	N/mm
CTE Load Cell Platens	6.5	$10^{-6}/^{\circ}\text{C}$	Active Force per Spring Stack at Room T.	703	N
Active Expanding Bolt Length	16.7	mm	Active Force per Spring Stack at Contact	363	N
Thickness Load Cell Top	15.5	mm	Active Force per Spring Stack at Bonding T.	367	N
Tensile Stress Area Bolt	20.5	$\text{mm}^2$	Tensile Stress of Bolts at Room Temp.	34	MPa
Nominal Load Disc Spring	800	N	Tensile Stress of Bolts at Contact Temp.	18	MPa
Nominal Compression D.S.	0.292	mm	Load Cell Compression at Room Temp.	257	$\mu\text{m}$
Number of Springs per Stack	1		Load Cell Compression at Contact Temp.	133	$\mu\text{m}$
Number of Spring Stacks	4		Load Cell Compression at Bonding Temp.	134	$\mu\text{m}$
			Expansion Potential CTE Fixture	19	$\mu\text{m}$
			Active CTE Compression of Load Cell	1	$\mu\text{m}$
			Starting Pressure at Contact Temperature	3.0	MPa
			Pressure Sensitivity CTE Fixture in f(T)	0.0005	$\text{MPa}/^{\circ}\text{C}$
			Pressure Sensitivity CTE Fixture in f(z)	0.0224	$\text{MPa}/\mu\text{m}$
			Adjustable Initial Gap	18	$\mu\text{m}$

**Table F2-4:  $T_B=800^{\circ}\text{C}$  /  $T_C=750^{\circ}\text{C}$  /  $p_B=6\text{MPa}$** 

Bonding Data Input			CTE Fixture Data Output: Preload Load Cell		
Room Temperature	20	$^{\circ}\text{C}$	Active Warpage Temperature Range	50	$^{\circ}\text{C}$
Bonding Temperature	800	$^{\circ}\text{C}$	Load Cell Force at Bonding Temperature	2934	N
Temperature of Contact	750	$^{\circ}\text{C}$	Load Cell Force at Contact Temperature	2921	N
Bonding Area (Test Article)	489	$\text{mm}^2$	Load Cell Force at Room Temperature	4279	N
Desired Bonding Pressure	6.0	MPa	Preload Force (Hot Press)	962	lbs
CTE Fixture Data Input			CTE Fixture Data Output: Initial Gap		
Gap Closure Function	0.024	$\mu\text{m}/^{\circ}\text{C}$	Additional Load Cell Compression	-124	$\mu\text{m}$
CTE Load Cell Fasteners	16.2	$10^{-6}/^{\circ}\text{C}$	Spring Constant per Stack	2740	N/mm
CTE Load Cell Platens	6.5	$10^{-6}/^{\circ}\text{C}$	Active Force per Spring Stack at Room T.	1070	N
Active Expanding Bolt Length	16.7	mm	Active Force per Spring Stack at Contact	730	N
Thickness Load Cell Top	15.5	mm	Active Force per Spring Stack at Bonding T.	734	N
Tensile Stress Area Bolt	20.5	$\text{mm}^2$	Tensile Stress of Bolts at Room Temp.	52	MPa
Nominal Load Disc Spring	800	N	Tensile Stress of Bolts at Contact Temp.	36	MPa
Nominal Compression D.S.	0.292	mm	Load Cell Compression at Room Temp.	390	$\mu\text{m}$
Number of Springs per Stack	1		Load Cell Compression at Contact Temp.	267	$\mu\text{m}$
Number of Spring Stacks	4		Load Cell Compression at Bonding Temp.	268	$\mu\text{m}$
			Expansion Potential CTE Fixture	19	$\mu\text{m}$
			Active CTE Compression of Load Cell	1	$\mu\text{m}$
			Starting Pressure at Contact Temperature	6.0	MPa
			Pressure Sensitivity CTE Fixture in f(T)	0.0005	$\text{MPa}/^{\circ}\text{C}$
			Pressure Sensitivity CTE Fixture in f(z)	0.0224	$\text{MPa}/\mu\text{m}$
			Adjustable Initial Gap	18	$\mu\text{m}$

### F3: Results Fin Warpage

**Table F3-1: Measurements Fin Warpage (Fin Center)**

Run	Mode	Bonding Temp. [°C]	Bonding Pressure [MPa]	Bonding Time [min]	Fin Warpage [μm]
1	Hot Press	800	3	60	5.51
					7.81
					7.00
					5.72
2	Fixture	500	3	30	2.91
					3.09
					1.96
					3.13
3	Hot Press	800	3	60	3.59
					2.52
					2.72
					1.99
4	Hot Press	500	6	30	1.82
					3.01
					2.26
					2.72
5	Fixture	500	6	30	2.94
					1.73
					2.89
					3.38
6	Hot Press	800	6	30	17.40
					14.94
					8.65
					5.92
7	Fixture	500	3	30	1.61
					3.17
					1.73
					2.69
8	Hot Press	800	6	60	5.15
					4.82
					5.04
					6.12
9	Fixture	800	3	60	4.90
					3.70
					5.23
					4.78
10	Fixture	500	3	60	1.81
					2.68
					1.79
					1.82

**Table F3-1: Measurements Fin Warpage (Continued)**

Run	Mode	Bonding Temp. [°C]	Bonding Pressure [MPa]	Bonding Time [min]	Fin Warpage [μm]
11	Hot Press	800	3	30	5.35
					4.83
					2.59
					7.71
12	Hot Press	500	6	60	2.01
					2.69
					1.45
					2.31
13	Hot Press	800	3	30	5.19
					2.48
					4.83
					5.39
14	Hot Press	800	6	30	4.56
					6.28
					5.52
					3.97
15	Hot Press	500	3	30	2.45
					2.46
					2.51
					1.12
16	Fixture	800	3	30	2.77
					4.16
					3.45
					4.24
17	Fixture	800	3	30	5.93
					4.66
					6.12
					9.94
18	Fixture	800	3	60	7.25
					5.48
					9.36
					5.78
19	Hot Press	500	6	60	1.14
					1.20
					1.73
					0.98
20	Fixture	500	6	60	2.32
					2.13
					2.92
					2.50

**Table F3-1: Measurements Fin Warpage (Continued)**

Run	Mode	Bonding Temp. [°C]	Bonding Pressure [MPa]	Bonding Time [min]	Fin Warpage [μm]
21	Hot Press	800	6	60	5.87
					7.55
					7.82
					8.93
22	Fixture	500	3	60	2.83
					1.65
					1.94
					1.43
23	Fixture	500	6	60	2.50
					1.31
					2.96
					1.81
24	Fixture	800	6	30	8.55
					8.72
					8.12
					5.91
25	Fixture	800	6	60	4.24
					6.54
					4.58
					5.38
26	Fixture	800	6	60	7.13
					5.96
					6.19
					5.45
27	Hot Press	500	3	60	1.79
					2.11
					1.52
					1.80
28	Hot Press	500	3	60	1.70
					1.47
					1.89
					1.54
29	Fixture	500	6	30	2.66
					1.63
					2.13
					1.72
30	Hot Press	500	6	30	1.42
					1.65
					2.23
					2.20

**Table F3-1: Measurements Fin Warpage (Continued)**

Run	Mode	Bonding Temp. [°C]	Bonding Pressure [MPa]	Bonding Time [min]	Fin Warpage [μm]
31	Hot Press	500	3	30	1.86
					3.27
					1.49
					1.77
32	Fixture	800	6	30	4.17
					4.53
					4.92
					5.46

**Table F3-2: Results Multifactor ANOVA Fin Warpage**

Analysis of Variance for Warpage - Type III Sums of Squares

Source	Sum of Squares	Df	Mean Square	F-Ratio	P-Value
MAIN EFFECTS					
A:Mode	0.0321945	1	0.0321945	0.01	0.9193
B:Temperature	457.645	1	457.645	146.66	0.0000
C:Pressure	21.7553	1	21.7553	6.97	0.0095
D:Time	6.58391	1	6.58391	2.11	0.1491
INTERACTIONS					
AB	3.90951	1	3.90951	1.25	0.2654
AC	9.02594	1	9.02594	2.89	0.0917
AD	3.02888	1	3.02888	0.97	0.3266
BC	19.5703	1	19.5703	6.27	0.0137
BD	0.216976	1	0.216976	0.07	0.7925
CD	3.62141	1	3.62141	1.16	0.2836
ABC	10.3683	1	10.3683	3.32	0.0710
ABD	1.95278	1	1.95278	0.63	0.4306
ACD	0.592688	1	0.592688	0.19	0.6638
BCD	5.93832	1	5.93832	1.90	0.1705
RESIDUAL	352.602	113	3.12037		
TOTAL (CORRECTED)	896.843	127			

All F-ratios are based on the residual mean square error.

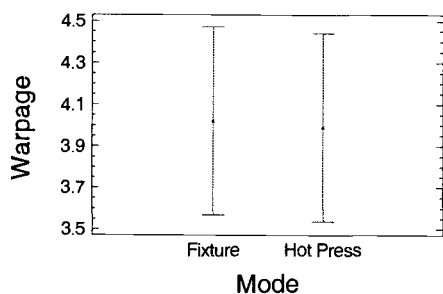
**Table F3-3: Results Multifactor ANOVA Fin Warpage (Table of Means)**

Table of Least Squares Means for Warpage  
with 95.0 Percent Confidence Intervals

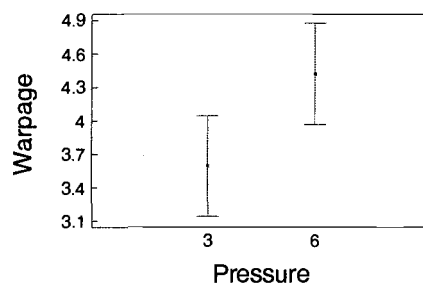
Level	Count	Mean	Std. Error	Lower Limit	Upper Limit
GRAND MEAN	128	4.00555			
Mode					
Fixture	64	4.02141	0.220807	3.58395	4.45887
Hot Press	64	3.98969	0.220807	3.55223	4.42715
Temperature					
500	64	2.11469	0.220807	1.67723	2.55215
800	64	5.89641	0.220807	5.45895	6.33387
Pressure					
3	64	3.59328	0.220807	3.15582	4.03074
6	64	4.41781	0.220807	3.98035	4.85527
Time					
30	64	4.23234	0.220807	3.79488	4.6698
60	64	3.77875	0.220807	3.34129	4.21621

**F3-4: Plot of Means with 95% Confidence Intervals**

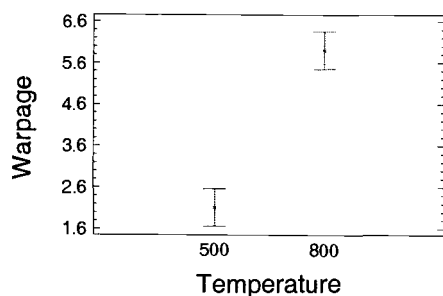
Means and 95.0 Percent Confidence Intervals



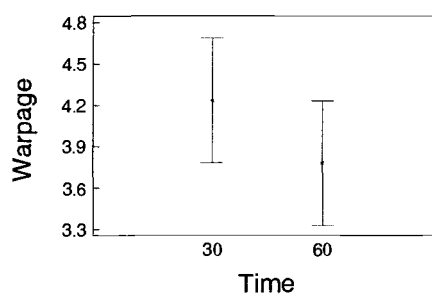
Means and 95.0 Percent Confidence Intervals



Means and 95.0 Percent Confidence Intervals

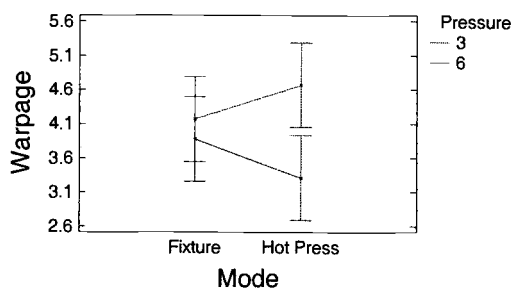


Means and 95.0 Percent Confidence Intervals

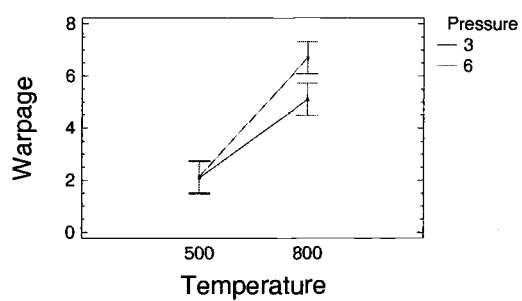


**F3-5: Interactions of Interest with 95% Confidence Intervals**

Interactions and 95.0 Percent Confidence Intervals



Interactions and 95.0 Percent Confidence Intervals



# F4: Results Void Fraction

Table F4-1: Bond Lines Hot Press at 500°C / 3MPa / 30min


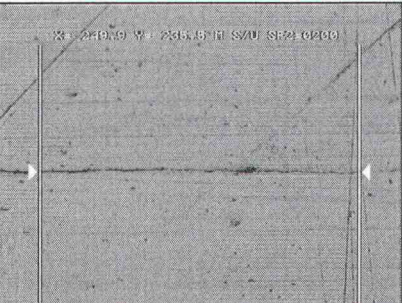


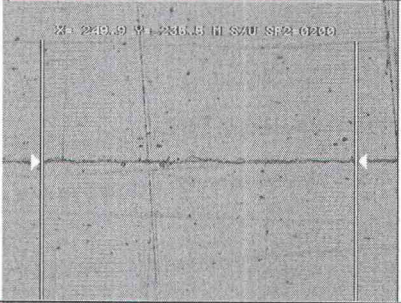
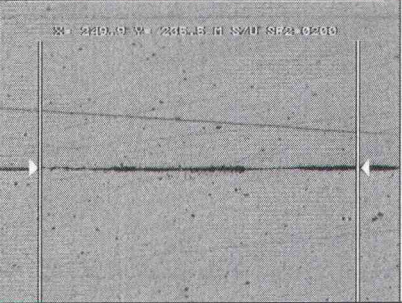

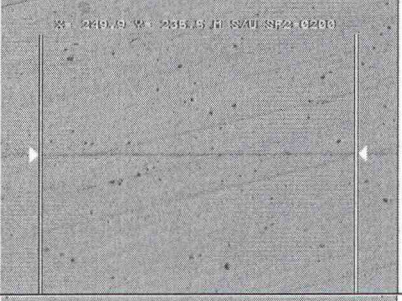
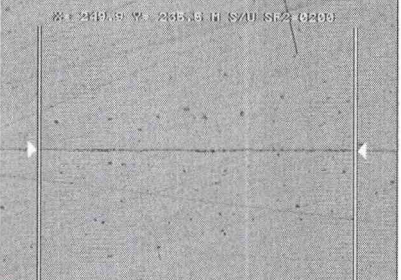
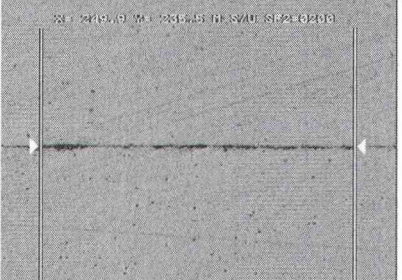
1		2	
3		4	
5		6	
7		8	
9		10	

Table F4-2: Bond Lines Hot Press at 500°C / 3MPa / 60min

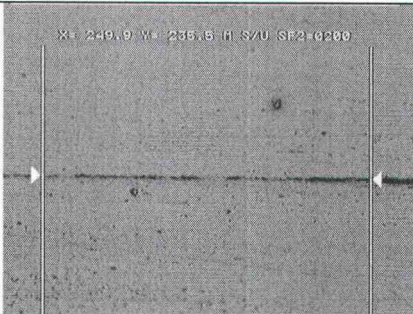





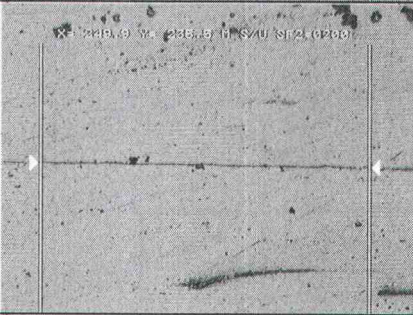

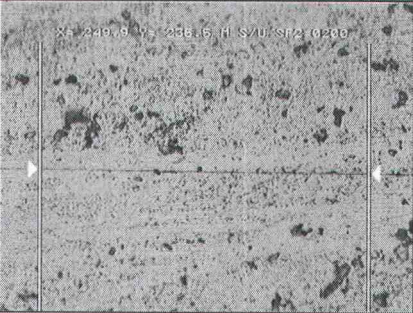
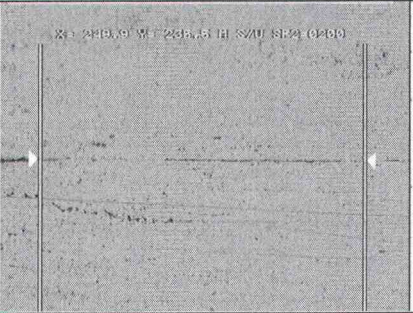
1		2	
3		4	
5		6	
7		8	
9		10	

Table F4-3: Void Fractions Hot Press at 500°C / 3MPa / 60min












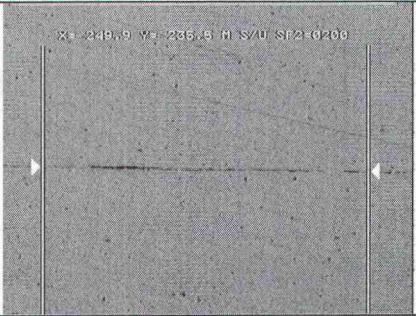
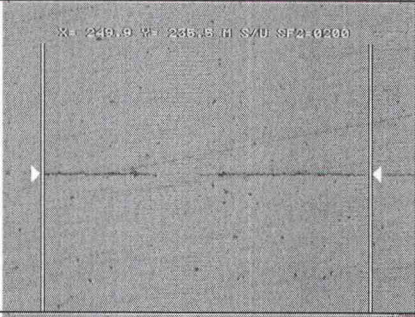
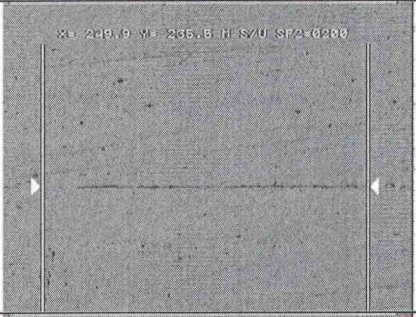



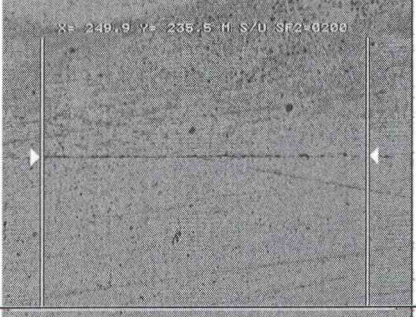
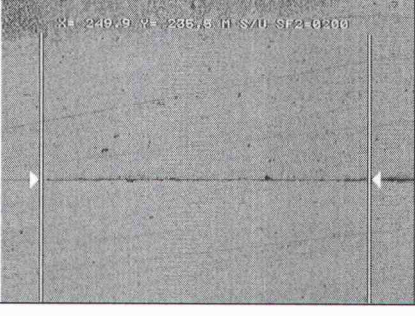
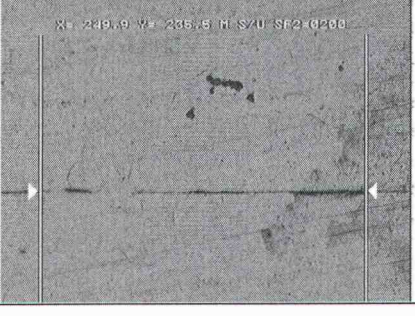
Bond Line	Void Inspection	Void Fraction
1		68%
2		78%
3		89%
4		67%
5		84%
6		78%
7		87%
8		84%
9		85%
10		68%
Average Void Fraction		78.8%

Table F4-4: Bond Lines Hot Press at 500°C / 6MPa / 30min

1		2	
3		4	
5		6	
7		8	
9		10	

**Table F4-5: Void Fractions Hot Press at 500°C / 6MPa / 30min**











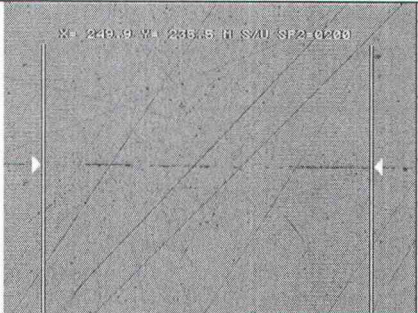
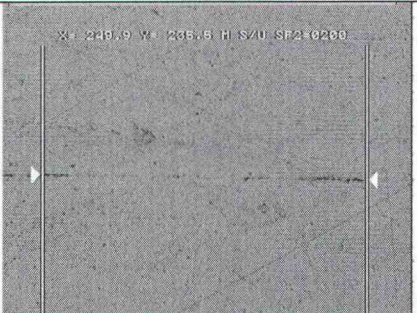



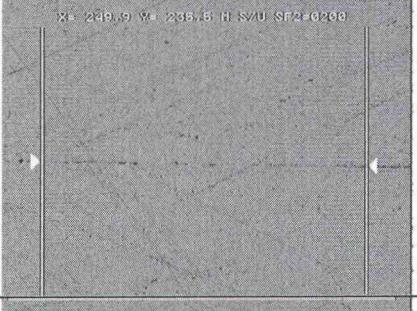
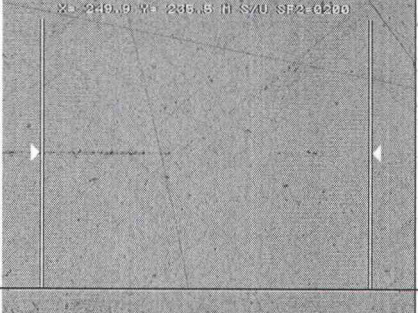
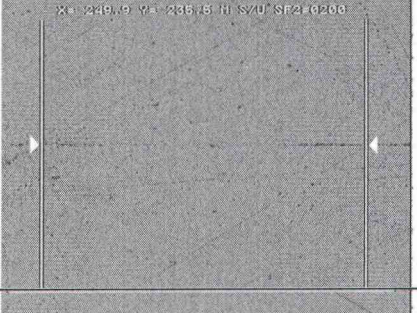

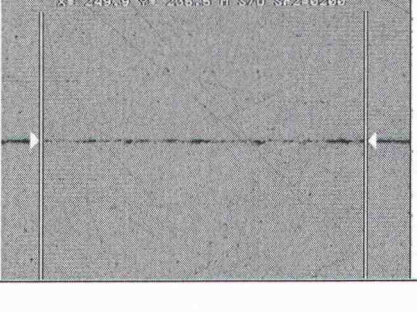
Bond Line	Void Inspection	Void Fraction
1		59%
2		56%
3		73%
4		52%
5		58%
6		69%
7		75%
8		58%
9		83%
10		74%
Average Void Fraction		<b>65.7%</b>

Table F4-6: Bond Lines Hot Press at 500°C / 6MPa / 60min

1		2	
3		4	
5		6	
7		8	
9		10	

**Table F4-7: Void Fractions Hot Press at 500°C / 6MPa / 60min**











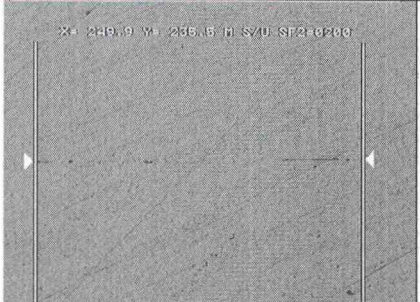
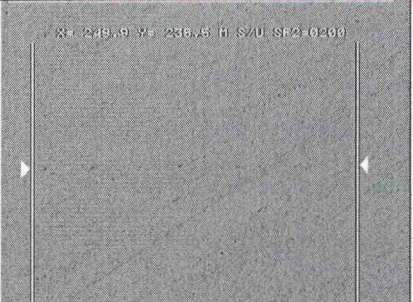
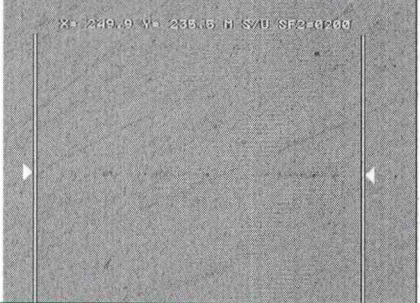
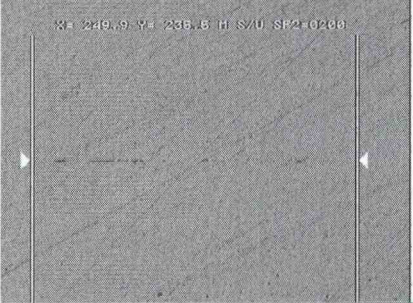


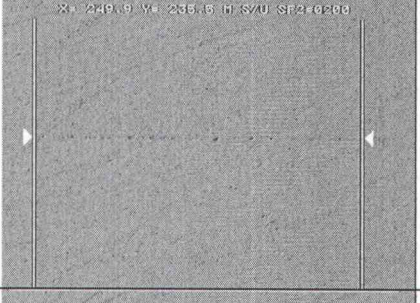

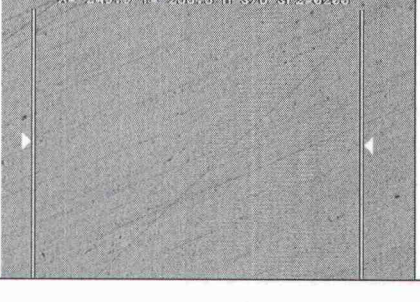
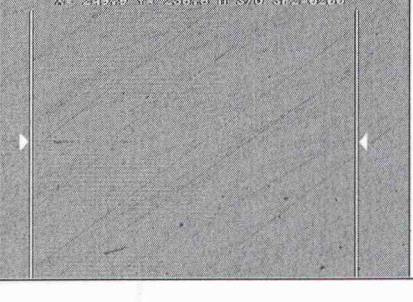
Bond Line	Void Inspection	Void Fraction
1		49%
2		30%
3		40%
4		26%
5		17%
6		27%
7		29%
8		39%
9		54%
10		48%
Average Void Fraction		<b>35.9%</b>

Table F4-8: Bond Lines Hot Press at 800°C / 3MPa / 30min

1		2	
3		4	
5		6	
7		8	
9		10	

**Table F4-9: Void Fractions Hot Press at 800°C / 3MPa / 30min**











Bond Line	Void Inspection	Void Fraction
1		31%
2		7%
3		16%
4		25%
5		17%
6		15%
7		21%
8		25%
9		26%
10		18%
Average Void Fraction		<b>20.1%</b>

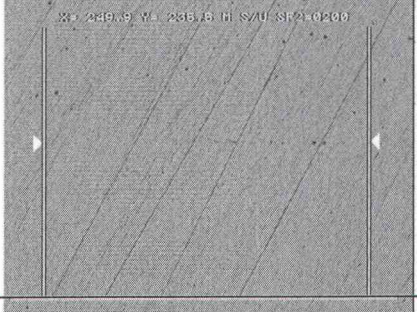
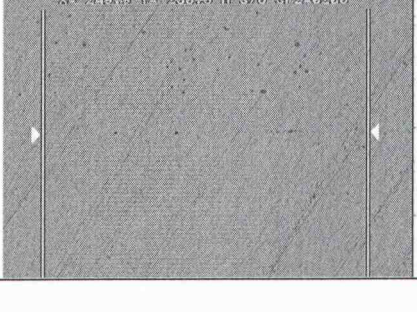
Table F4-10: Bond Lines Hot Press at 800°C / 3MPa / 60min

1		2	
3		4	
5		6	
7		8	
9		10	

**Table F4-11: Void Fractions Hot Press at 800°C / 3MPa / 60min**

Bond Line	Void Inspection	Void Fraction
1		35%
2		9%
3		9%
4		8%
5		5%
6		14%
7		11%
8		23%
9		25%
10		19%
Average Void Fraction		15.8%

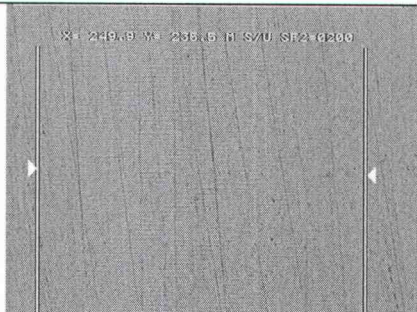
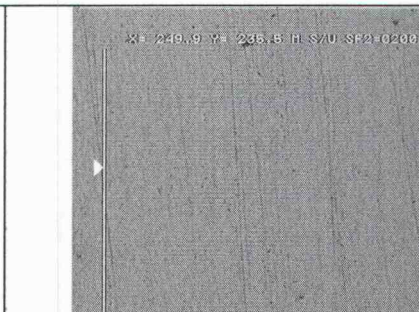

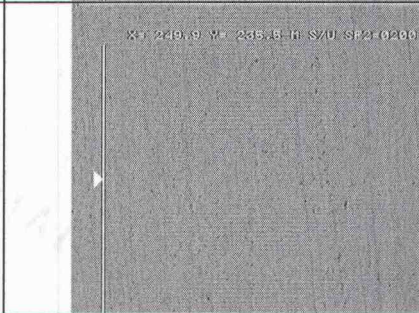
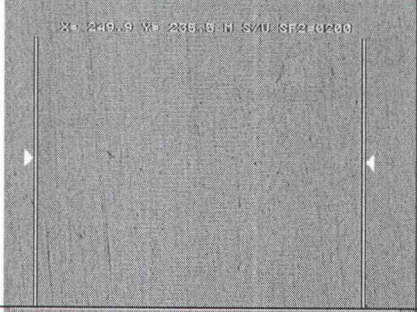
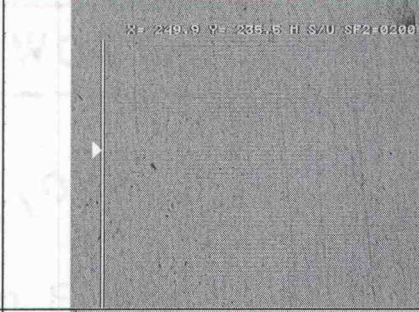

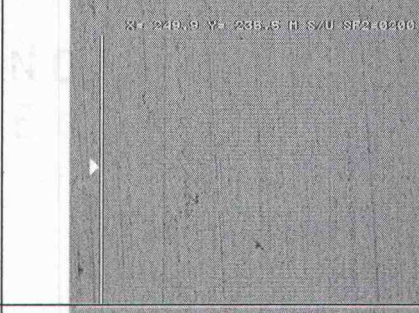
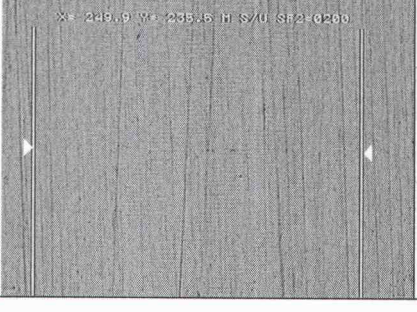
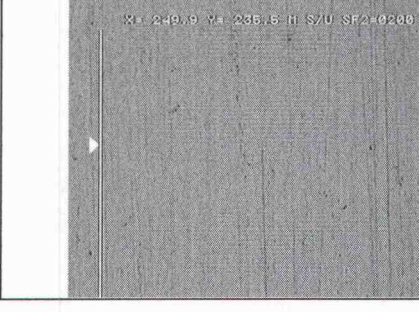
**Table F4-12: Bond Lines Hot Press at 800°C / 6MPa / 30min**

1		2	
3		4	
5		6	
7		8	
9		10	

**Table F4-13: Void Fractions Hot Press at 800°C / 6MPa / 30min**

Bond Line	Void Inspection	Void Fraction
1	"    .            - -	8%
2	" " " " " "    .            .    .	12%
3	" " "                    -    " " " " " "	19%
4	.            " " " "                    " " " "	17%
5	.            .    .    " " " "    " " " "    .    .	20%
6	" "            .            .    " "            " " " "	14%
7	" " "            .    .            .            .            " "	15%
8	.    "            " " " "            .            .            " " "	18%
9	.            " " " " " "            .            .            .	18%
10	.    " "                    " " " "            .	14%
Average Void Fraction		<b>15.5%</b>

Table F4-14: Bond Lines Hot Press at 800°C / 6MPa / 60min

1		2	
3		4	
5		6	
7		8	
9		10	

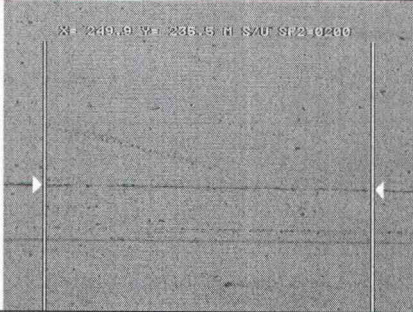
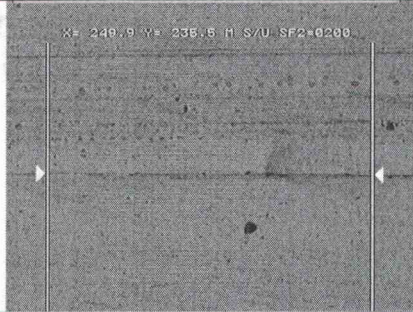
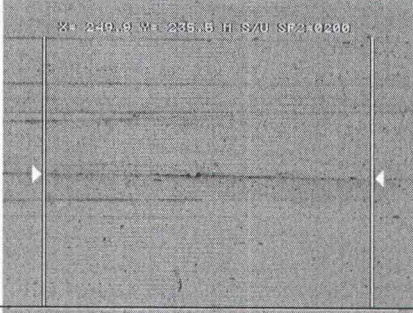
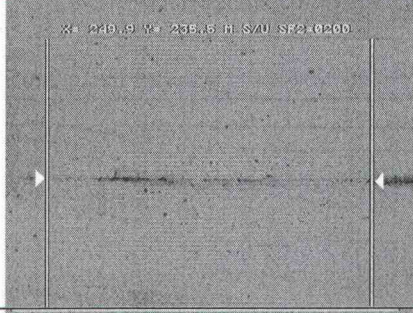
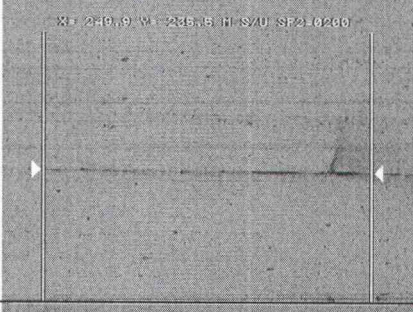

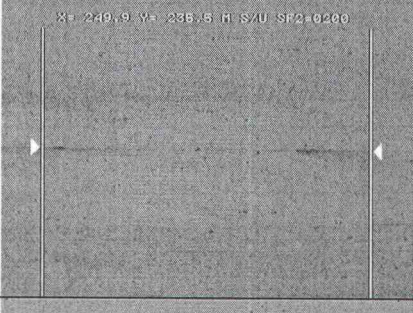

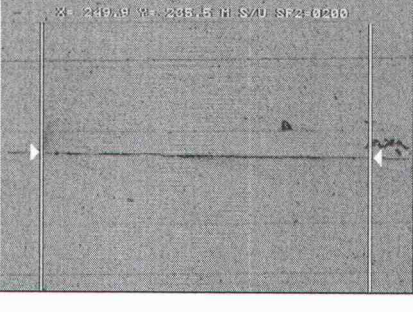

**Table F4-15: Void Fractions Hot Press at 800°C / 6MPa / 60min**

Bond Line	Void Inspection	Void Fraction
1	. . . . .	9%
2	. . . . .	11%
3	. . . . .	7%
4	. . . . .	9%
5	. . . . .	8%
6	. . . . .	8%
7	. . . . .	6%
8	. . . . .	3%
9	. . . . .	11%
10	. . . . .	8%
Average Void Fraction		8.0%

Table F4-16: Bond Lines  $\Delta$ CTE Fixture at 500°C / 3MPa / 30min

1		2	
3		4	
5		6	
7		8	
9		10	

Table F4-17: Bond Lines  $\Delta$ CTE Fixture at 500°C / 3MPa / 60min

1		2	
3		4	
5		6	
7		8	
9		10	

**Table F4-18: Void Fractions  $\Delta$ CTE Fixture at 500°C / 3MPa / 60min**











Bond Line	Void Inspection	Void Fraction
1		70%
2		78%
3		70%
4		55%
5		59%
6		77%
7		67%
8		75%
9		70%
10		84%
Average Void Fraction		<b>70.5%</b>

Table F4-19: Bond Lines  $\Delta$ CTE Fixture at 500°C / 6MPa / 30min


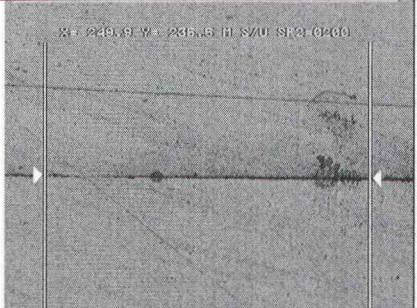
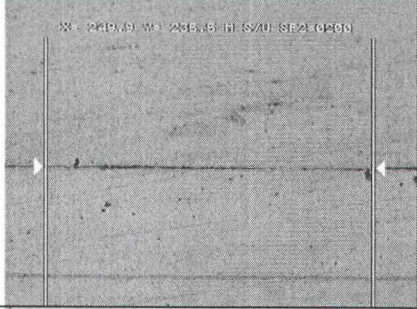
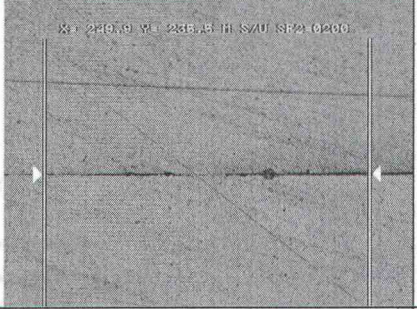
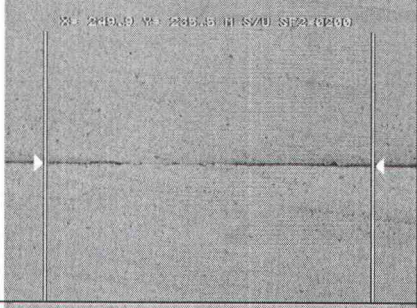
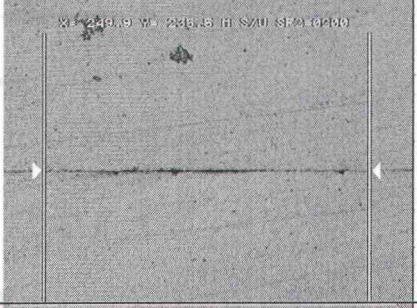
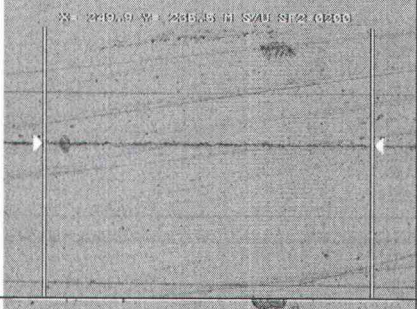
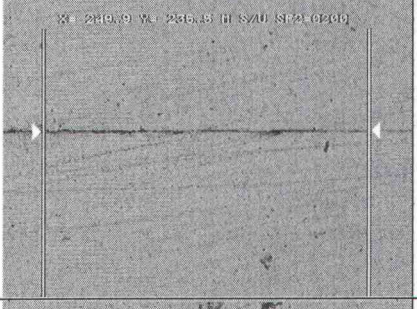
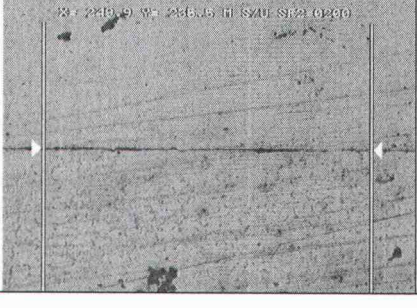

1		2	
3		4	
5		6	
7		8	
9		10	

Table F4-20: Void Fractions  $\Delta$ CTE Fixture at 500°C / 6MPa / 30min











Bond Line	Void Inspection	Void Fraction
1		79%
2		90%
3		81%
4		86%
5		80%
6		83%
7		75%
8		75%
9		83%
10		68%
Average Void Fraction		80.0%

Table F4-21: Bond Lines  $\Delta$ CTE Fixture at 500°C / 6MPa / 60min






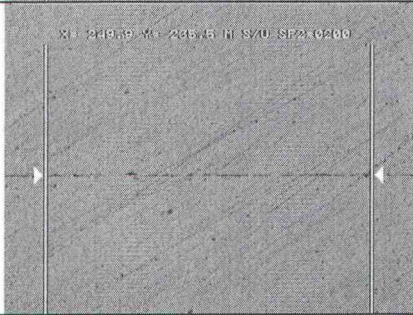
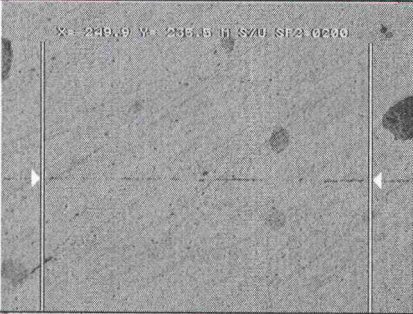



1		2	
3		4	
5		6	
7		8	
9		10	

Table F4-22: Void Fractions  $\Delta$ CTE Fixture at 500°C / 6MPa / 60min

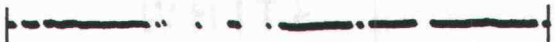











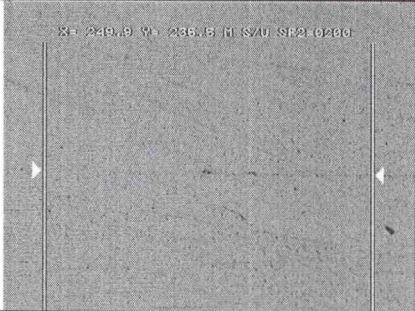







Bond Line	Void Inspection	Void Fraction
1		72%
2		63%
3		59%
4		68%
5		51%
6		61%
7		50%
8		61%
9		67%
10		68%
Average Void Fraction		<b>62.0%</b>

Table F4-23: Bond Lines  $\Delta$ CTE Fixture at 800°C / 3MPa / 30min

1		2	
3		4	
5		6	
7		8	
9		10	

**Table F4-24: Void Fractions  $\Delta$ CTE Fixture at 800°C / 3MPa / 30min**














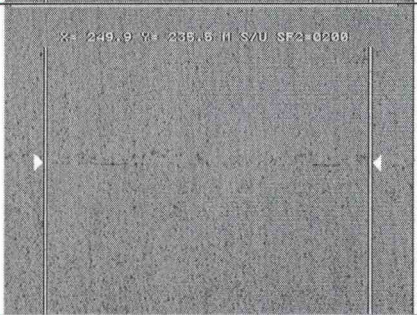


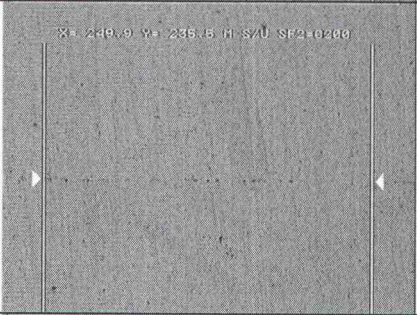



Bond Line	Void Inspection	Void Fraction
1		30%
2		53%
3		16%
4		35%
5		26%
6		27%
7		23%
8		25%
9		28%
10		40%
Average Void Fraction		<b>30.3%</b>

Table F4-25: Bond Lines  $\Delta$ CTE Fixture at 800°C / 3MPa / 60min

1	 Micrograph showing the bond line between two materials. The text 'X= 249.9 Y= 235.5 H S/U SF2=0200' is visible at the top.	2	 Micrograph showing the bond line between two materials. The text 'X= 249.9 Y= 235.5 H S/U SF2=0200' is visible at the top.
3	 Micrograph showing the bond line between two materials. The text 'X= 249.9 Y= 235.5 H S/U SF2=0200' is visible at the top.	4	 Micrograph showing the bond line between two materials. The text 'X= 249.9 Y= 235.5 H S/U SF2=0200' is visible at the top.
5	 Micrograph showing the bond line between two materials. The text 'X= 249.9 Y= 235.5 H S/U SF2=0200' is visible at the top.	6	 Micrograph showing the bond line between two materials. The text 'X= 249.9 Y= 235.5 H S/U SF2=0200' is visible at the top.
7	 Micrograph showing the bond line between two materials. The text 'X= 249.9 Y= 235.5 H S/U SF2=0200' is visible at the top.	8	 Micrograph showing the bond line between two materials. The text 'X= 249.9 Y= 235.5 H S/U SF2=0200' is visible at the top.
9	 Micrograph showing the bond line between two materials. The text 'X= 249.9 Y= 235.5 H S/U SF2=0200' is visible at the top.	10	 Micrograph showing the bond line between two materials. The text 'X= 249.9 Y= 235.5 H S/U SF2=0200' is visible at the top.

**Table F4-26: Void Fractions  $\Delta$ CTE Fixture at 800°C / 3MPa / 60min**











Bond Line	Void Inspection	Void Fraction
1		28%
2		24%
3		18%
4		29%
5		21%
6		28%
7		22%
8		24%
9		17%
10		21%
Average Void Fraction		<b>23.2%</b>

Table F4-27: Bond Lines  $\Delta$ CTE Fixture at 800°C / 6MPa / 30min

1		2	
3		4	
5		6	
7		8	
9		10	

**Table F4-28: Void Fractions  $\Delta$ CTE Fixture at 800°C / 6MPa / 30min**











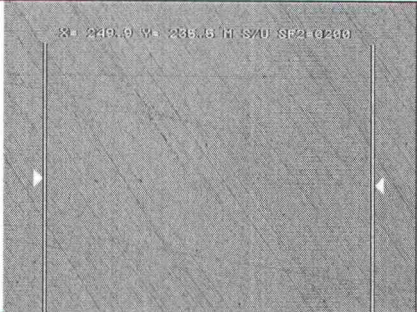
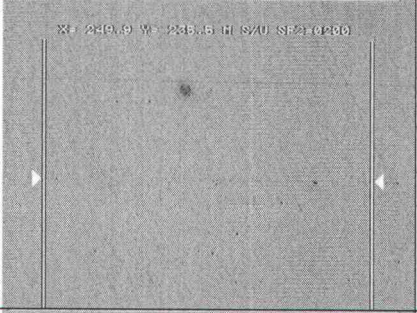
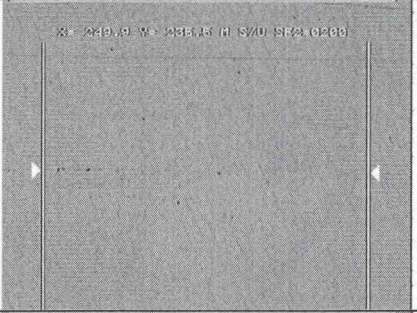
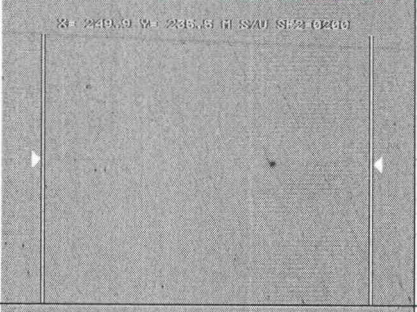
Bond Line	Void Inspection	Void Fraction
1		17%
2		18%
3		18%
4		38%
5		19%
6		13%
7		31%
8		11%
9		17%
10		13%
Average Void Fraction		<b>19.5%</b>

Table F4-29: Bond Lines  $\Delta$ CTE Fixture at 800°C / 6MPa / 60min

1		2	
3		4	
5		6	
7		8	
9		10	

**Table F4-30: Void Fractions  $\Delta$ CTE Fixture at 800°C / 6MPa / 60min**

Bond Line	Void Inspection	Void Fraction
1	. . . . .	8%
2	. . . . .	11%
3	. . . . .	9%
4	. . . . .	16%
5	. . . . .	8%
6	. . . . .	7%
7	. . . . .	11%
8	. . . . .	7%
9	. . . . .	11%
10	. . . . .	8%
Average Void Fraction		<b>9.6%</b>

Table F4-31: Results Multifactor ANOVA Void Fraction

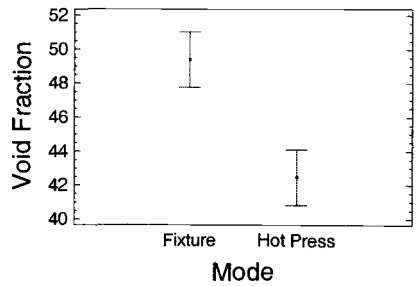
Analysis of Variance for Void Fraction - Type III Sums of Squares

Source	Sum of Squares	Df	Mean Square	F-Ratio	P-Value
MAIN EFFECTS					
A:Mode	1911.31	1	1911.31	35.16	0.0000
B:Temperature	127069.0	1	127069.0	2337.24	0.0000
C:Pressure	12691.4	1	12691.4	233.44	0.0000
D:Time	10128.3	1	10128.3	186.29	0.0000
INTERACTIONS					
AB	49.5062	1	49.5062	0.91	0.3415
AC	841.806	1	841.806	15.48	0.0001
AD	1.80625	1	1.80625	0.03	0.8556
BC	2967.01	1	2967.01	54.57	0.0000
BD	3036.31	1	3036.31	55.85	0.0000
CD	6.00625	1	6.00625	0.11	0.7401
ABC	2302.81	1	2302.81	42.36	0.0000
ABD	47.3062	1	47.3062	0.87	0.3525
ACD	262.656	1	262.656	4.83	0.0295
BCD	49.5062	1	49.5062	0.91	0.3415
RESIDUAL	7883.26	145	54.3673		
TOTAL (CORRECTED)	169248.0	159			

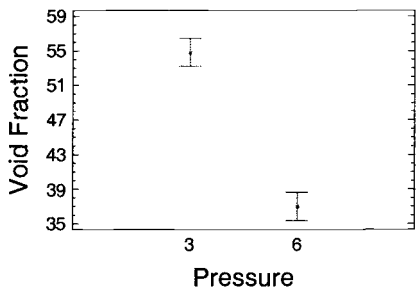
All F-ratios are based on the residual mean square error.

F4-32: Plot of Means with 95% Confidence Intervals

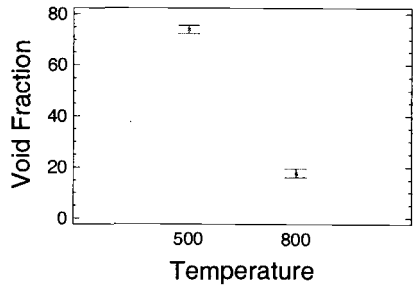
Means and 95.0 Percent Confidence Intervals



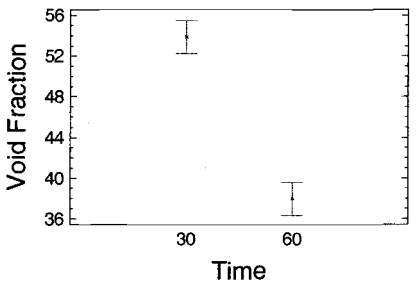
Means and 95.0 Percent Confidence Intervals



Means and 95.0 Percent Confidence Intervals



Means and 95.0 Percent Confidence Intervals



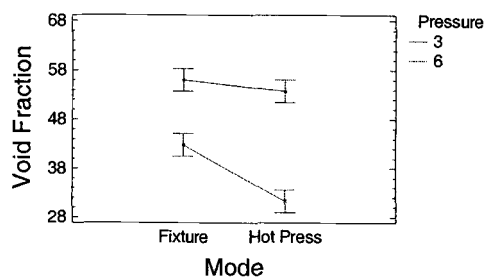
**Table F4-33: Results Multifactor ANOVA Void Fraction (Table of Means)**

Table of Least Squares Means for Void Fraction  
with 95.0 Percent Confidence Intervals

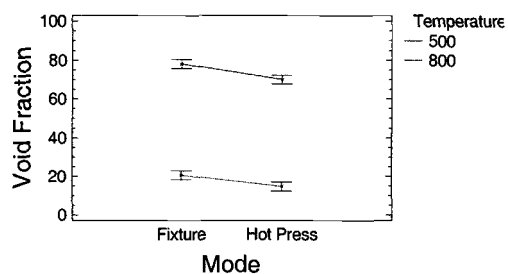
Level	Count	Mean	Std. Error	Lower Limit	Upper Limit
GRAND MEAN	160	45.9313			
Mode					
Fixture	80	49.3875	0.824373	47.7582	51.0168
Hot Press	80	42.475	0.824373	40.8457	44.1043
Temperature					
500	80	74.1125	0.824373	72.4832	75.7418
800	80	17.75	0.824373	16.1207	19.3793
Pressure					
3	80	54.8375	0.824373	53.2082	56.4668
6	80	37.025	0.824373	35.3957	38.6543
Time					
30	80	53.8875	0.824373	52.2582	55.5168
60	80	37.975	0.824373	36.3457	39.6043
Mode by Temperature					
Fixture 500	40	78.125	1.16584	75.8208	80.4292
Fixture 800	40	20.65	1.16584	18.3458	22.9542
Hot Press 500	40	70.1	1.16584	67.7958	72.4042
Hot Press 800	40	14.85	1.16584	12.5458	17.1542
Mode by Pressure					
Fixture 3	40	56.0	1.16584	53.6958	58.3042
Fixture 6	40	42.775	1.16584	40.4708	45.0792
Hot Press 3	40	53.675	1.16584	51.3708	55.9792
Hot Press 6	40	31.275	1.16584	28.9708	33.5792
Mode by Time					
Fixture 30	40	57.45	1.16584	55.1458	59.7542
Fixture 60	40	41.325	1.16584	39.0208	43.6292
Hot Press 30	40	50.325	1.16584	48.0208	52.6292
Hot Press 60	40	34.625	1.16584	32.3208	36.9292
Temperature by Pressure					
500 3	40	87.325	1.16584	85.0208	89.6292
500 6	40	60.9	1.16584	58.5958	63.2042
800 3	40	22.35	1.16584	20.0458	24.6542
800 6	40	13.15	1.16584	10.8458	15.4542
Temperature by Time					
500 30	40	86.425	1.16584	84.1208	88.7292
500 60	40	61.8	1.16584	59.4958	64.1042
800 30	40	21.35	1.16584	19.0458	23.6542
800 60	40	14.15	1.16584	11.8458	16.4542
Pressure by Time					
3 30	40	62.6	1.16584	60.2958	64.9042
3 60	40	47.075	1.16584	44.7708	49.3792
6 30	40	45.175	1.16584	42.8708	47.4792
6 60	40	28.875	1.16584	26.5708	31.1792

**F4-34: Interactions of Interest with 95% Confidence Intervals**

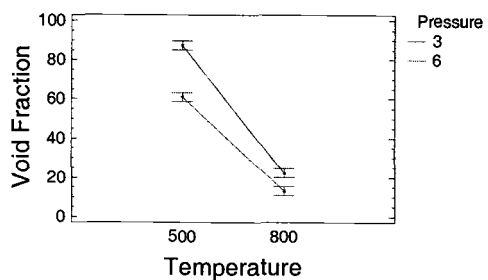
Interactions and 95.0 Percent Confidence Intervals



Interactions and 95.0 Percent Confidence Intervals



Interactions and 95.0 Percent Confidence Intervals



Interactions and 95.0 Percent Confidence Intervals

